

Cooperative Self-Assembly of Pyridine-2,6-Diimine-Linked Macrocycles into Mechanically Robust Nanotubes

Michael J. Strauss¹, Darya Asheghali², Austin M. Evans¹, Rebecca L. Li¹, Anton D. Chavez^{1,3},
Chao Sun^{1,3}, Matthew L. Becker^{2,*}, and William R. Dichtel^{1,*}

¹*Department of Chemistry, Northwestern University, 2145 Sheridan Road, Evanston, Illinois
60208, United States*

²*Department of Polymer Science, The University of Akron, Akron, Ohio 44325, United States*

³*Department of Chemistry and Chemical Biology, Baker Laboratory, Cornell University, Ithaca,
New York 14853, United States*

Supplementary Information

Correspondence Address
Professor William R. Dichtel Department of Chemistry Northwestern University 2145 Sheridan Road Evanston, IL 60208 (USA) wdichtel@northwestern.edu

Table of Contents

A. Materials and Instrumentation	S-3
I. Materials	
II. Instrumentation	
B. Synthetic Procedures	S-8
C. Additional Macrocycle Characterization	S-16
I. Characterization of MC 1	
II. Characterization of MC 2	
D. ^1H and ^{13}C NMR Spectra	S-20
E. Nanotube Characterization	S-26
I. Atomic Force Microscopy	
II. Scanning Electron Microscopy	

III.	X-Ray Diffraction	
IV.	Matrix Assisted Laser Desorption Ionization Mass Spectrometry	
V.	UV-Vis Spectroscopy	
VI.	Gel Permeation Chromatography	
VII.	Fluorescence	
VIII.	Comparison of Fluorescence and Gel Permeation Chromatography Data	
F.	Touch-Spun Fiber Characterization	S-64
I.	Transmission Electron Microscopy	
II.	Scanning Electron Microscopy	
III.	Atomic Force Microscopy	
IV.	Infrared Spectroscopy	
V.	Matrix Assisted Laser Desorption Ionization Mass Spectrometry	
VI.	Mechanical Testing of Touch-Spun Nanofibers	
VII.	Touch-Spinning of MC 1 with No Acid	
G.	References	S-72

A. Materials and Instrumentation.

I. Materials.

Reagents were purchased in reagent grade from commercial suppliers and used without further purification, unless otherwise described. Anhydrous solvents (Toluene, THF, DMF, DCM) were obtained from a solvent purification system (JC Meyer System). Reaction progress was monitored by thin layer chromatography (TLC) carried out on EMD 250 μm silica gel 60-F254 plates. Visualization was performed by UV light irradiation. For the preparation of touch-spun nanofibers, poly(ethylene oxide) (PEO) ($M_n = 4,000,000 \text{ g}\cdot\text{mol}^{-1}$) was purchased from Sigma-Aldrich; polycaprolactone (PCL) ($M_n = 60,000 \text{ g}\cdot\text{mol}^{-1}$) and a phenylalanine-based poly(ester urea) (PEU) ($M_n = 36,000 \text{ g}\cdot\text{mol}^{-1}$) were prepared according to literature procedures.¹⁻²

II. Instrumentation.

Nuclear Magnetic Resonance (NMR). ^1H and ^{13}C NMR spectra were acquired on a Bruker AvanceIII-500 MHz spectrometer with a CryoProbe 5mm DCH w/ Z-Gradient, or on a 400 MHz Agilent DD MR-400 spectrometer using an AutoX 5mm probe w/ Z-Gradient. All spectra were recorded at 25°C. All spectra were calibrated using residual solvent as an internal reference (CDCl_3 : 7.26 ppm for ^1H NMR, 77.00 for ^{13}C NMR; $\text{THF}-d_8$: 3.58, 1.73 ppm for ^1H NMR, 67.57, 25.37 ppm for ^{13}C NMR).

Infrared Spectroscopy (IR). Infrared spectra were recorded on a Nicolet iS10 FT-IR spectrometer equipped with a diamond ATR attachment and are uncorrected.

High-Resolution Mass Spectrometry (HRMS). High-resolution mass spectra were acquired on an Agilent 6210A LC-TOF Mass Spectrometer, with Atmospheric Pressure Photoionization (APPI) as an ion source. The instrument is equipped with an Agilent Series 1200 HPLC binary pump and autosampler. All samples were run using direct injection.

Matrix Assisted Laser Desorption Ionization Time of Flight (MALDI-TOF) Mass Spectrometry. MALDI-TOF mass spectra were recorded on a Bruker AutoFlex III with a 2,5-dihydroxybenzoic acid (DHB) matrix. All measurements were taken in reflectron positive (RP) mode.

Gel Permeation Chromatography (GPC). Gel permeation chromatography (GPC) was performed in stabilized, HPLC-grade tetrahydrofuran using an Agilent 1260 Infinity II system with variable-wavelength diode array (254, 450, and 530 nm) and refractive index detectors, guard column (Agilent PLgel; 5 μ m; 50 x 7.5 mm), and three analytical columns (Agilent PLgel; 5 μ m; 300 x 7.5 mm; 105, 104, and 103 Å pore sizes). The instrument was calibrated with narrow dispersity polystyrene standards between 640 Da and 2300 kDa (Polymer Standards Service GmbH). All runs were performed at 1.0 mL/min flow rate and 40 °C. All samples were dissolved in THF (1 mg/mL) and sonicated for 10 minutes before being filtered through a 0.45 μ m syringe filter (PTFE membrane). The calibration curve for the quantitative GPC studies was developed by diluting a stock solution of 0.5 mg/mL of macrocycle in THF with 0.3 mM tetrabutylammonium perchlorate. The solutions were filtered through a 0.45 μ m syringe filter (PTFE membrane) prior to measurement. All data for the quantitative GPC studies was conducted by acidifying 1 mL of a 0.15 mg/mL macrocycle solution in THF with 0.3 mM tetrabutylammonium perchlorate. The solutions were allowed to equilibrate undisturbed at room temperature for 2 h. before being filtered through a 0.45 μ m syringe filter (PTFE membrane) prior to measurement.

UV-Vis Absorption Spectroscopy. UV-Vis absorption spectra were acquired using a UV-3600 Shimadzu UV-Vis-NIR Spectrophotometer from 600 to 200 nm with a medium scan speed; λ_{max} in nm (ϵ in L · mol⁻¹ · cm⁻¹). All spectra were recorded at room temperature in the presence of air. UV-Vis solutions were prepared from a 0.1 mg/mL solution of macrocycle in THF with 0.3 mM tetrabutylammonium perchlorate. The appropriate amount of CF₃CO₂H was added, the resulting solution was allowed to equilibrate at room temperature for 12 h. before being analyzed.³

Fluorescence Spectroscopy. Fluorescence data was obtained on a Molecular Devices Gemini EM Fluorescence/Cheiluminescence Plate Reader maintained by the Keck Biophysics core facility at Northwestern University. All measurements were taken using the top read mode, in a clear 96 well plate. All samples were prepared from a 0.5 mg/mL solution of macrocycle in THF with 0.3 mM tetrabutylammonium perchlorate. After adding the appropriate amount of acid, the resulting solutions were allowed to equilibrate at room temperature for 12 h. before being analyzed.

Atomic Force Microscopy (AFM). Atomic force microscopy (AFM) was conducted using the facilities at the Northwestern Atomic and Nanoscale Characterization Experiment Center (NUANCE) on a SPID Bruker FastScan AFM under the non-contact mode in air. AFM samples

were prepared from a 0.1 mg/mL solution of macrocycle in THF with 0.3 mM tetrabutylammonium perchlorate. The solution was subjected to a brief bath sonication to ensure dissolution of the macrocycle. The appropriate amount of CF₃CO₂H was then added, the solution was allowed to equilibrate at room temperature for 12 h., and was then drop cast onto a silicon native oxide substrate and allowed to air dry for 30 minutes. The substrate was then washed with EtOH and allowed to once again air dry for 3 h. before images were taken.³

Scanning Electron Microscopy (SEM). Scanning electron microscopy (SEM) was conducted using the facilities at Northwestern's Electron Probe Instrumentation Center (EPIC) on an SEM Hitachi SU8030 microscope with an accelerating voltage of 15 kV. Samples were prepared from a 0.1 mg/mL solution of macrocycle in THF with 0.3 mM tetrabutylammonium perchlorate. The solution was subjected to a brief bath sonication to ensure dissolution of the macrocycle. The appropriate amount of CF₃CO₂H was then added, the solution was allowed to equilibrate at room temperature for 12 h., and was then drop cast onto a silicon native oxide substrate and allowed to air dry for 30 minutes. The substrate was then washed with EtOH and allowed to air dry for 3 h. The samples were then mounted onto a flat aluminum sample holder and coated with 2 nm of Osmium before images were taken.

Grazing-Incidence X-Ray Diffraction (GI-XRD). Grazing-incidence x-ray diffraction (GI-XRD) patterns were collected at Sector 12-ID-B of the Advanced Photon Source (APS) at Argonne National Laboratory. Samples were prepared by drop casting approximately 1 mL of 0.1 mg/mL of acidified macrocycle solutions onto a silicon wafer. Patterns were collected with a photon energy of 12 keV at an incidence angle of 0.14° on a Pilatus 100k 2D detector. The detector frames were then merged and pixel coordinates transformed into q space. 2D patterns were then radially integrated from $\phi = 90^\circ - 180^\circ$ to yield an anisotropic 1D pattern. Background was subtracted using a polynomial fitting through the Biovia Materials Studio Reflex Module.

Macrocyclic and Nanotube Modeling and Structure Refinement. Initial nanotube structures were constructed in Materials Studio ver 4.2 (Accelrys Inc.) with a primitive unit cell with a P1 space group. The *a* cell parameter was estimated according to the distance between the center of the vertices for each macrocycle and *c* parameter was estimated as a typical π -stacking distance of 4 Å. Based on this analysis, it was determined that the nitrogen's of the pyridine pointed towards the inside of the macrocycle. The structures were optimized using the Geometry Optimization

routine including energy minimization with cell parameters optimization, using the parameters from the Universal Force Field. The final molecular structure in a P1 unit cell was prepared by using geometrical parameters from the optimized structure. Higher order symmetry was not possible due to random scrambling by the aliphatic sidechains in the structure. Diffraction simulation and Pawley refinement were carried out using the Reflex software package.

Nanotube models and their simulated patterns were Pawley refined to experimental patterns iteratively until the RWP value converges. The pseudo-Voigt profile function was used for whole profile fitting. The final discrepancy index values were calculated to be less than 5% in all cases. Simulated XRD patterns were calculated from the refined unit cell and compared with the experimentally observed patterns. Crystallite size was then estimated by the LeBail method which was Pawley refined to the experimental data.

Sonication. Sonication was performed with a Branson 3510 ultrasonic cleaner with a power output of 100 W and a frequency of 42 kHz.

Touch-Spun Fibers Preparation. In the touch-spinning of fibers from polymer samples,⁴ the polymer droplet ejects from the tip of a nozzle in close proximity to the bars attached to a rotating disk. As the disk rotates, the tip of the bar touches the droplet at the nozzle and a liquid bridge forms between the bar and the nozzle. As the disk continues to rotate, the liquid bridge stretches and solvent evaporates, therefore allowing the fiber to solidify. The continuous mechanical force applied from the bars on the rotating disk onto the fiber stretches the fiber and enhances the mechanical properties of the fiber. A collector is placed at the center of the disk in the form of a frame or any other chemical substrates. The touch-spun samples presented in this work were prepared at 1000 RPM. A solution of nanotubes, prepared with 0.5 wt% poly(ethylene oxide) (PEO) in 1,4-dioxane, was supplied to the rotating disk by an automated variable speed syringe pump (Razel Scientific Instruments, E99-e), through a Hamilton 1000 series gastight syringe (1 mL), at a flow rate of 5 μ L/min. All touch-spinning was carried out at room temperature. PEO nanofibers were touch-spun from an 0.5 wt/v% stock solution of PEO in 1,4-dioxane, which was prepared at 60 °C overnight. PCL nanofibers were touch-spun from an 8 wt/v% stock solution in chloroform, which was prepared at 60 °C overnight. PEU nanofibers were touch-spun from a 5 wt/v% stock solution in 1,1,1,3,3-hexafluoro-2-propanol (HFIP), which was prepared at 60 °C overnight.

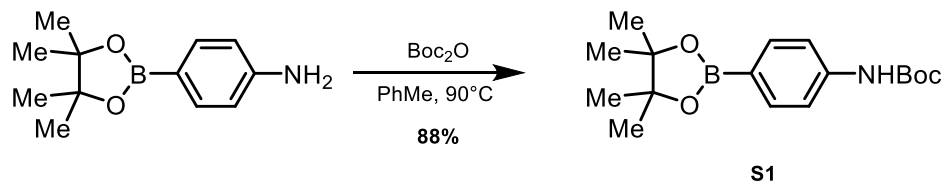
Touch-Spun Fibers Characterization. All fiber characterization was conducted at the University of Akron. Transmission electron microscopy (TEM) was carried out on a JEOL JSM-1230 microscope, and field emission scanning electron microscopy (SEM) was carried out on a JEOL-7401 microscope. These two techniques were used to assess the dimensions and alignment of the nanotubes on the prepared fibers. All samples were sputter-coated with gold for 15 seconds at a coating rate of 0.1 nm/s prior to imaging with the SEM. A Fiji software was used to measure the diameter of the fibers.⁵

Attenuated Total Reflection Fourier Transform Infrared (ATR-FTIR) spectroscopy spectra were obtained on a Shimadzu MIRACLE 10 spectrometer with 4 cm⁻¹ resolution.

Mechanical Testing of Touch-Spun Nanofibers. The mechanical properties of the fiber samples investigated using a NanoBionix tensile tester (MTS Systems Corp., Oak Ridge, TN, U.S.A.), with a load resolution of 50 nN and an extension resolution of 35 nm. Fibers were extended at a constant rate of 1% strain per second, until failure.⁶ The fiber samples were prepared for the mechanical tests by collecting them on rectangular frames (20 cm x 30 cm). Fiber samples were prepared in triplicate. All fibers were trimmed to rectangular sheets (3 mm x 30 mm), and clasped on each end by mechanical grips. Young's modulus was calculated by dividing the force on the sample by the effective cross-sectional area of the fiber bundle. The effective cross-sectional area, A , was determined using the equation: $A=W / (L \times PD)$, where W represents the weight of the fiber bundles, L represents the length of the fiber bundles, and PD represents the density of the polymer (PEO: 1.21 g·mL⁻¹; PCL: 1.14 g·mL⁻¹; and PEU: 1.05 g·mL⁻¹)

B. Synthetic Procedures

Scheme S1. Synthesis of **S1**.



Synthesis of **S1**:

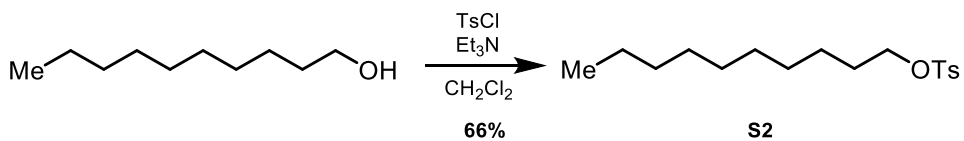
S1 was prepared using a slight modification of a reported procedure.⁷

4-(4,4,5,5-Tetramethyl-1,3,2-dioxaborolan-2-yl)-aniline (10.0 g, 45.6 mmol) and di-*tert*-butyldicarbonate (12.45 g, 54.1 mmol, 1.25 equiv.) were dissolved in toluene (365 mL) in a 1L round bottom flask equipped with a magnetic stir bar. The resulting solution was heated to 90°C for 18 h. under a constant flow of N₂. After cooling to room temperature, the resulting solution was washed with a saturated NaHCO₃ solution (3x50 mL), 2M HCl (3x50 mL), and brine (3x50 mL) before being dried over MgSO₄. The solvent was then removed *in vacuo* and the resulting solid was washed with hot hexanes (3x100 mL) to afford **S1** (12.78 g, 88%) as a light brown powder.

¹H NMR (500 MHz, CDCl₃) δ 7.76 (d, J=8.5 Hz, 2H), 7.38 (d, J=8.5 Hz, 2H), 1.54 (s, 9H), 1.36 (s, 12H). ¹³C NMR (126 MHz, CDCl₃) δ 152.35, 141.09, 135.86, 117.20, 83.64, 80.71, 28.34, 24.87.

ESI HRMS *m/z* calcd. For C₁₇H₂₆BNNaO₄ ([M+Na]⁺) 342.1850, found 342.1843.

Scheme S2. Synthesis of **S2**.



Synthesis of S2:

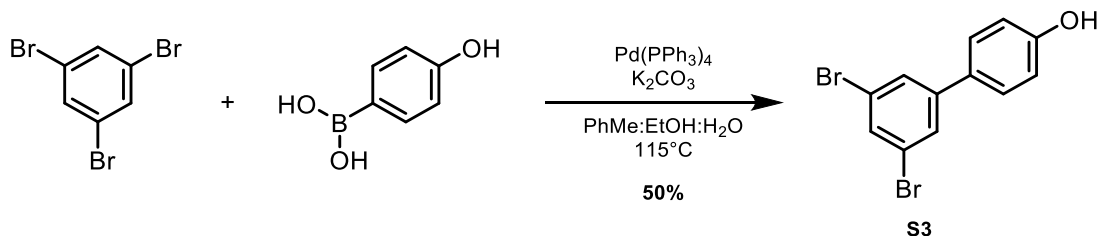
S2 was prepared using a slight modification of a reported procedure.⁸

Decanol (9.64 mL, 50.5 mmol) was dissolved in dry CH_2Cl_2 (50 mL) in a 250 mL round bottom flask equipped with a magnetic stir bar. Et_3N (8.81 mL, 63.2 mmol, 1.25 equiv.) was added to the stirring solution, followed by TsCl (12.05 g, 63.2 mmol, 1.25 equiv.). The reaction mixture was stirred at room temperature for 12 h. before being washed with 1M HCl (3x25 mL), followed by NaHCO_3 (3x25 mL). The organic layers were then isolated, combined, and dried over MgSO_4 . The solvent was removed *in vacuo*, and the resulting crude material was purified via column chromatography (SiO_2 , 1:9 CH_2Cl_2 /Hexanes) to afford **S2** (10.42 g, 66%) as a clear, colorless oil.

^1H NMR (500 MHz, CDCl_3) δ 7.74 (d, $J=8.3$ Hz, 2H), 7.30 (d, $J=8.3$ Hz, 2H), 3.97 (t, $J=6.6$ Hz, 3 H), 2.39 (s, 3H), 1.58 (m, 2H), 1.21 (br, 14H), 0.83 (t, $J=6.9$ Hz, 3H). ^{13}C NMR (126 MHz, CDCl_3) δ 144.62, 133.25, 129.79, 127.81, 70.67, 31.84, 9.42, 29.36, 23.23, 28.88, 28.78, 25.30, 22.63, 21.53, 14.06.

ESI HRMS *m/z* calcd. For $\text{C}_{17}\text{H}_{28}\text{NaO}_3\text{S}$ ($[\text{M}+\text{Na}]^+$) 335.1657, found 335.1646.

Scheme S3. Synthesis of **S3**.



Synthesis of S3:

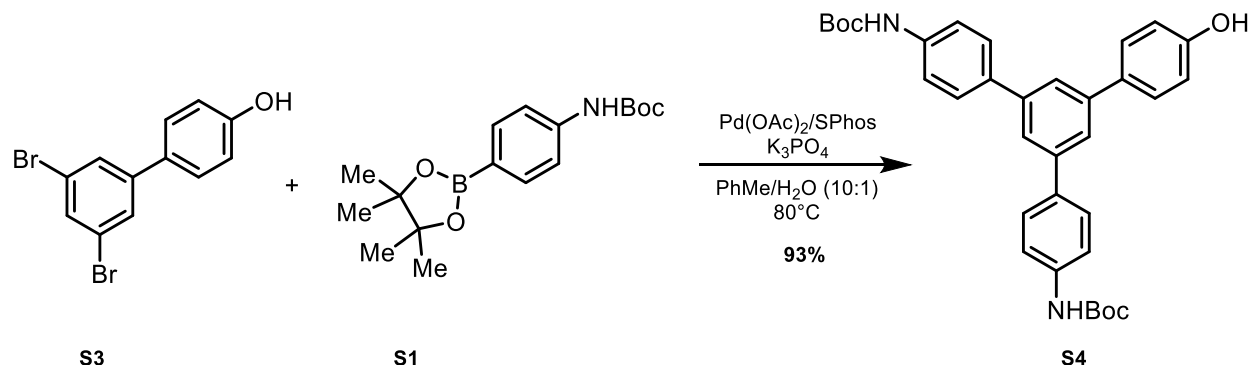
S3 was prepared using a slight modification of a reported procedure.⁹

4-hydroxyphenyl boronic acid (5.0 g, 36.3 mmol), 1,3,5-tribromobenzene (28.5 g, 90.6 mmol, 2.50 equiv.), and K₂CO₃ (10.0 g, 72.5 mmol, 2.00 equiv.) were loaded into a three neck round bottom flask equipped with a magnetic stir bar and a condenser. The flask was evacuated and backfilled with N₂ three times. After the final backfill, a PhMe:EtOH:H₂O solvent mixture (3:1:1, 240 mL) was added and the resulting solution was sparged with N₂ for 30 minutes. After the 30 minute sparge, Pd(PPh₃)₄ (1.67 g, 1.45 mmol, 0.04 equiv.) was quickly added and the solution was sparged with N₂ for an additional 30 minutes. The reaction mixture was then heated at 115°C for 24 h. After cooling to room temperature, the reaction mixture was diluted with CH₂Cl₂ (150 mL) and filtered through a bed of Celite®. The solvent was then removed *in vacuo*, and the resulting crude reaction mixture was purified via column chromatography (SiO₂, 100% Hexanes, then 100% CH₂Cl₂). Further purification was gained through recrystallization from cold CH₂Cl₂ to yield **S3** (6.12 g, 50%) as an off-white crystalline solid.

¹H NMR (500 MHz, CDCl₃) δ 7.52 (m, 3H), 7.34 (d, J=8.7 Hz, 2H), 6.83 (d, J=8.7 Hz, 2H), 4.77 (s, 1H). ¹³C NMR (126 MHz, CDCl₃) δ 155.96, 144.31, 131.99, 131.12, 128.51, 128.49, 129.23, 115.94.

ESI HRMS *m/z* calcd. For C₁₂H₇Br₂O ([M-H]⁻) 326.8849, found 326.8847.

Scheme S4. Synthesis of S4.



Synthesis of S4:

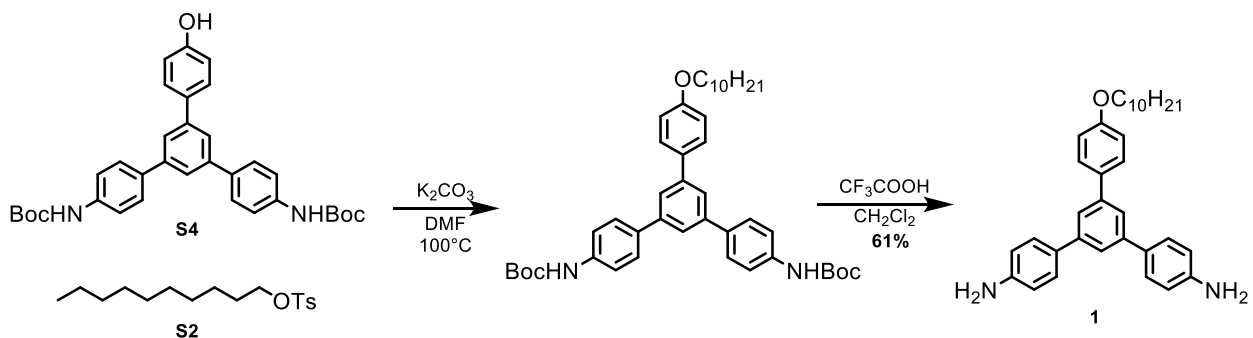
S4 was prepared using a slight modification of a reported procedure.¹⁰

S3 (2.75 g, 8.4 mmol), **S1** (6.69 g, 20.96 mmol, 2.50 equiv.), K₃PO₄ (7.12 g, 33.54 mmol, 4.00 equiv.), and SPhos (0.344 g, 0.84 mmol, 0.10 equiv.) were loaded into a 250 mL three neck round bottom flask equipped with a magnetic stir bar and a cold-water condenser. The flask was then evacuated and backfilled with N₂ three times. After the final backfill, a solvent duo of PhMe:H₂O (10:1, 85 mL) was added, and the resulting solution was sparged with N₂ for 30 minutes. Pd(OAc)₂ (0.094 g, 0.42 mmol, 0.050 equiv.) was then quickly added under a positive pressure of N₂, and the resulting solution was sparged for an additional 20 minutes. The solution was then heated to 80°C for 18 h. After cooling to room temperature, the solution was diluted with CH₂Cl₂ (100 mL) and filtered through a plug of Celite®. The solvent was then removed *in vacuo*, and the resulting crude material was purified via column chromatography (SiO₂, 1:2 EtOAc/Hex) to yield **S4** (4.63 g, 93%) as a slightly yellow fluffy powder.

¹H NMR (500 MHz, CDCl₃) δ 7.64 (m, 3H), 7.60 (d, J=8.7 Hz, 4H), 7.54 (d, J=8.7 Hz, 4H), 7.45 (d, J=8.7 Hz, 4H), 6.93 (d, J=8.7 Hz, 2H), 6.61 (s, 2H), 1.54 (s, 18H). ¹³C NMR (126 MHz, CDCl₃) δ 153.73, 152.84, 141.97, 141.64, 137.82, 136.01, 133.61, 128.55, 127.82, 124.08, 123.80, 118.94, 115.78, 80.76, 28.39.

ESI HRMS *m/z* calcd. For C₃₄H₃₆N₂NaO₅ ([M+Na]⁺) 575.2516, found 575.2582.

Scheme S5. Synthesis of **1**.



Synthesis of **1:**

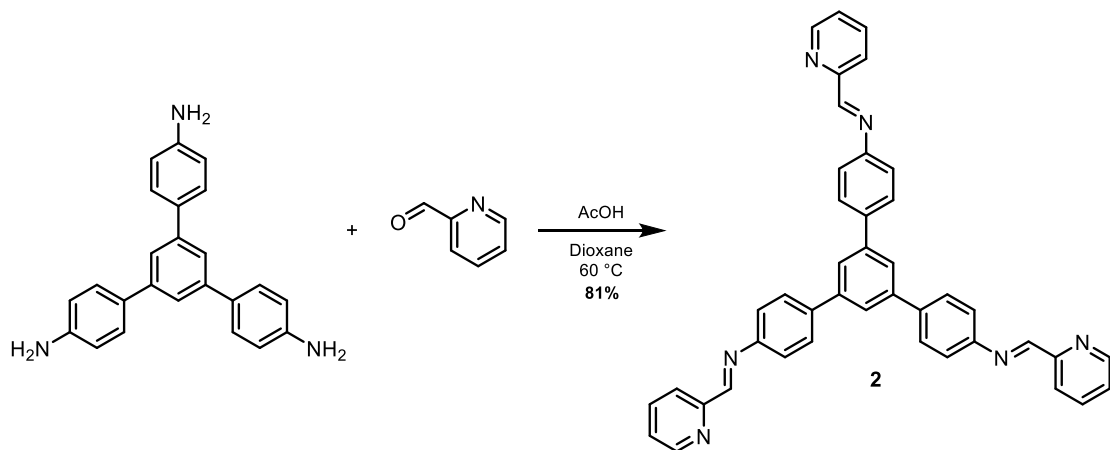
1 was prepared using a slight modification of a reported procedure.⁹

S4 (1.75 g, 3.17 mmol), **S2** (2.97g, 9.50 mmol, 3.00 equiv.), and K_2CO_3 (1.31 g, 9.50 mmol, 3.00 equiv.) were dissolved in dry DMF (13 mL) in a flame dried Schlenk flask equipped with a magnetic stir bar. The solution was sparged with N_2 for 10 minutes before being heated to 100°C for 6 h. The solution was then cooled to room temperature and poured into H_2O (10 mL) and extracted into CH_2Cl_2 (3x10 mL). The organic layers were then combined and dried over MgSO_4 . Solvent was then removed *in vacuo* and the resulting crude material was dissolved in CH_2Cl_2 (10 mL). The solution was acidified with $\text{CF}_3\text{CO}_2\text{H}$ (4 mL, 52 mmol, 15.0 equiv.), and the resulting solution was allowed to stir at room temperature for 1 h. The solution was poured into a saturated NaHCO_3 solution (200 mL) and extracted into CH_2Cl_2 (3x50 mL). The combined organic layers were then washed with 1M KOH (3x25 mL), and dried over MgSO_4 before being purified via column chromatography (SiO_2 , 1:1 Hexanes/EtOAc) to yield **1** (0.951 g, 61% overall) as a white powder.

^1H NMR (500 MHz, CDCl_3) δ 7.61 (m, 5H), 7.51 (d, $J=8.6$ Hz, 4H), 6.99 (d, $J=8.8$ Hz, 2H), 6.78 (d, $J=8.6$ Hz, 4H), 4.01 (t, $J=6.6$ Hz, 2H), 3.58 (br, 4H), 1.81 (m, 2H), 1.48 (m, 2H), 1.29 (br, 12H), 0.89, t, $J=6.8$ Hz, 3H). ^{13}C NMR (126 MHz, CDCl_3) δ 158.80, 145.94, 142.05, 141.73, 133.89, 131.8, 128.30, 128.22, 123.20, 115.40, 114.78, 68.15, 31.92, 29.61, 29.59, 29.44, 29.34, 26.09, 22.70, 14.14.

ESI HRMS *m/z* calcd. For $\text{C}_{34}\text{H}_{41}\text{N}_2\text{O} ([\text{M}+\text{H}]^+)$ 493.3213, found 493.3240.

Scheme S6. Synthesis of **2**.



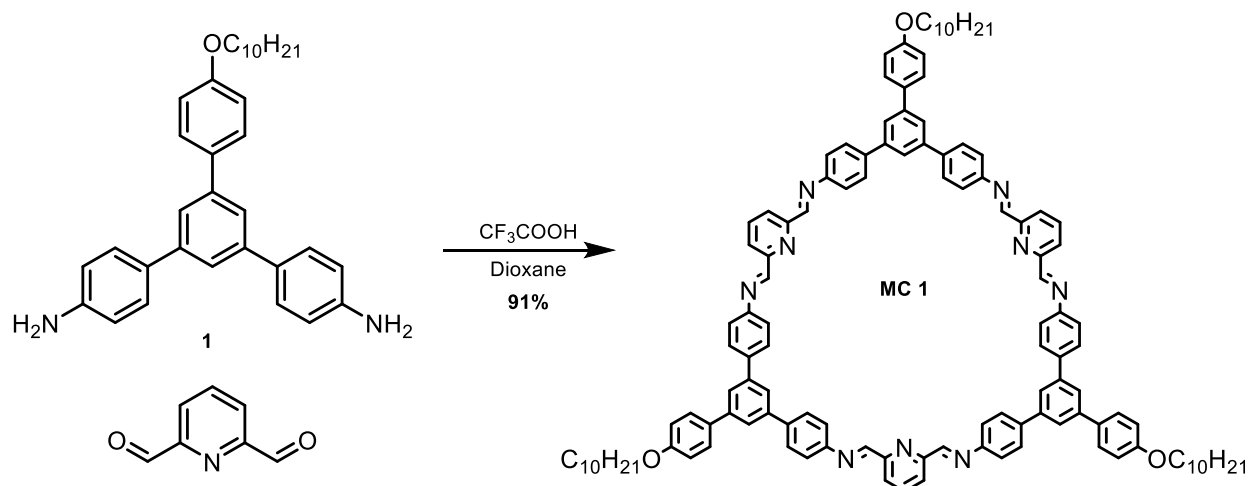
Synthesis of **2:**

1,3,5-Tris(4-aminophenyl)benzene (2.00 g, 5.69 mmol) was combined with 1,4-dioxane (40 mL) in a 250 mL round bottom flask equipped with a magnetic stir bar. 2-pyridinecarboxaldehyde (2.17 mL, 22.76 mmol, 4.0 equiv.) was then added to the slurry, followed by glacial AcOH (1.63 mL, 28.45 mmol, 5.0 equiv.). The resulting solution was stirred at 60°C for 16 h under a positive pressure of N₂. After cooling to room temperature, the solution was poured into a saturated NaHCO₃ solution (150 mL), extracted into CH₂Cl₂ (3x50 mL), and dried over MgSO₄. The solvent was removed *in vacuo* and the resulting crude material was triturated with EtOH to yield **2** (2.83 g, 81%) as an off-white powder.

¹H NMR (500 MHz, CDCl₃) δ 8.74 (d, J=4.34 Hz, 3H), 8.70 (s, 3H), 8.25 (d, J=7.9 Hz, 3H), 7.82 (m, 12H), 7.44 (m, 9H). ¹³C NMR (126 MHz, CDCl₃) δ 160.60, 154.62, 150.40, 149.80, 141.78, 139.54, 136.72, 128.20, 125.21, 124.85, 122.02.

ESI HRMS *m/z* calcd. For C₄₂H₃₁N₆ ([M+H]⁺) 619.2610, found 619.3481.

Scheme S7. Synthesis of MC 1.

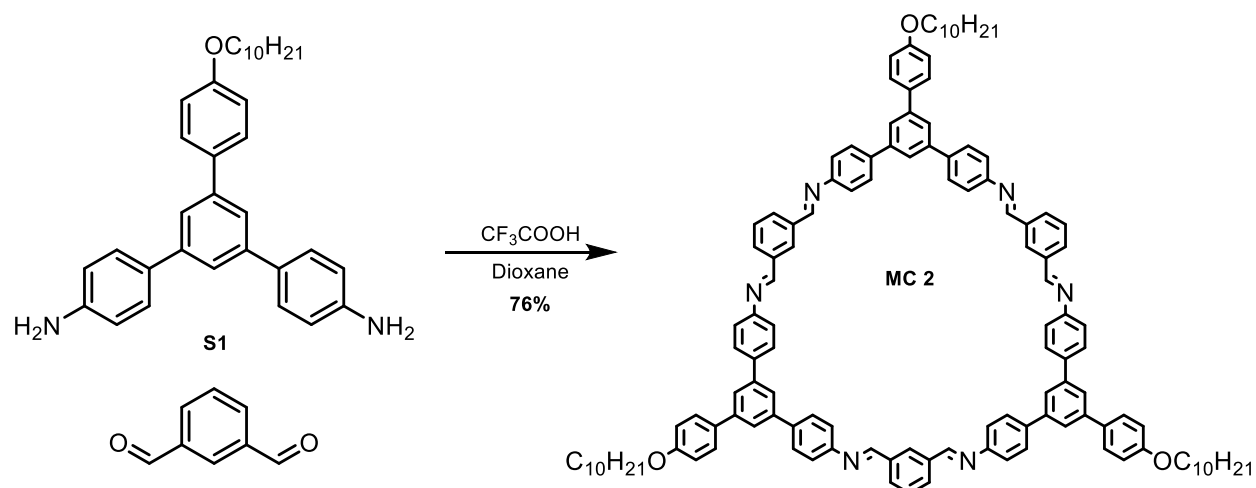


Synthesis of MC 1:

MC 1 was prepared using a slight modification of a reported procedure.⁹

1 (0.05 g, 0.101 mmol) and 2,6-pyridinedicarboxaldehyde (0.014 g, 0.101 mmol, 1.0 equiv.) were combined in 1,4-dioxane (4.00 mL) and sonicated until completely dissolved. 25 μL of a 2.0 M solution of $\text{CF}_3\text{CO}_2\text{H}$ in 1,4-dioxane (0.051 mmol, 0.5 equiv.) was then added. The solution immediately turned yellow and a precipitate began to form. The solution was then left undisturbed for 18 h. After 18 h., the reaction mixture was neutralized with Et_3N (3.0 mL) and poured into Et_2O (c.a. 10 mL). The precipitate was isolated by centrifugation and subsequently rinsed with additional Et_2O (3x10 mL). The resulting solid was dried under high vacuum at room temperature to yield **A** (0.055 g, 91%) as a light brown solid.

Scheme S8. Synthesis of MC 2.



Synthesis of MC 2:

MC 2 was prepared using a slight modification of a reported procedure.⁹

1 (0.05 g, 0.101 mmol) and isophthalaldehyde (0.014 g, 0.101 mmol, 1.0 equiv.) were combined in 1,4-dioxane (4.00 mL) and sonicated until completely dissolved. 25 μL of a 2.0 M solution of $\text{CF}_3\text{CO}_2\text{H}$ in 1,4-dioxane (0.051 mmol, 0.5 equiv.) was then added. The solution immediately turned yellow and a precipitate began to form. The solution was then left undisturbed for 18 h. After 18 h., the reaction mixture was neutralized with Et_3N (3.0 mL) and poured into Et_2O (c.a. 10 mL). The precipitate was isolated by centrifugation and subsequently rinsed with additional Et_2O (3x10 mL). The resulting solid was dried under high vacuum at room temperature to yield **B** (0.048 g, 80%) as a yellow solid.

C. Additional Macrocycle Characterization

I. Characterization of MC 1

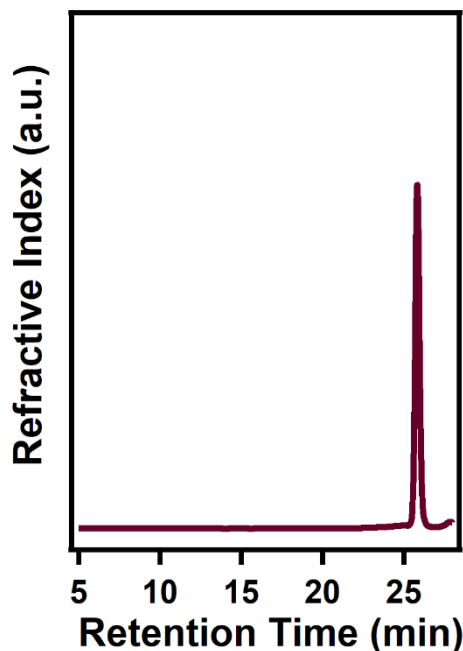


Figure S1. GPC trace of MC 1 in THF showing a single, narrow elution band.

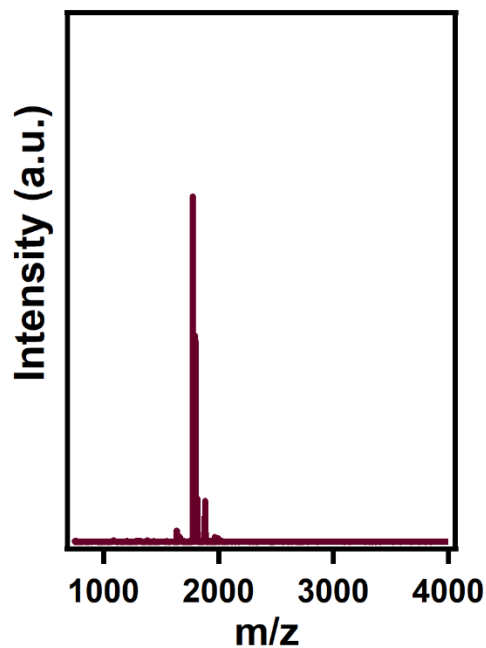


Figure S2. MALDI-MS spectra of MC 1 showing the desired $[M+H]^+$, $[M+Na]^+$, and $[M+K]^+$ adducts. ($m/z=1774.61$ $[M+H]^+$; $m/z= 1796.44$ $[M+Na]^+$; $m/z= 1813.92$ $[M+K]^+$).

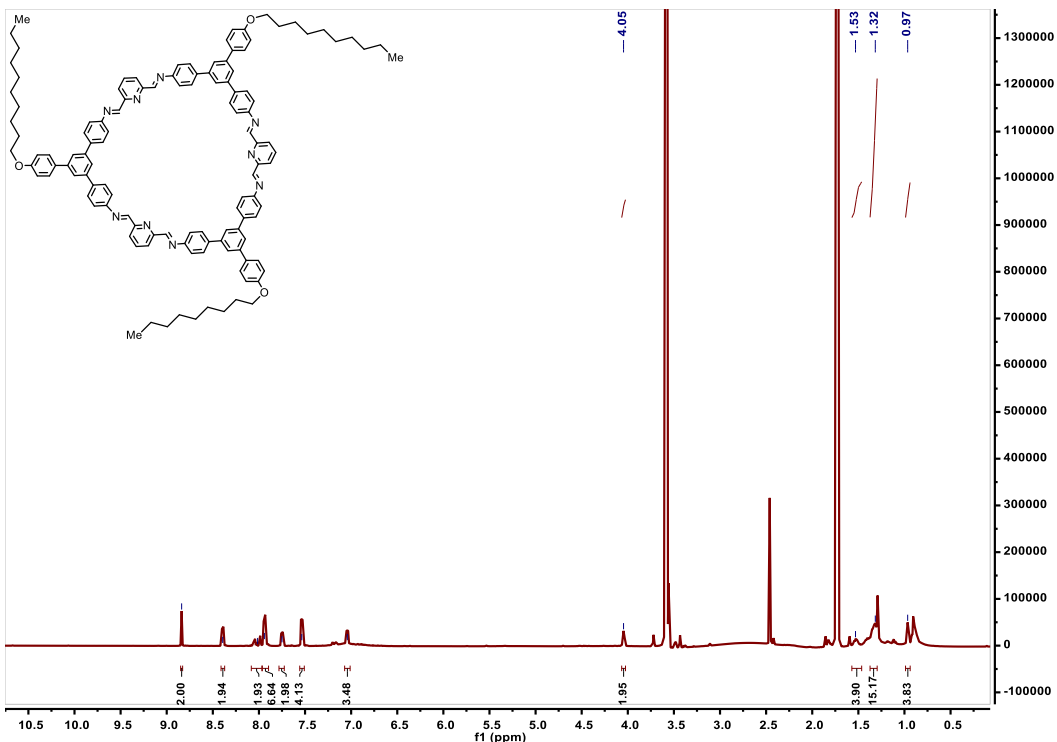


Figure S3. ^1H NMR ($\text{THF}-d_8$, 500 MHz, 298 K) of MC 1.

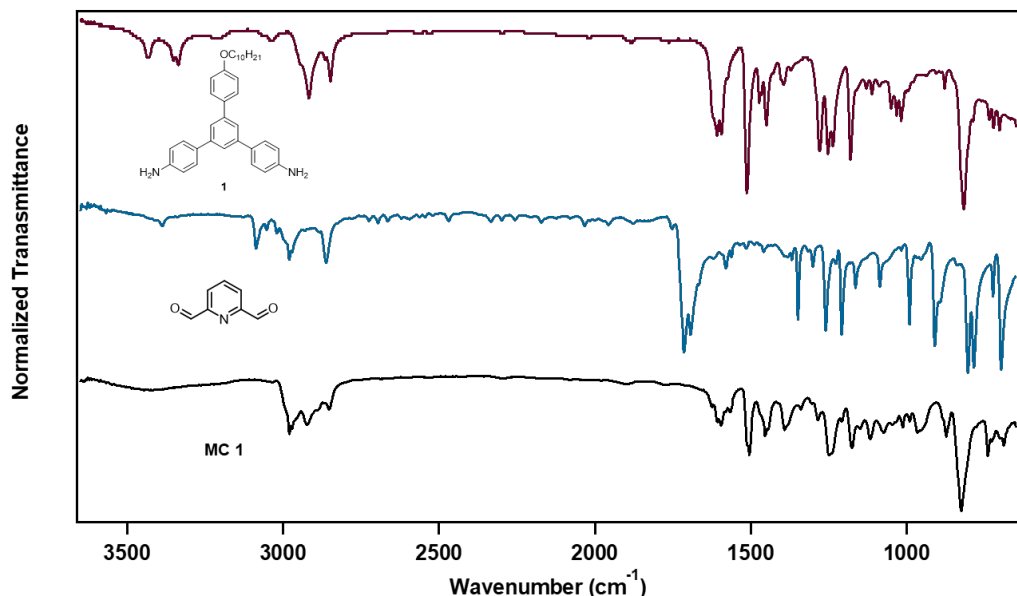


Figure S4. FT-IR spectra of 1, 2,6-pyridinedicarboxaldehyde, and MC 1.

II. Characterization of MC 2

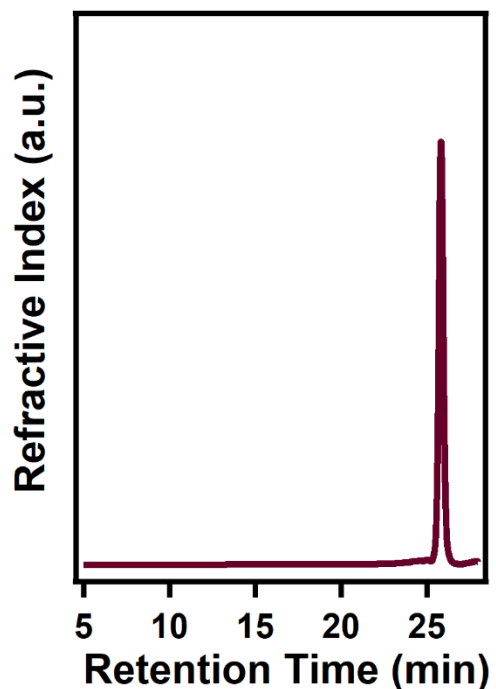


Figure S5. GPC trace of MC 2 in THF showing a single narrow elution band.

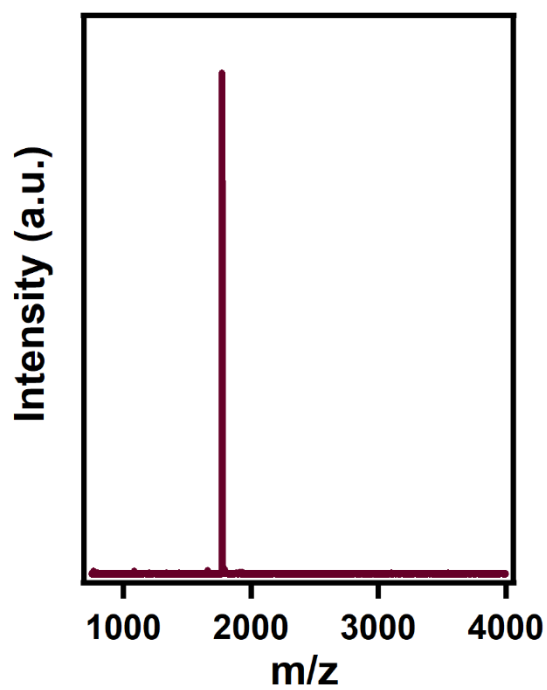


Figure S6. MALDI-MS of MC 2 showing the desired $[M + H]^+$ adduct. ($m/z = 1771.74$ $[M + H]^+$)

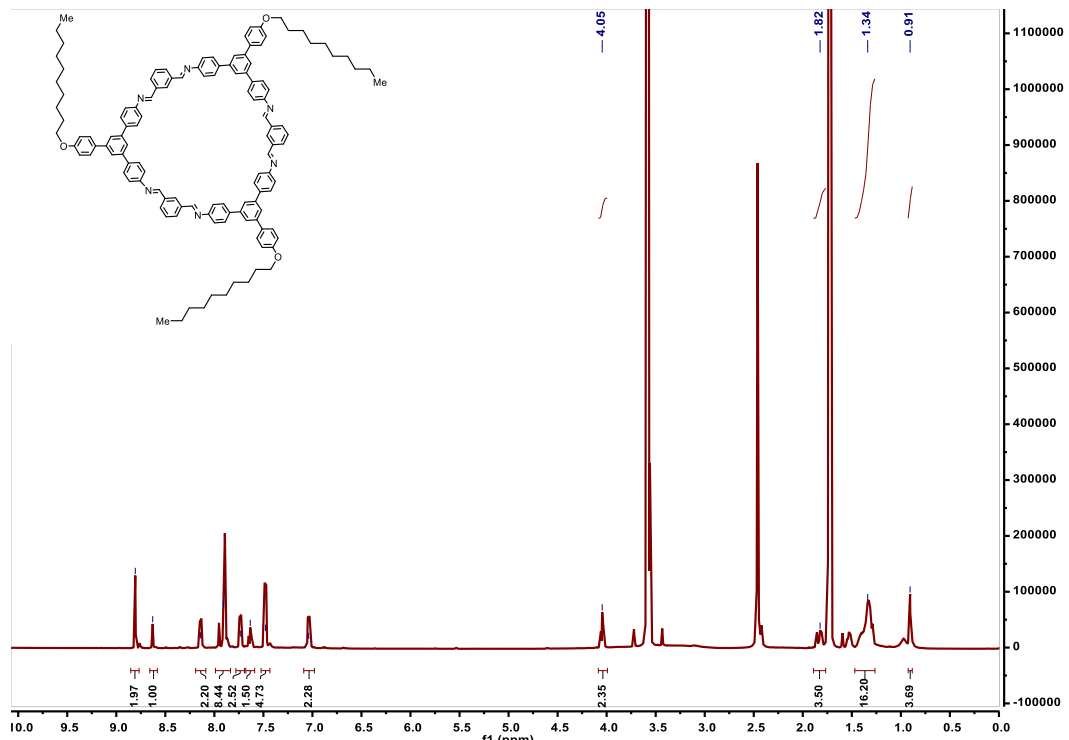


Figure S7. ^1H NMR ($\text{THF}-d_8$, 500 MHz, 298 K) of MC 2.

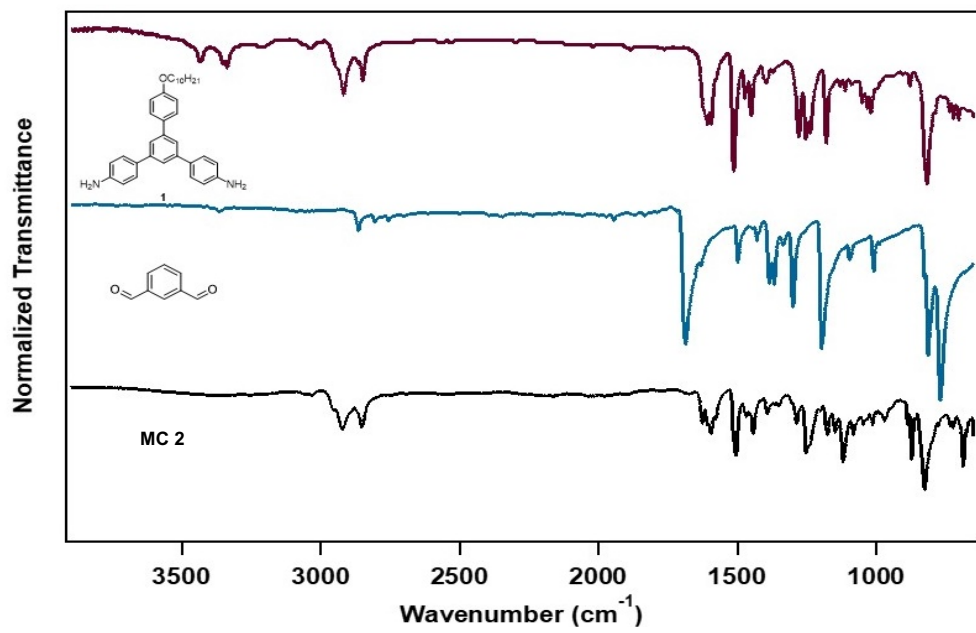


Figure S8. FT-IR spectra of **1**, isophthalaldehyde, and MC 2.

D. ^1H and ^{13}C NMR Spectra

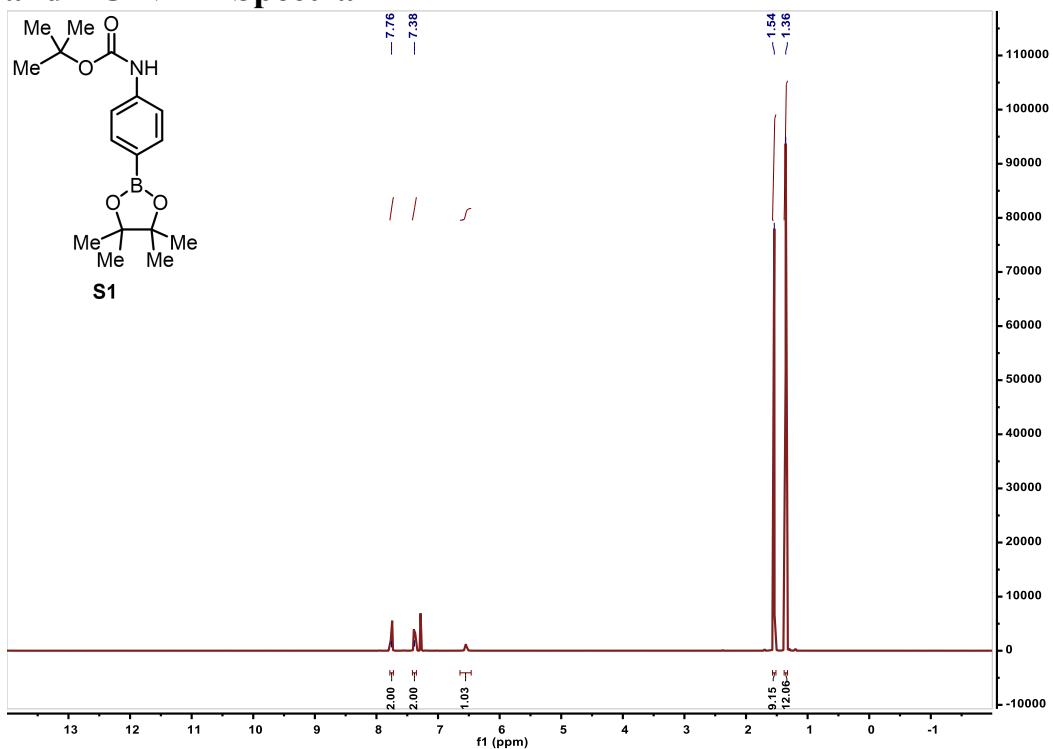


Figure S9. ^1H NMR (CDCl_3 , 500 MHz, 298 K) of S1.

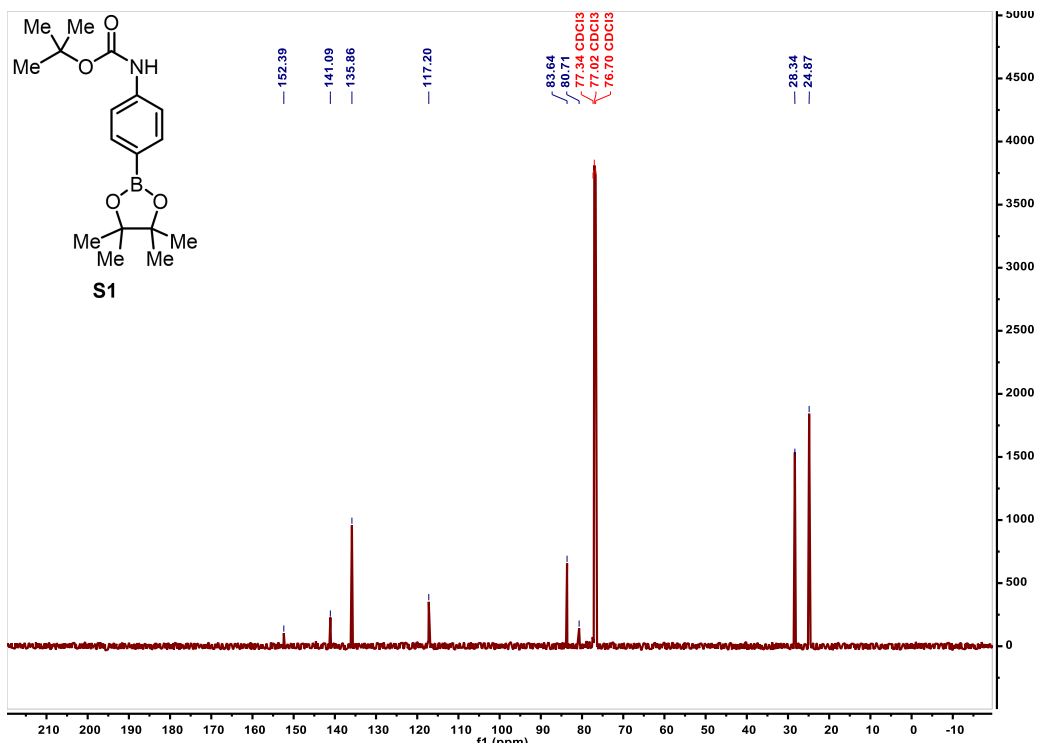


Figure S10. ^{13}C NMR (CDCl_3 , 126 MHz, 298 K) of S1.

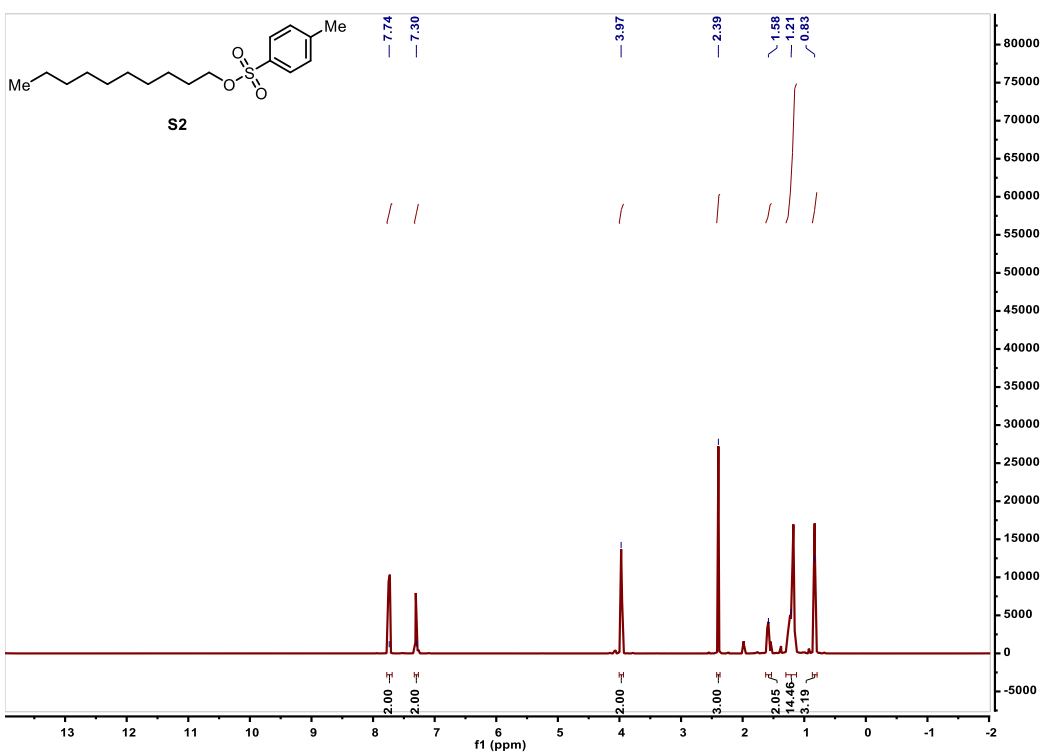


Figure S11. ¹H NMR (CDCl₃, 500 MHz, 298 K) of S2.

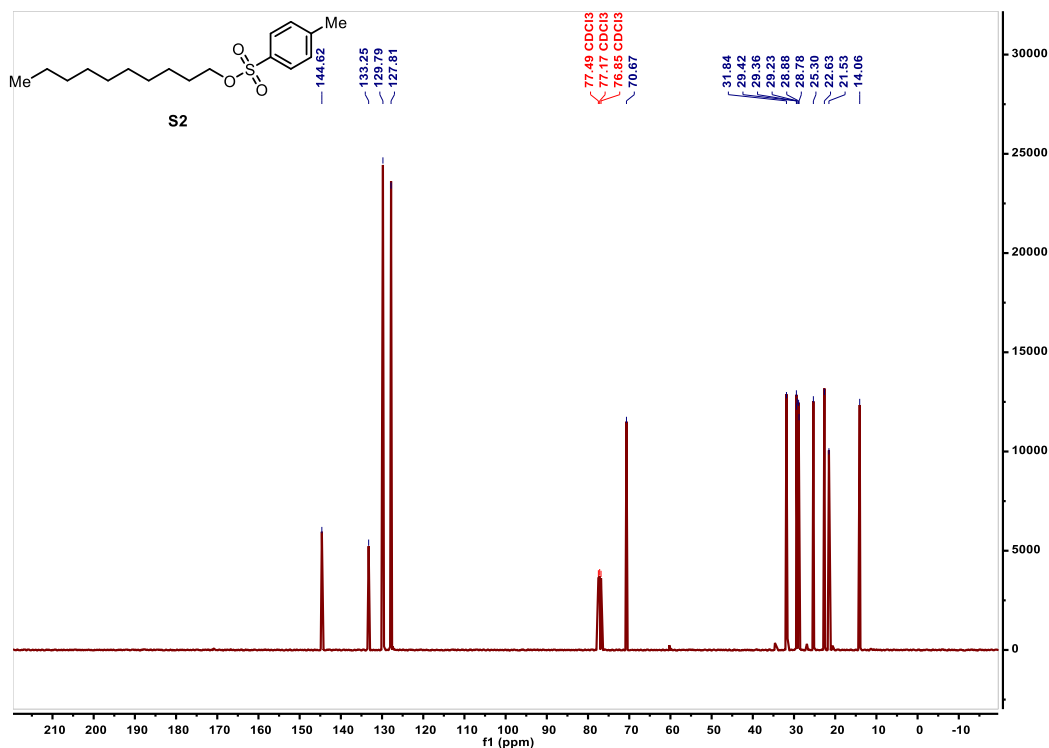


Figure S12. ¹³C NMR (CDCl₃, 126 MHz, 298 K) of S2.

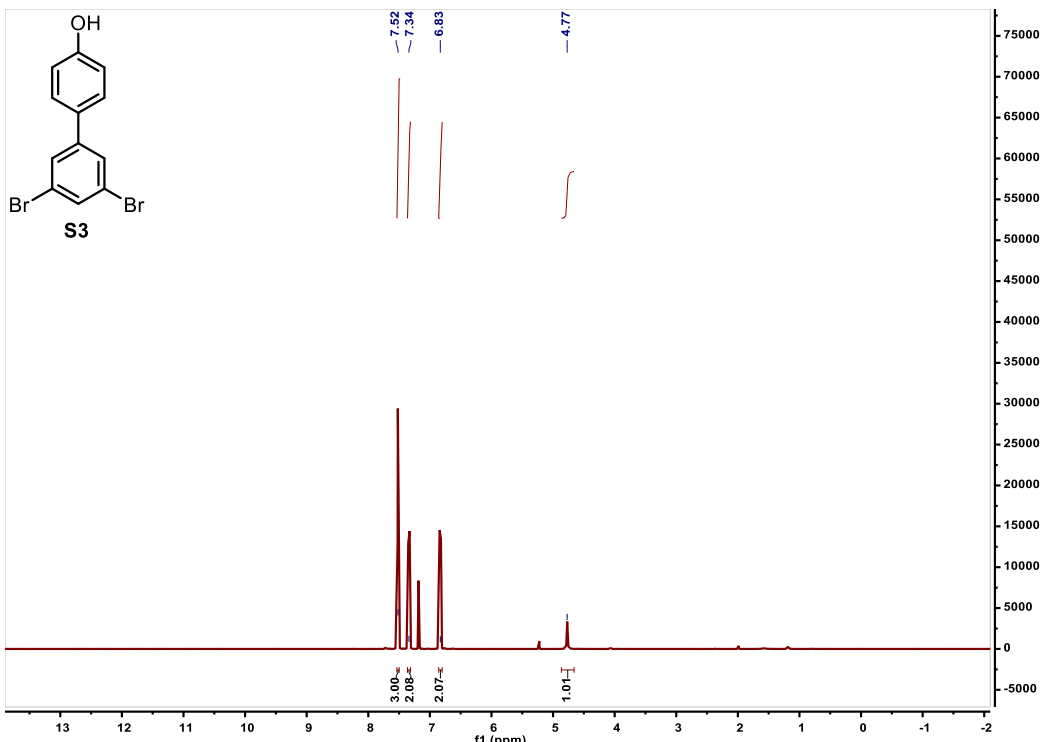


Figure S13. ¹H NMR (CDCl₃, 500 MHz, 298 K) of S3.

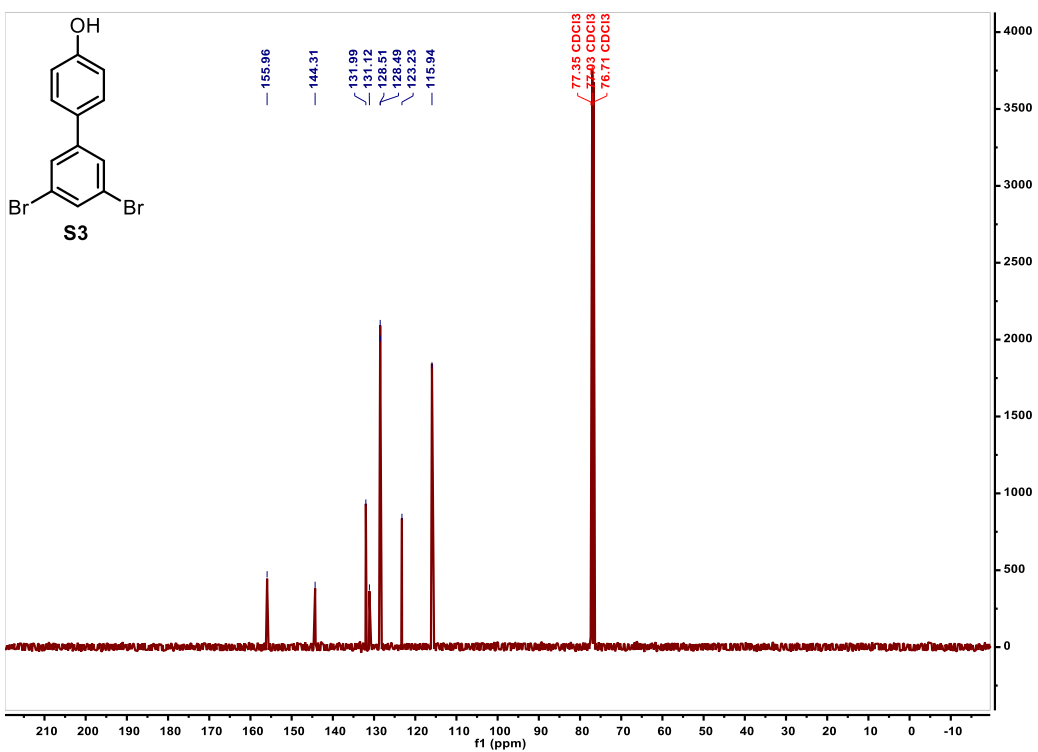


Figure S14. ¹³C NMR (CDCl₃, 126 MHz, 298 K) of S3.

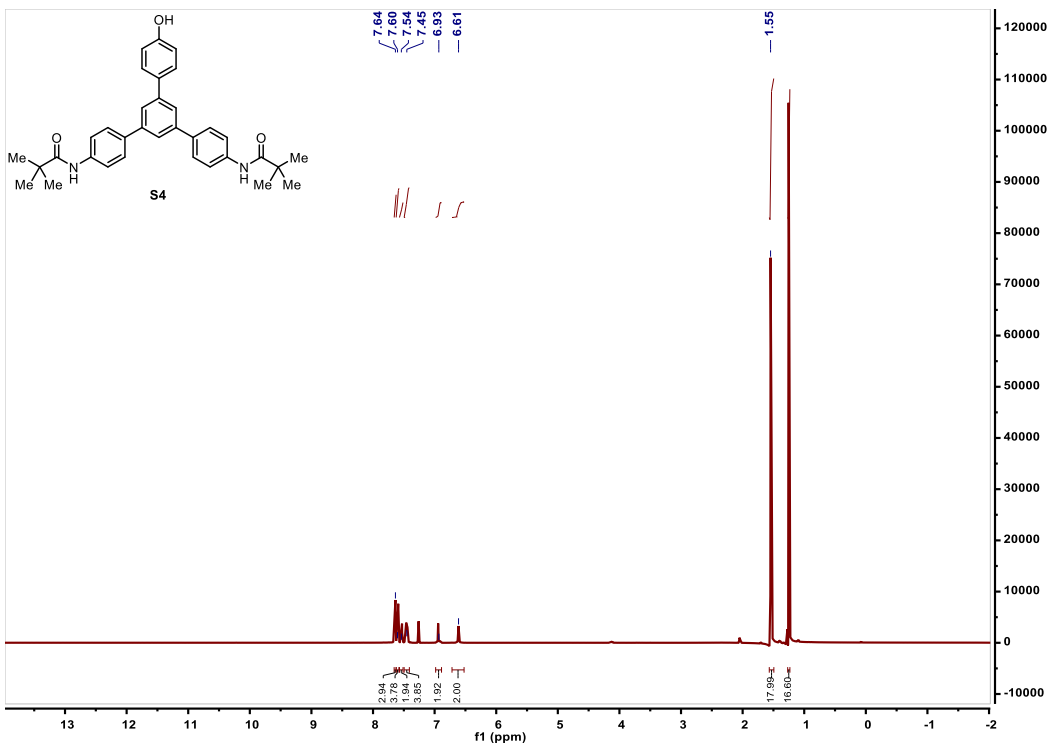


Figure S15. ^1H NMR (CDCl_3 , 500 MHz, 298 K) of S4. Note: Singlet at 1.25 assigned to pinacol impurity and was not removed before subsequent synthetic steps.

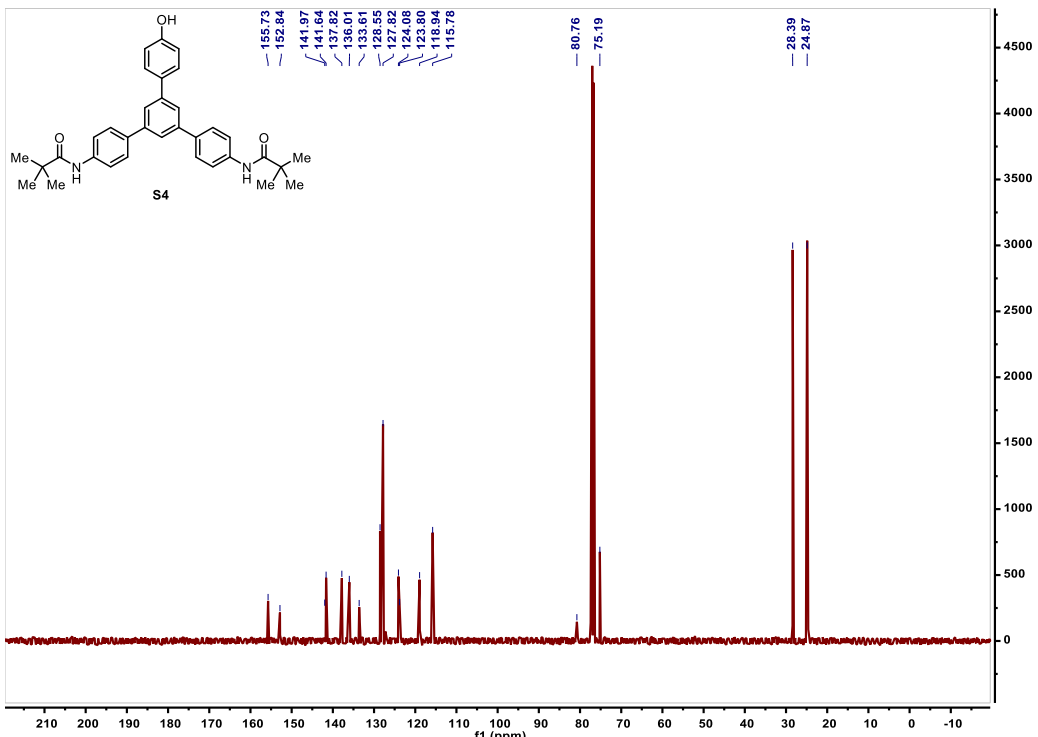


Figure S16. ^{13}C NMR (CDCl_3 , 126 MHz, 298 K) of S4. Note: Peaks at 75.19 and 24.87 assigned to pinacol impurity and was not removed before subsequent synthetic steps.

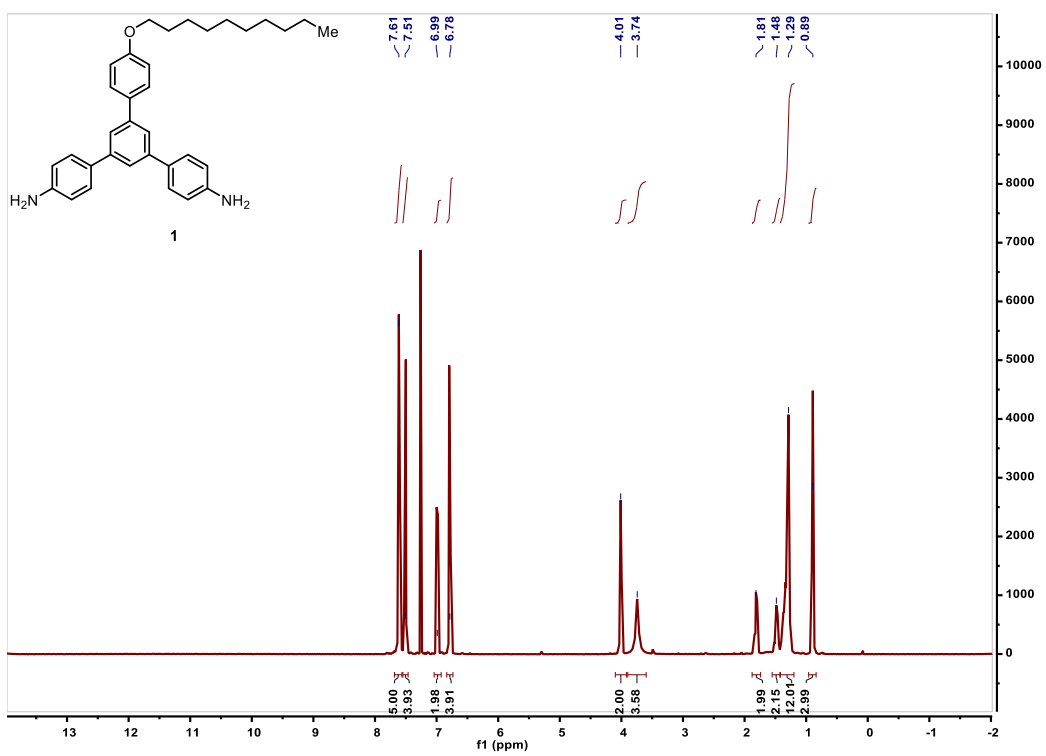


Figure S17. ^1H NMR (CDCl_3 , 500 MHz, 298 K) of 1.

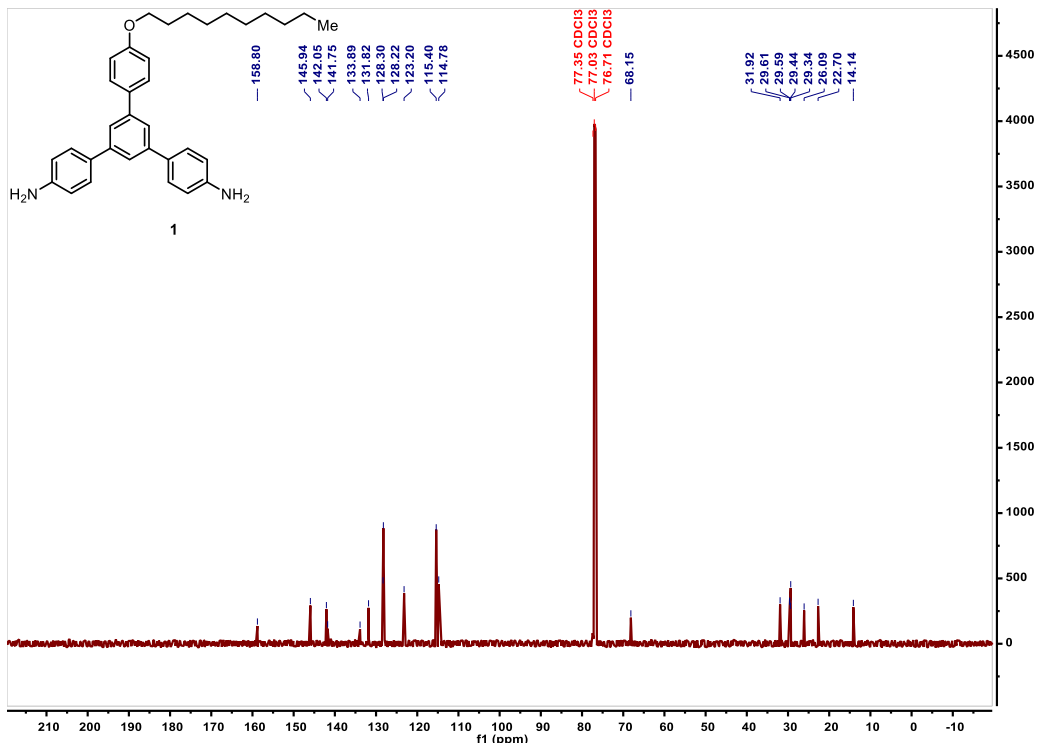


Figure S18. ^{13}C NMR (CDCl_3 , 126 MHz, 298 K) of **1**.

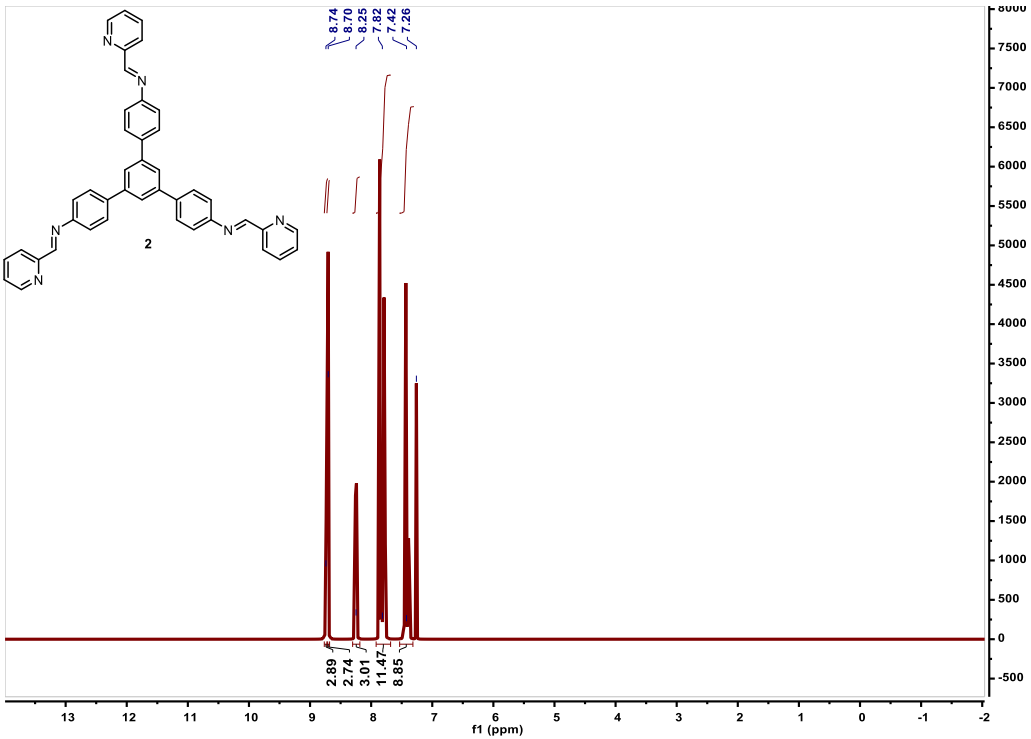


Figure S19. ^1H NMR (CDCl_3 , 500 MHz, 298 K) of **2**.

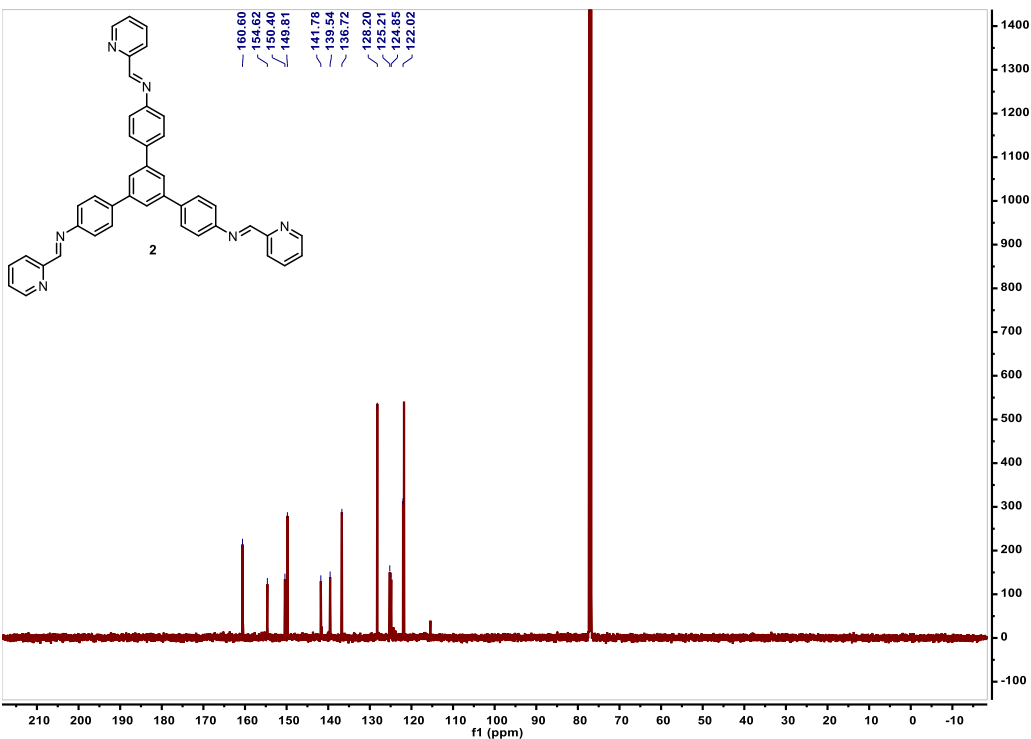


Figure S20. ^{13}C NMR (CDCl_3 , 126 MHz, 298 K) of **2**.

E. Nanotube Characterization

I. Atomic Force Microscopy

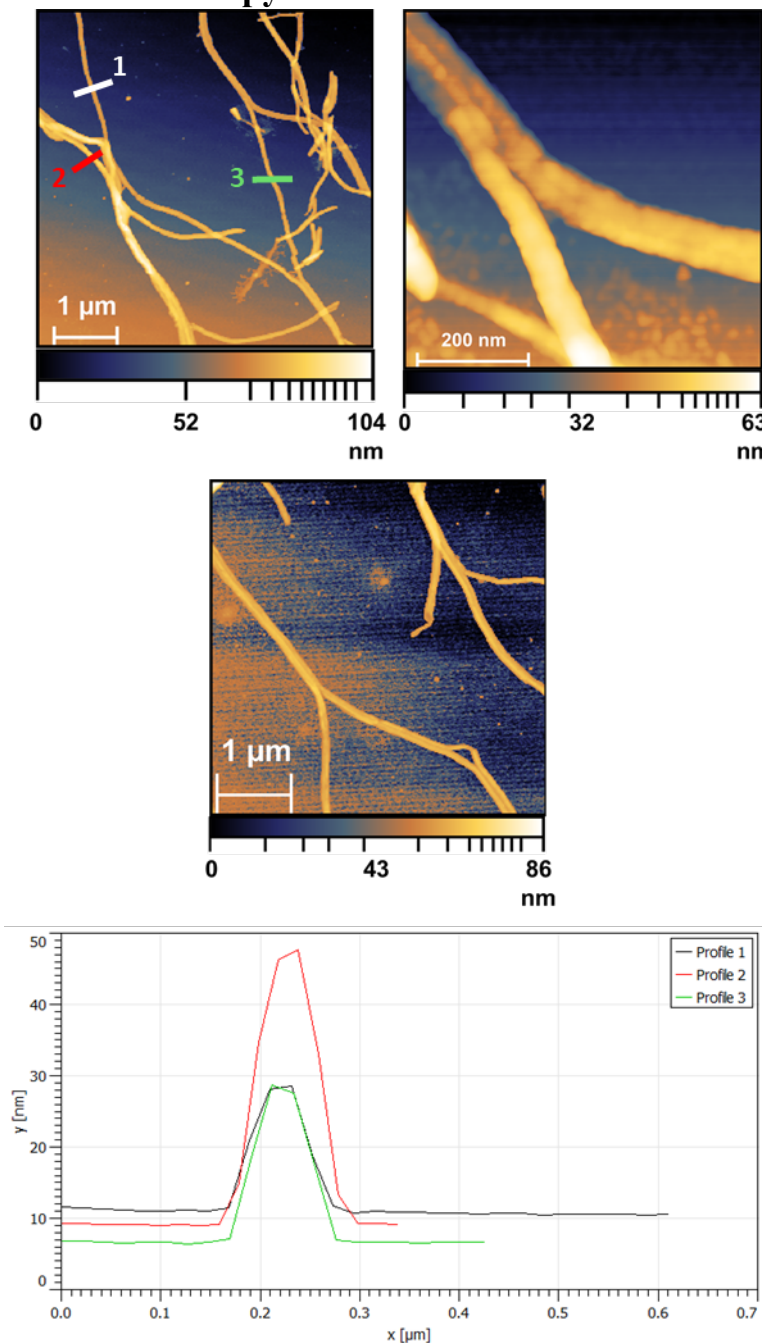


Figure S21. Atomic force microscopy images of a drop cast solution of MC 2 in THF with 0.3 mM tetrabutylammonium perchlorate, which was acidified with 2000 equivalents of $\text{CF}_3\text{CO}_2\text{H}$, onto silicon with a layer of native oxide. Additionally, height profiles (1-3) were extracted from the images to highlight the degree of bundling observed.

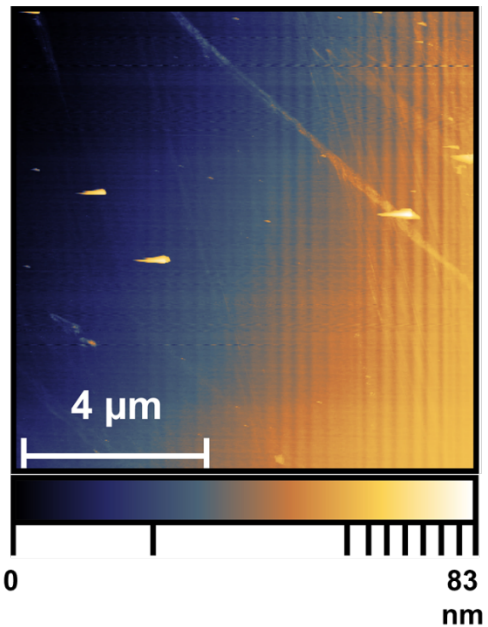


Figure S22. Atomic force microscopy image representing a drop cast solution of MC 2 in THF with 0.3 mM tetrabutylammonium perchlorate, which was acidified with 6.0 equivalents of $\text{CF}_3\text{CO}_2\text{H}$, onto silicon with a layer of native oxide. The lack of nanotube formation corroborates the finding of MALDI-MS experiments which show the hydrolysis of macrocycles at low acid loadings.

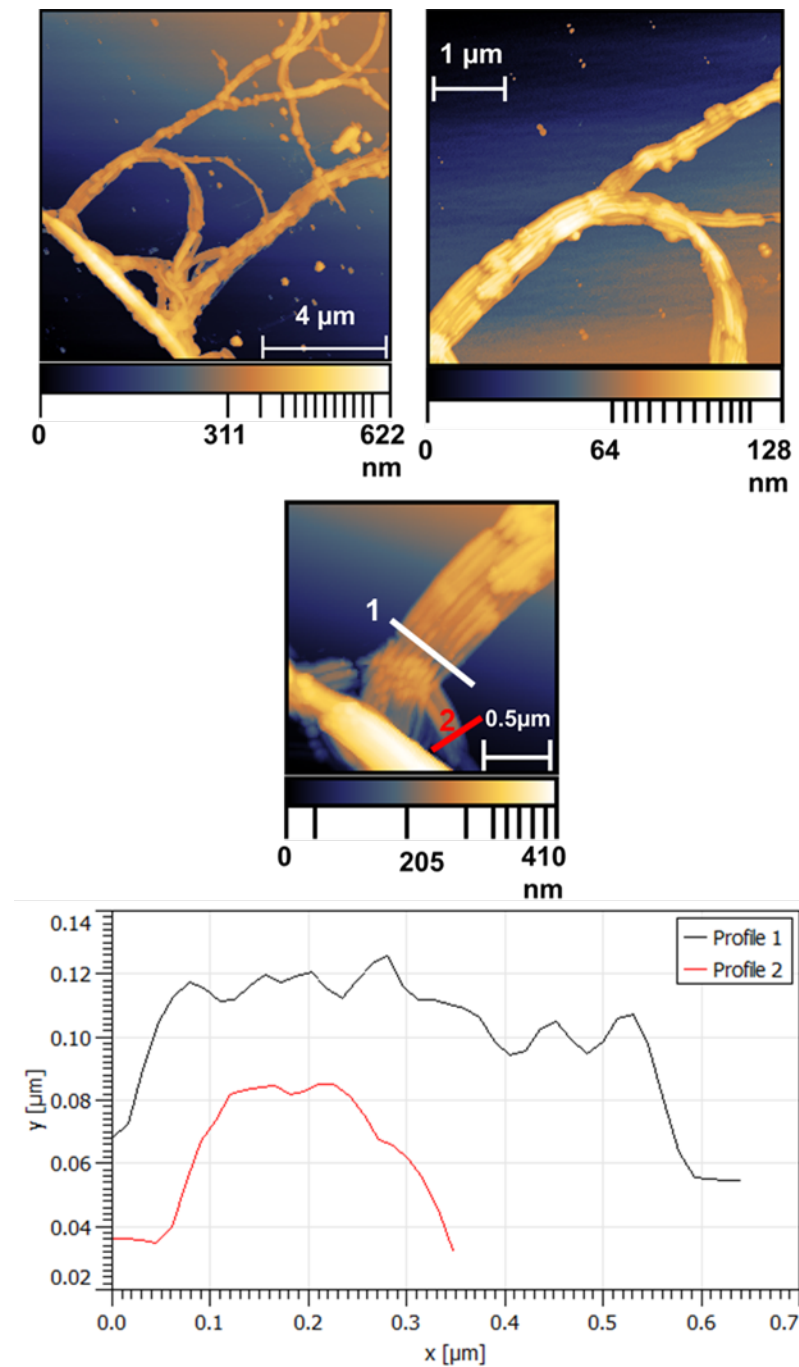


Figure S23. Atomic force microscopy images of a drop cast solution of MC 1 in THF with 0.3 mM tetrabutylammonium perchlorate, which was acidified with 2000 equivalents of $\text{CF}_3\text{CO}_2\text{H}$, onto silicon with a layer of native oxide. Additionally, height profiles (1-2) were extracted from the images to highlight the degree of bundling observed.

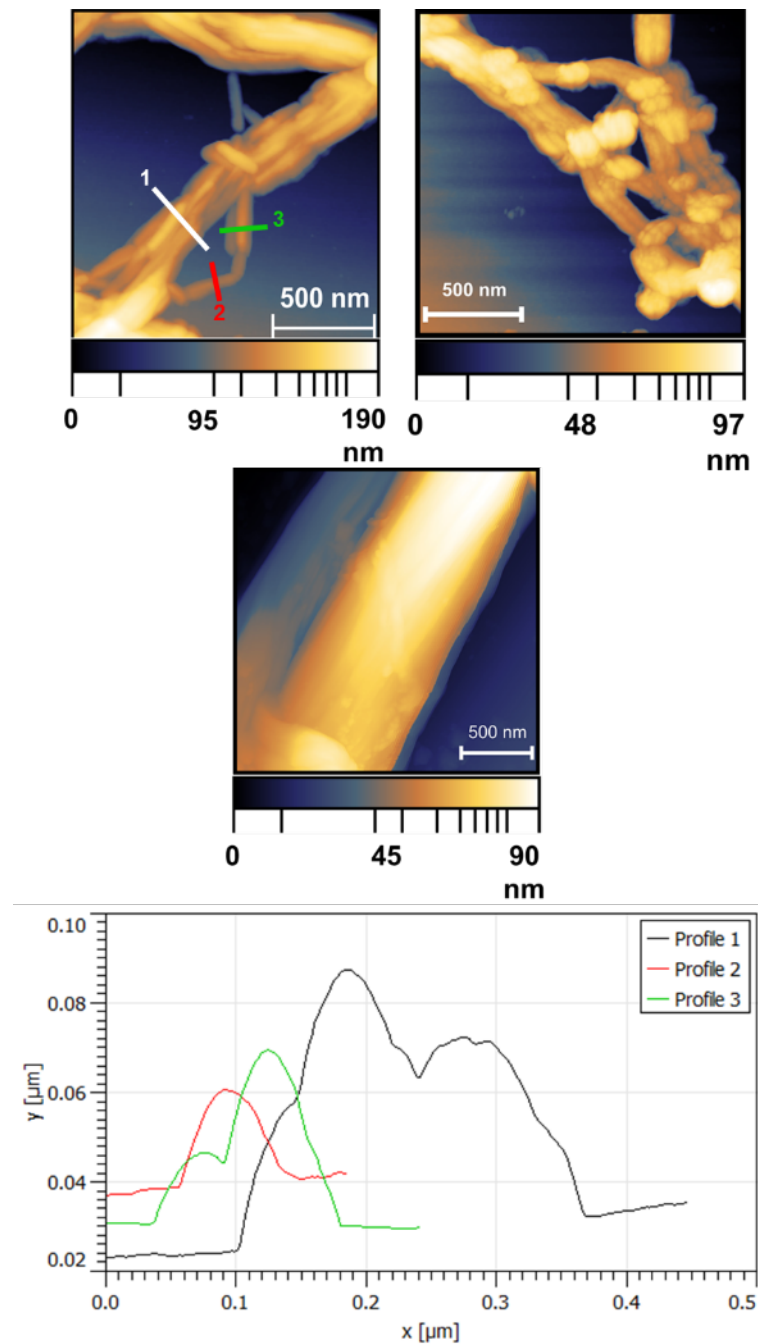


Figure S24. Atomic force microscopy images of a drop cast solution of MC 1 in THF with 0.3 mM tetrabutylammonium perchlorate, which was acidified with 3.0 equivalents of $\text{CF}_3\text{CO}_2\text{H}$, onto silicon with a layer of native oxide. Additionally, height profiles (**1-3**) were extracted from the images to highlight the degree of bundling observed.

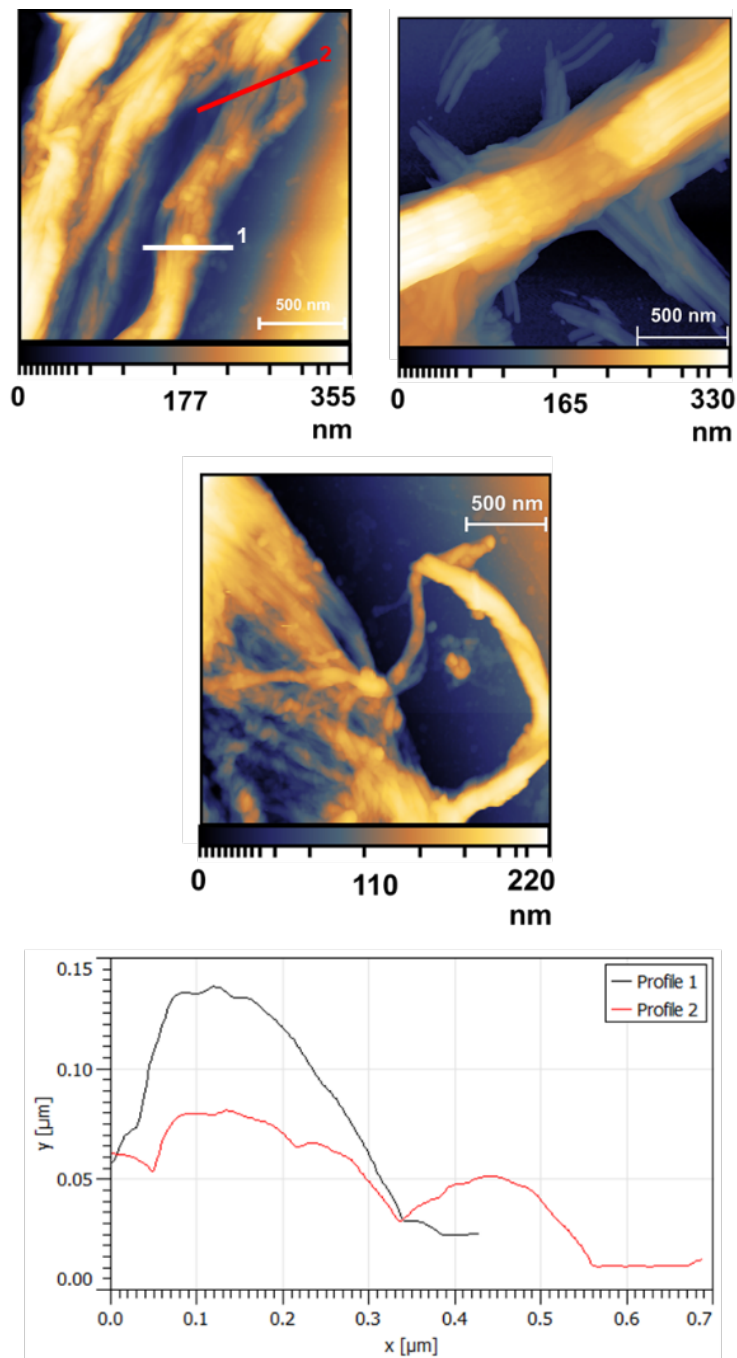


Figure S25. Atomic force microscopy images of a drop cast solution of MC 1 in THF with 0.3 mM tetrabutylammonium perchlorate, which was acidified with 2.0 equivalents of $\text{CF}_3\text{CO}_2\text{H}$ onto silicon with a layer of native oxide. Additionally, height profiles (1-2) were extracted from the images to highlight the degree of bundling observed.

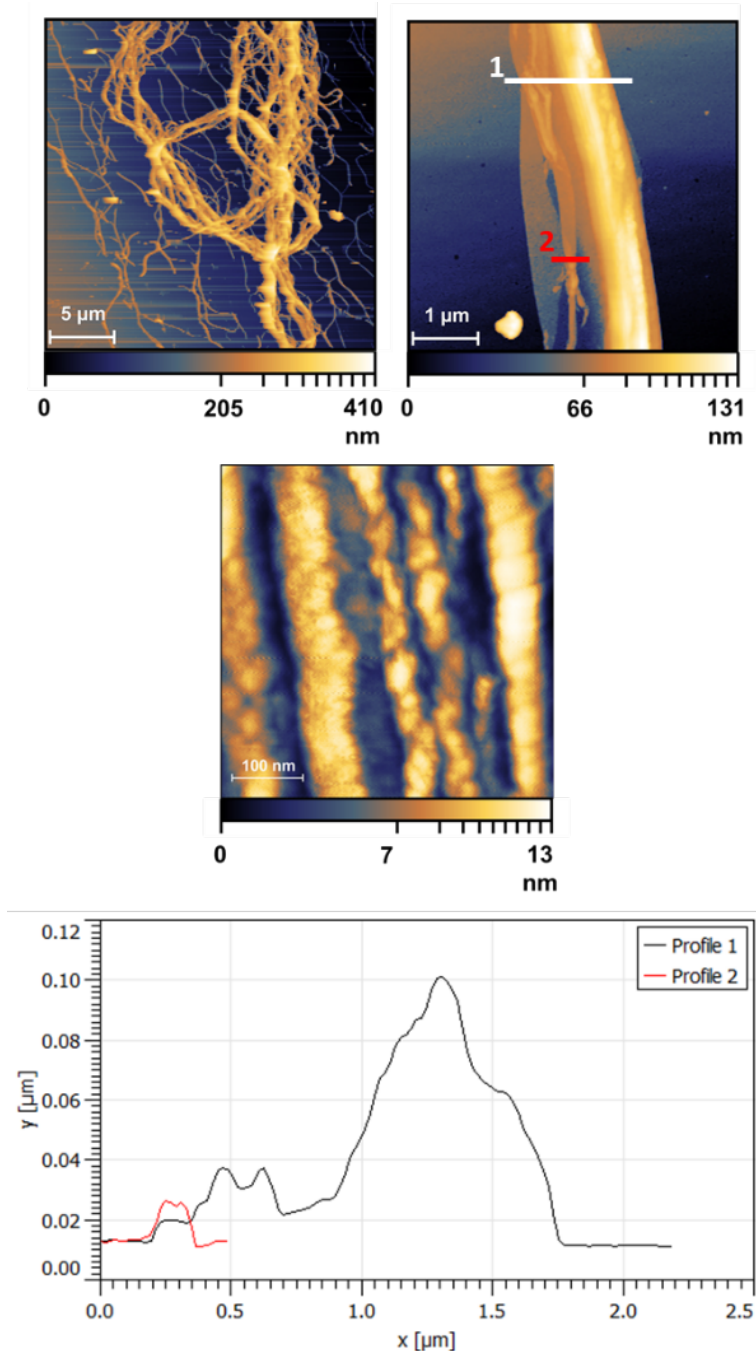


Figure S26. Atomic force microscopy images of a drop cast solution of MC 1 in THF with 0.3 mM tetrabutylammonium perchlorate, which was acidified with 1.0 equivalents of $\text{CF}_3\text{CO}_2\text{H}$, onto silicon with a layer of native oxide. Additionally, height profiles (1-2) were extracted from the images to highlight the degree of bundling observed.

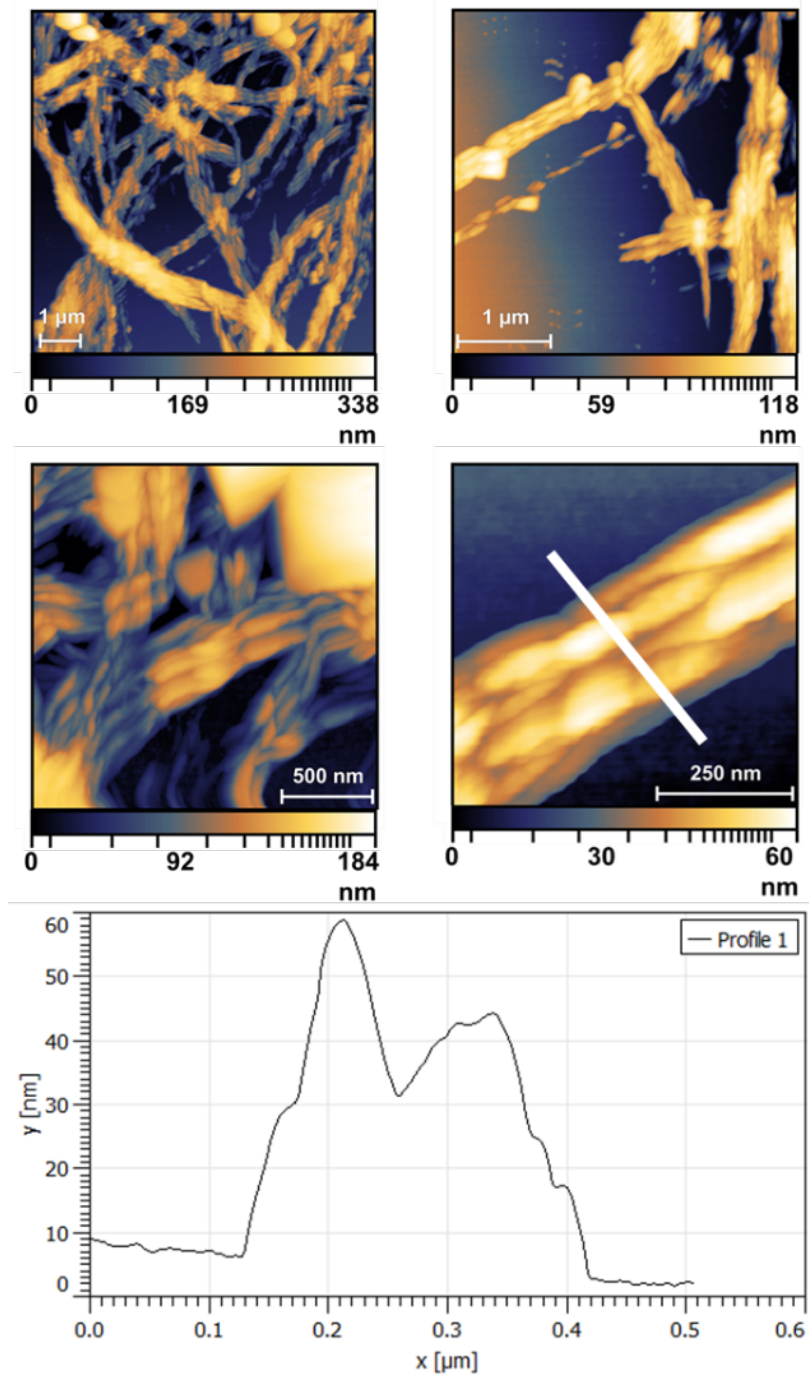


Figure S27. Atomic force microscopy images of a drop cast solution of MC 1 in THF with 0.3 mM tetrabutylammonium perchlorate, which was acidified with 0.4 equivalents of $\text{CF}_3\text{CO}_2\text{H}$, onto silicon with a layer of native oxide. Additionally, a height profile was extracted from the images to highlight the degree of bundling observed.

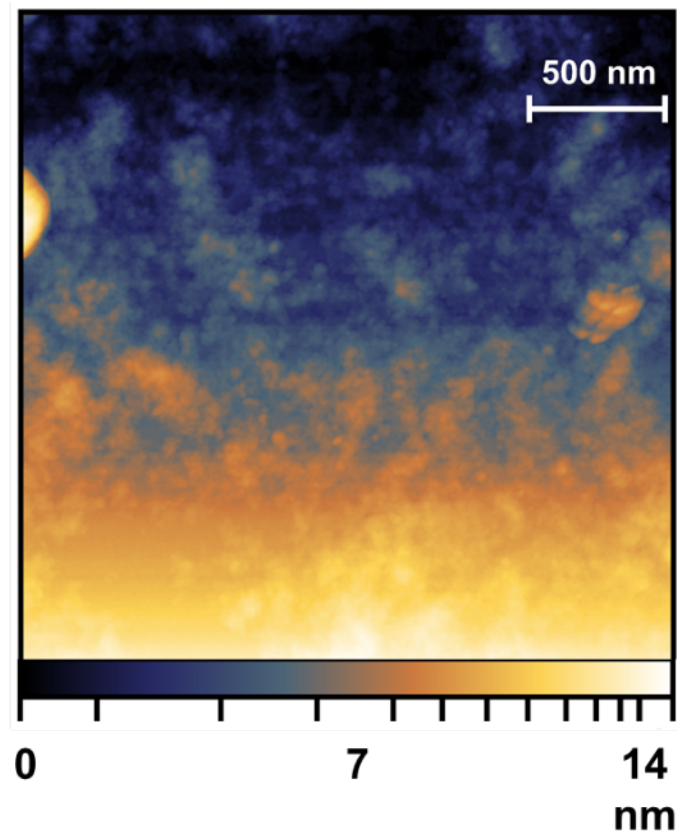


Figure S28. Atomic force microscopy image representing a drop cast solution of MC 1 in THF with 0.3 mM tetrabutylammonium perchlorate, which was not acidified. The image shows no presence of superstructure

II. Scanning Electron Microscopy (SEM)

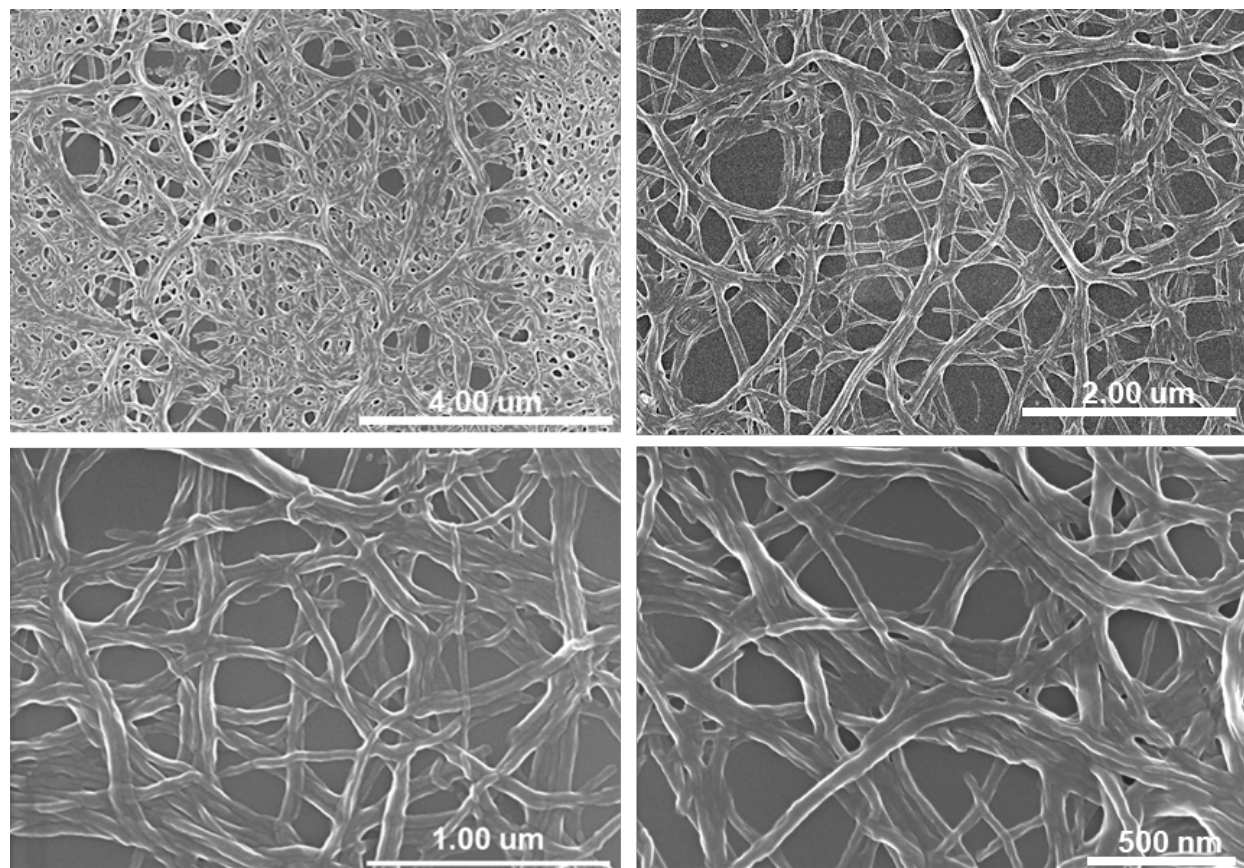


Figure S29. Scanning electron microscopy images of a drop cast solution of MC 2 in THF with 0.3 mM tetrabutylammonium perchlorate, which was acidified with 2000 equivalents of $\text{CF}_3\text{CO}_2\text{H}$, onto silicon with a layer of native oxide.

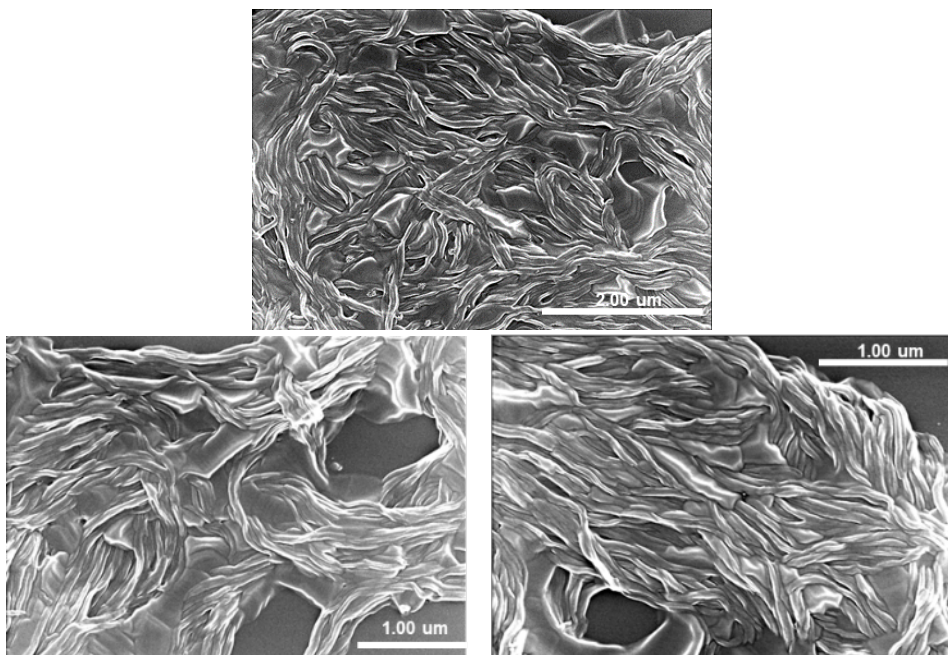


Figure S30. Scanning electron microscopy images of a drop cast solution of MC 1 in THF with 0.3 mM tetrabutylammonium perchlorate, which was acidified with 2000 equivalents of $\text{CF}_3\text{CO}_2\text{H}$, onto silicon with a layer of native oxide.

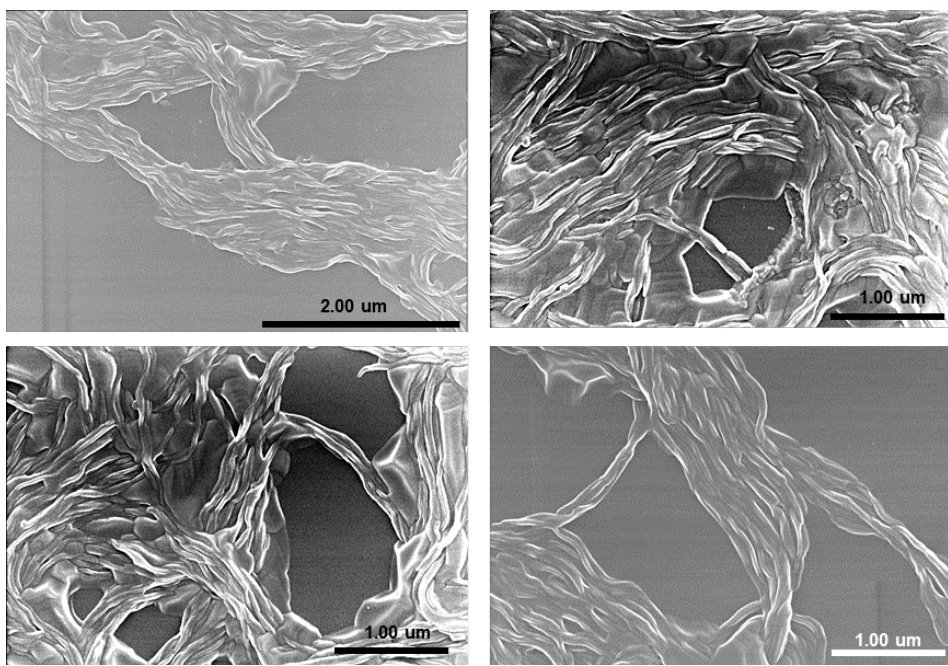


Figure S31. Scanning electron microscopy images of a drop cast solution of MC 1 in THF with 0.3 mM tetrabutylammonium perchlorate, which was acidified with 3.0 equivalents of $\text{CF}_3\text{CO}_2\text{H}$, onto silicon with a layer of native oxide.

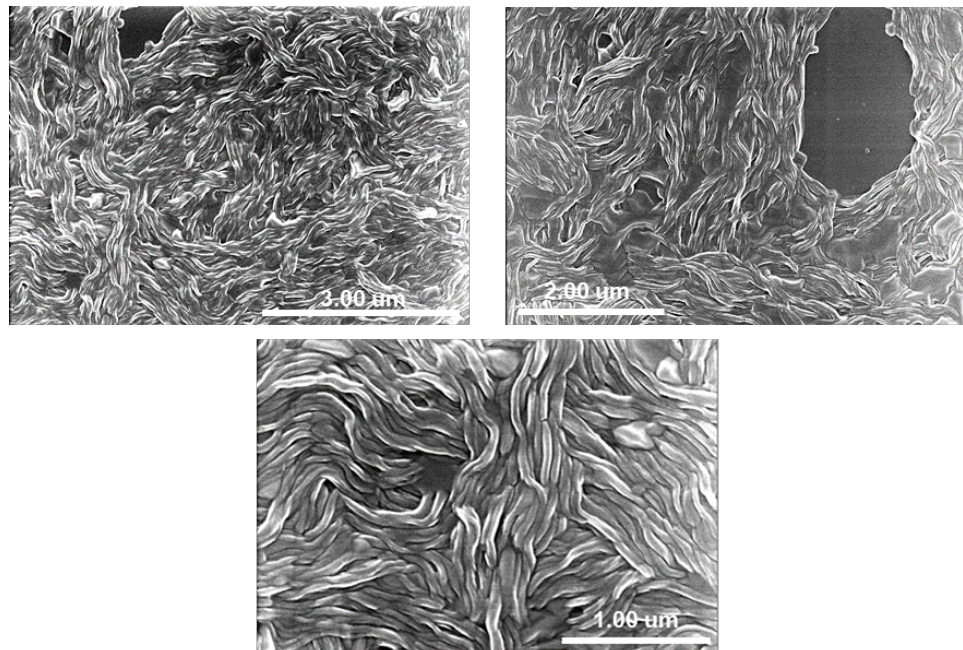


Figure S32. Scanning electron microscopy images of a drop cast solution of MC 1 in THF with 0.3 mM tetrabutylammonium perchlorate, which was acidified with 2.0 equivalents of $\text{CF}_3\text{CO}_2\text{H}$, onto silicon with a layer of native oxide.

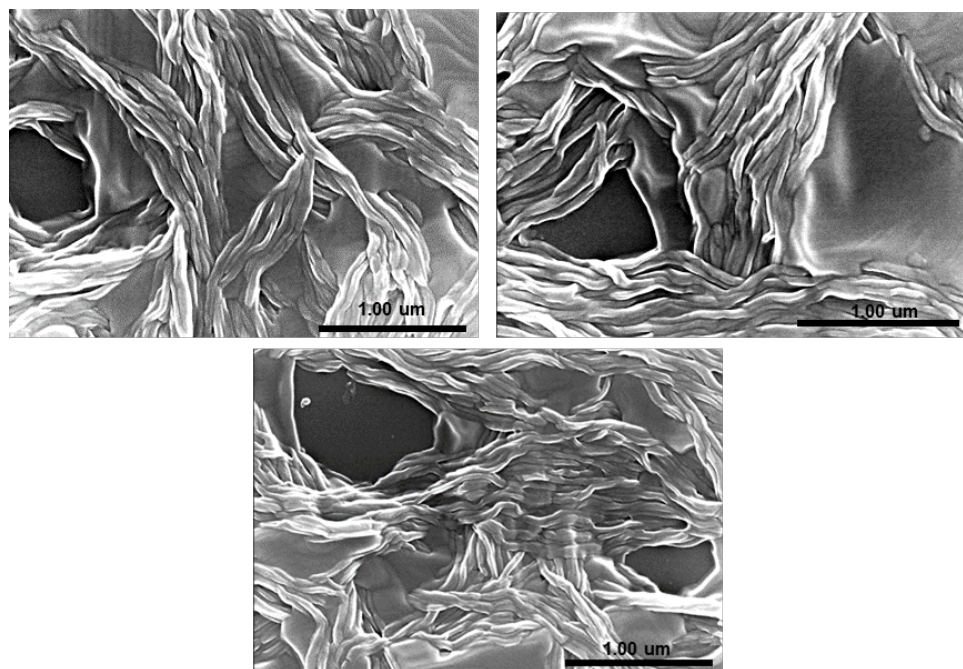


Figure S33. Scanning electron microscopy images of a drop cast solution of MC 1 in THF with 0.3 mM tetrabutylammonium perchlorate, which was acidified with 1.0 equivalents of $\text{CF}_3\text{CO}_2\text{H}$, onto silicon with a layer of native oxide.

III. X-Ray Diffraction

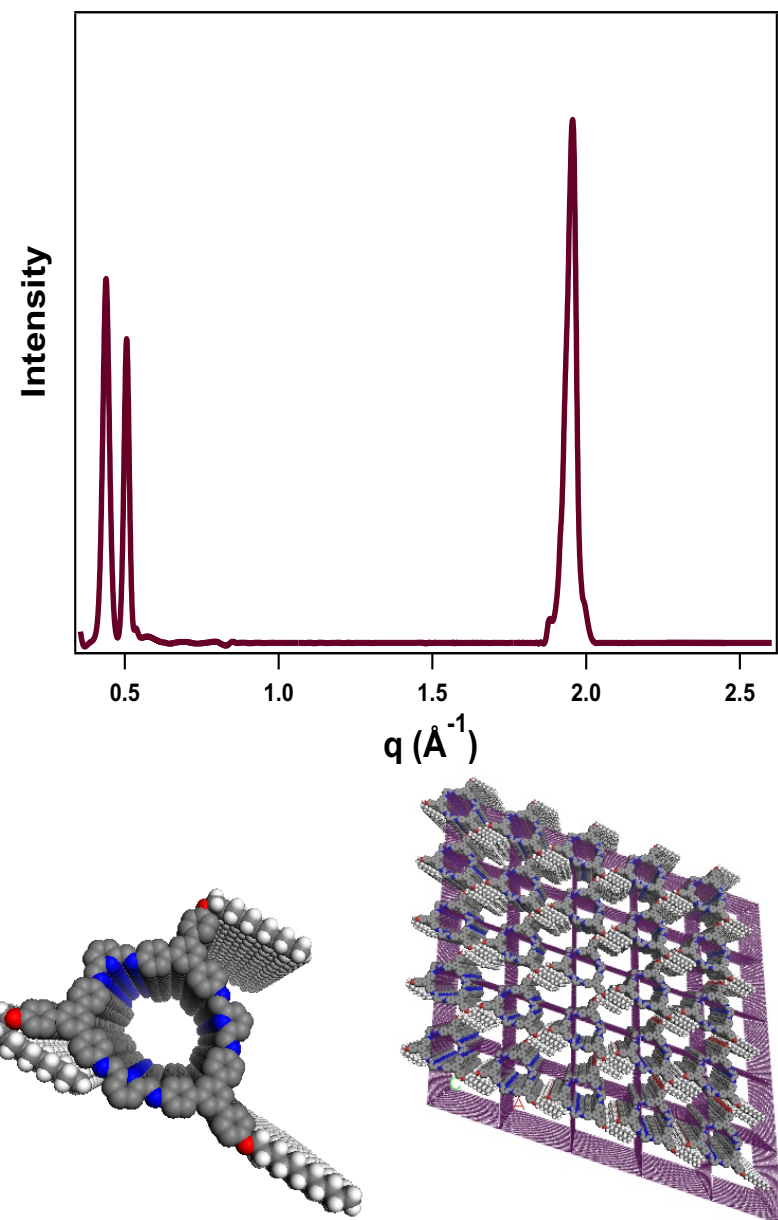


Figure S34. Refined X-Ray Diffraction (XRD) pattern of MC 2 assembled into nanotubes.

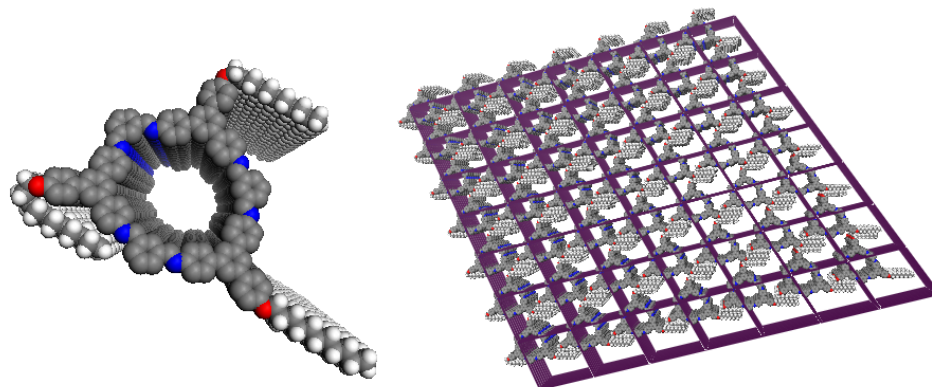
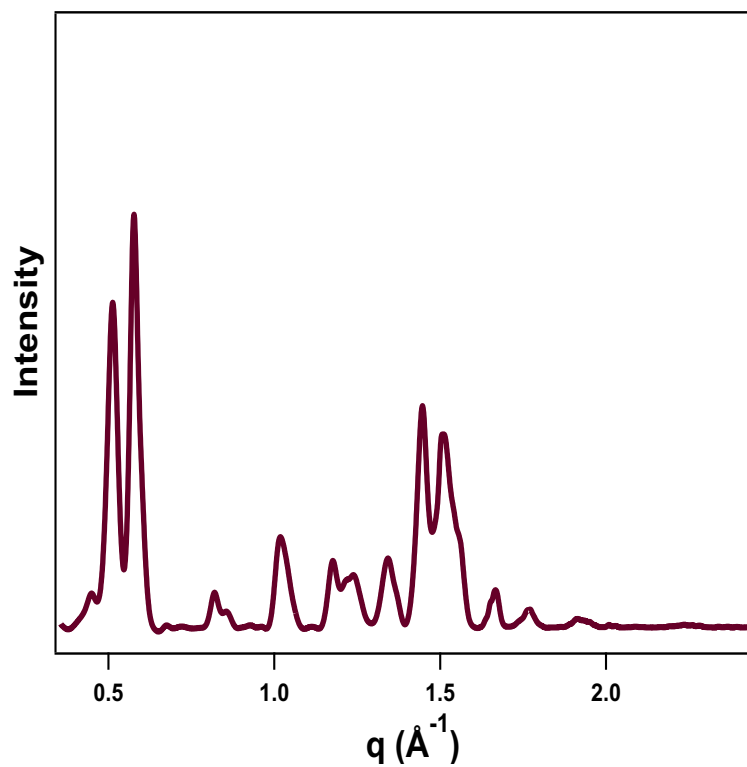


Figure S35. Refined X-Ray Diffraction (XRD) pattern of MC 1 assembled into nanotubes.

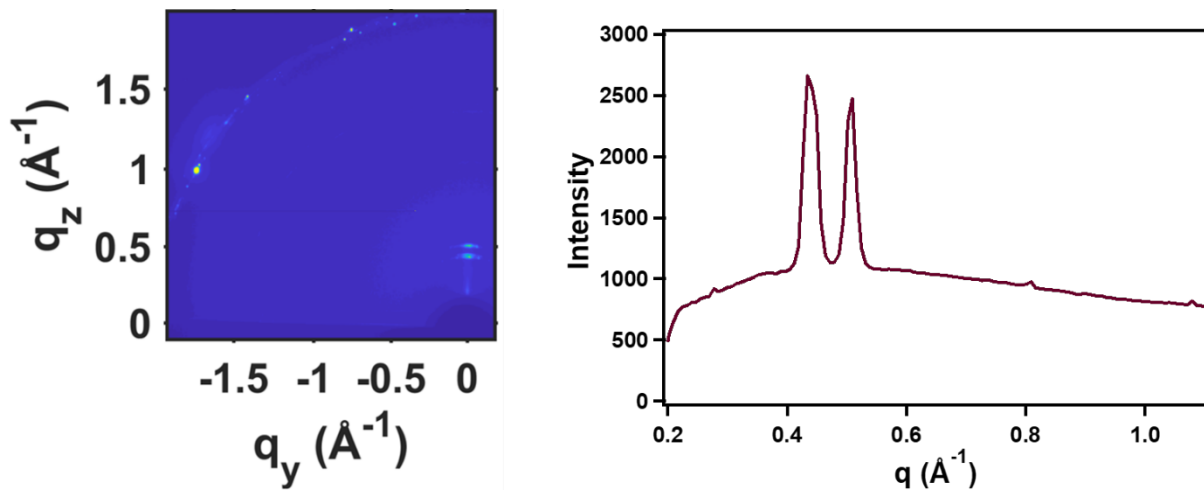


Figure S36. GI-WAXS patterns of MC 1 after being prepared for AFM with 2000 equivalents of acid.

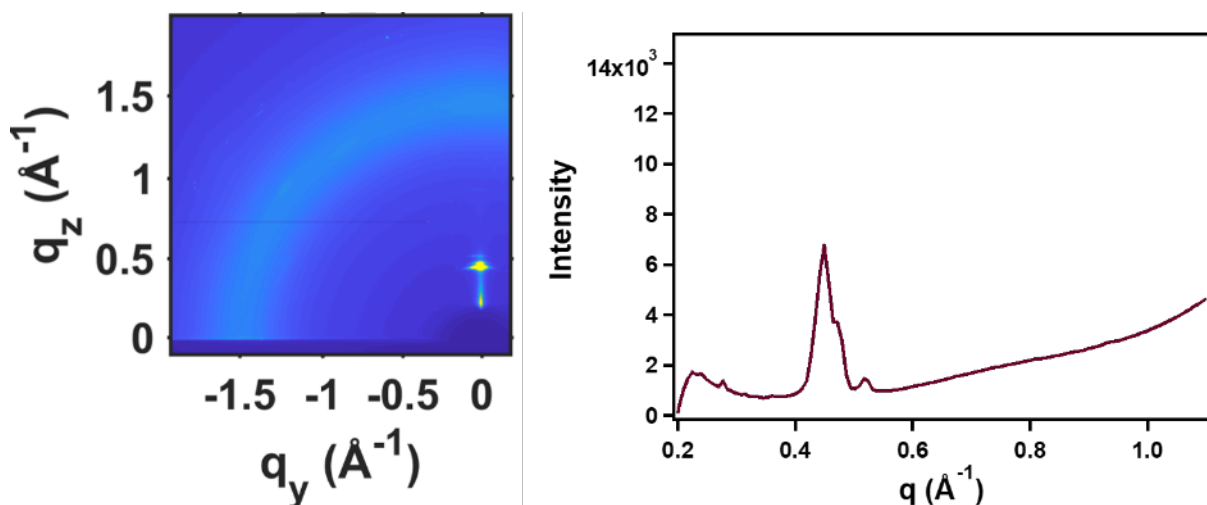


Figure S37. GI-WAXS patterns of MC 1 after being prepared for AFM with 3.0 equivalents of acid.

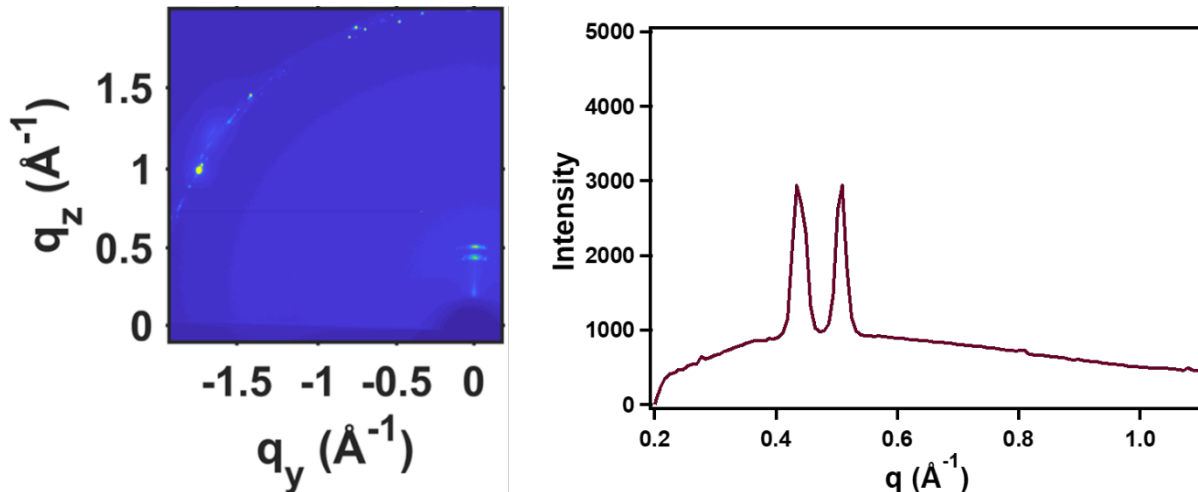


Figure S38. GI-WAXS patterns of MC 1 after being prepared for AFM with 2.0 equivalents of acid.

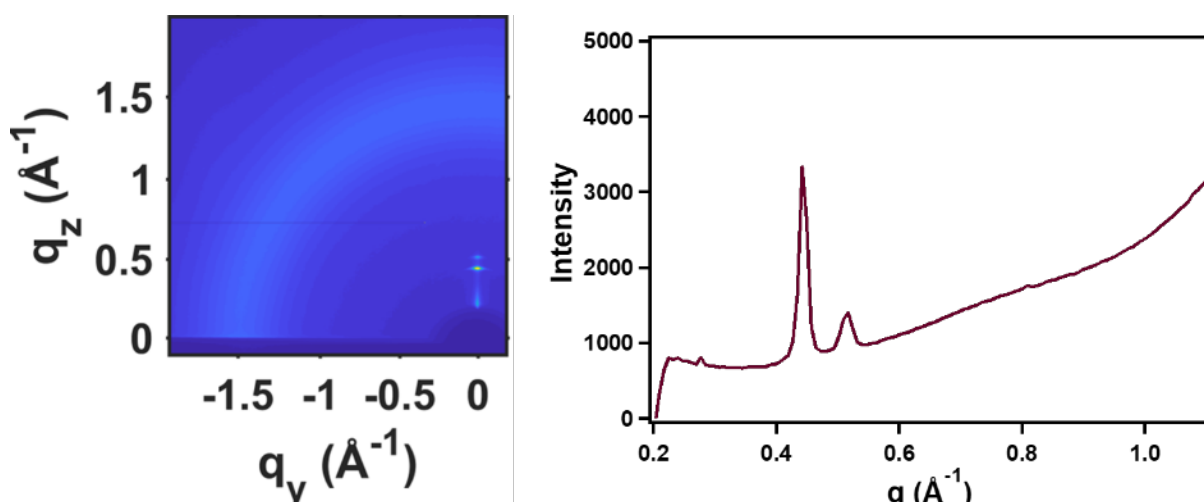


Figure S39. GI-WAXS patterns of MC 1 after being prepared for AFM with 1.0 equivalents of acid.

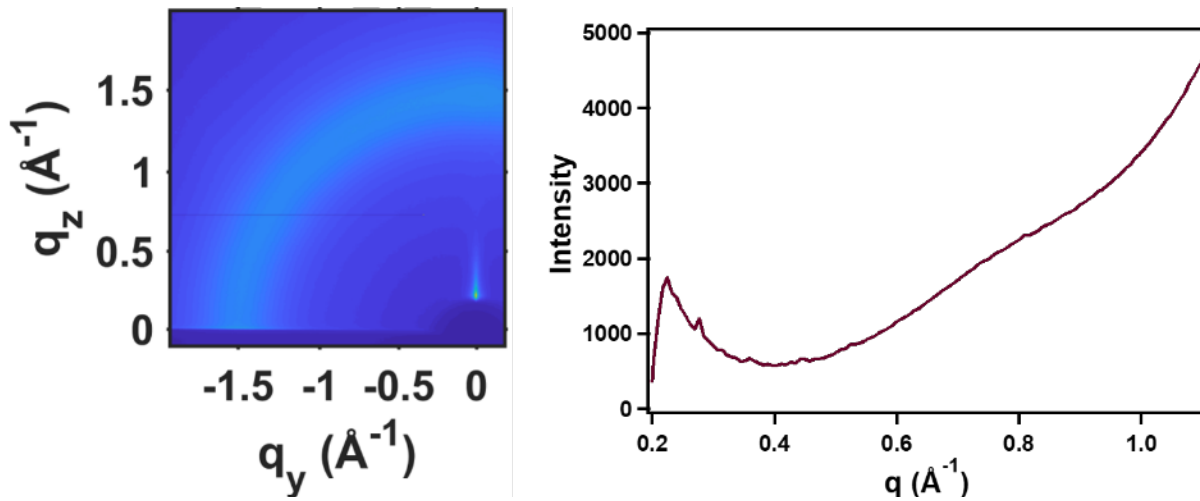


Figure S40. GI-WAXS patterns of MC 1 after being prepared for AFM with 0.0 equivalents of acid showing no self-assembly.

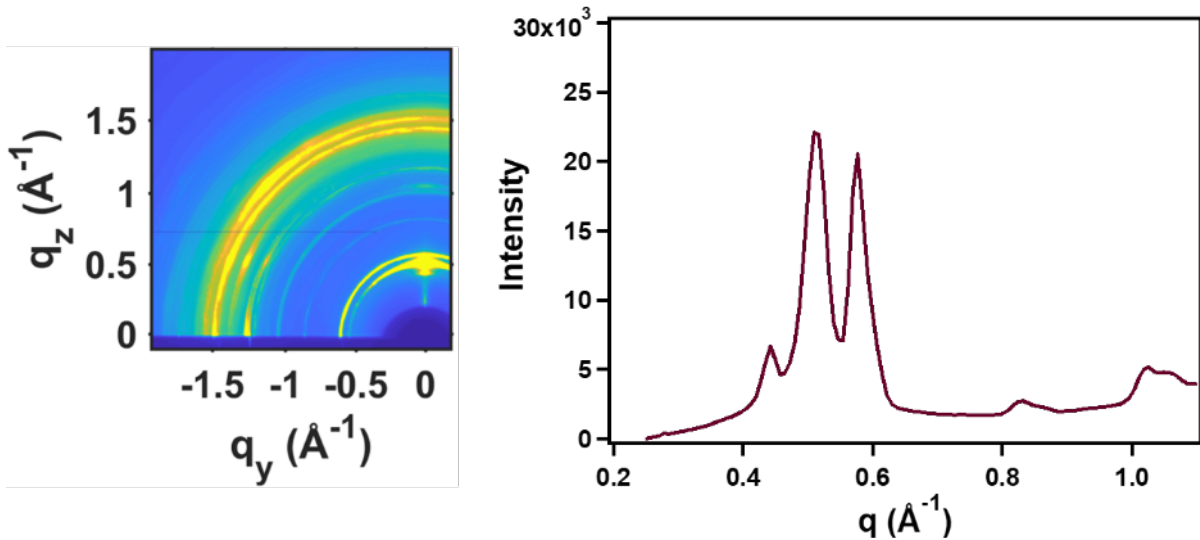


Figure S41. GI-WAXS patterns of MC 2 after being prepared for AFM with 2000 equivalents of acid.

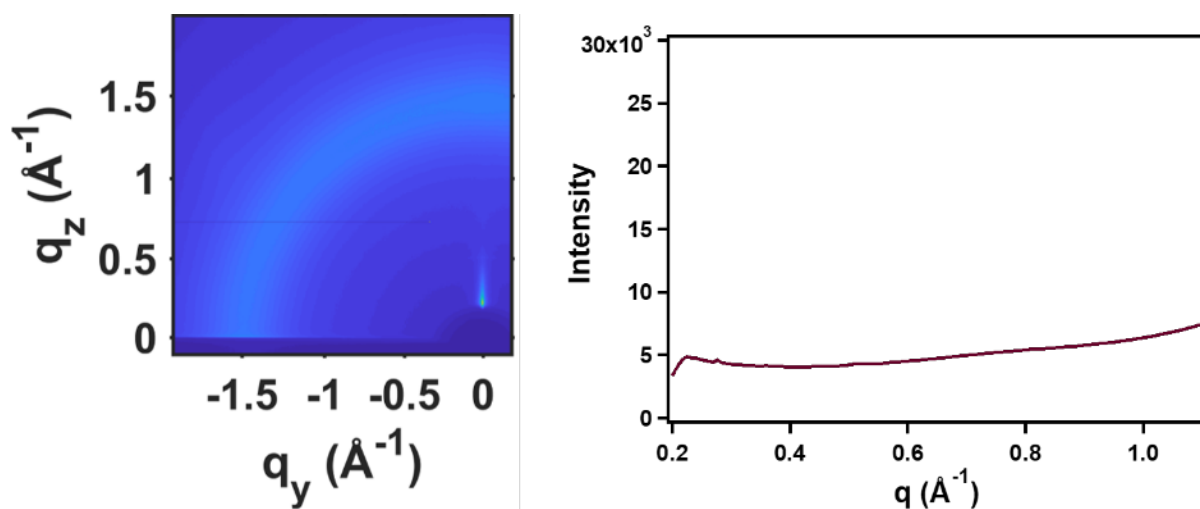


Figure S42. GI-WAXS patterns of MC 2 after being prepared for AFM with 6.0 equivalents of acid.

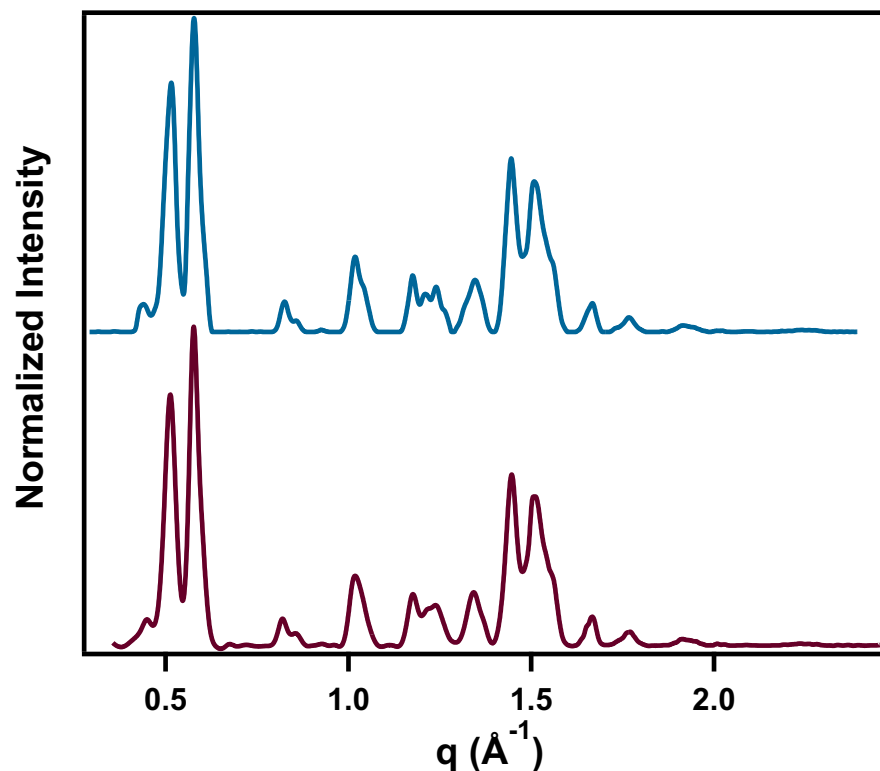


Figure S43. Stacked spectra of the refined diffraction pattern of MC 1 assembled into nanotubes and the experimental diffraction pattern of MC 1 after being prepared for AFM with 2000 equivalents of acid.

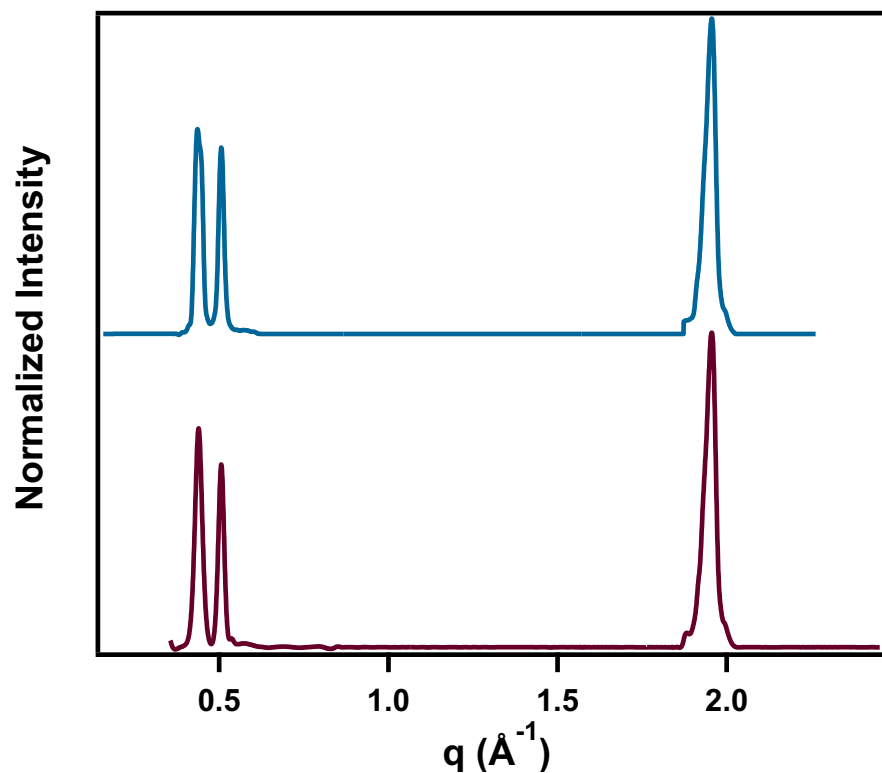


Figure S44. Stacked spectra of the refined diffraction pattern of MC 2 assembled into nanotubes and the experimental diffraction pattern of MC 2 after being prepared for AFM.

IV. MALDI-MS

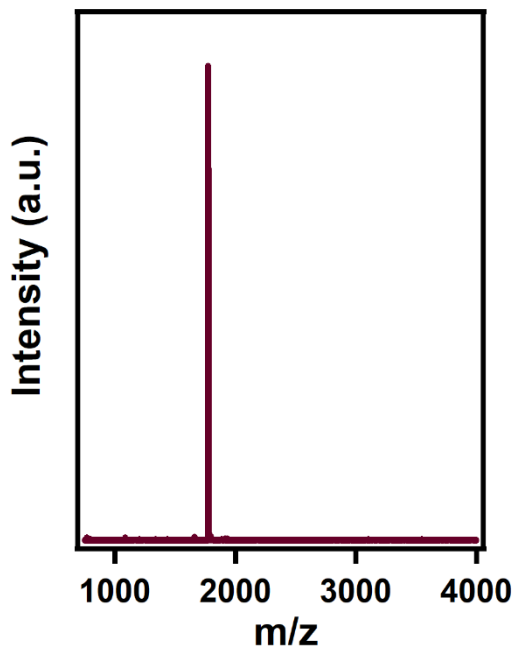


Figure S45. MALDI-MS spectra of MC 2 after acidification with 2000 equivalents of $\text{CF}_3\text{CO}_2\text{H}$, equilibration for 1 hour, and neutralization with Et_3N showing the recovery of the initial macrocycle. ($m/z=1771.74 \text{ [M+H]}^+$)

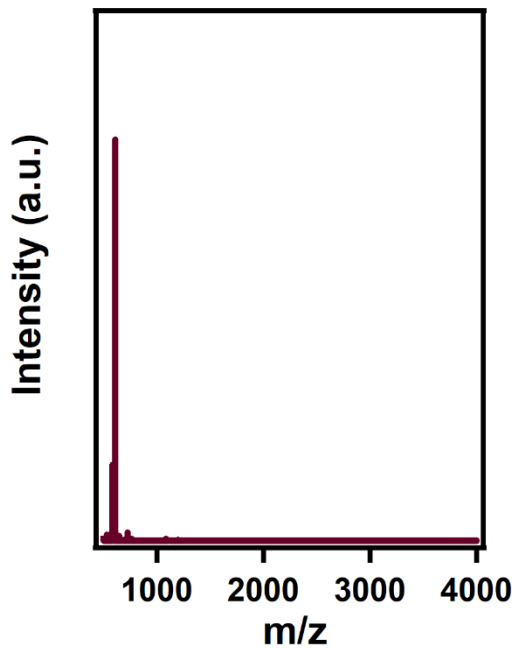


Figure S46. MALDI-MS spectra of MC 2 after acidification with 6.0 equivalents of $\text{CF}_3\text{CO}_2\text{H}$, equilibration for 1 hour, and neutralization with Et_3N , showing hydrolysis of the initial macrocycle rather than recovery. ($m/z=609.48: [1+\text{IDA}+\text{H}]^+$; $m/z=763.42: [1+2\text{IDA}+\text{H}]^+$)

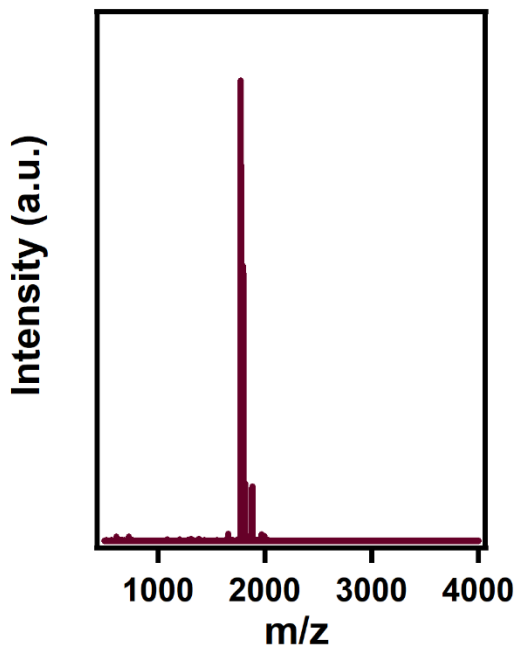


Figure S47. MALDI-MS spectra of MC 1 after acidification with 2000 equivalents of $\text{CF}_3\text{CO}_2\text{H}$, equilibration for 1 hour, and neutralization with Et_3N showing the recovery of the initial macrocycle. ($m/z= 1774.59 \text{ [M+H]}^+$; $m/z=1796.61 \text{ [M+Na]}^+$; $m/z=1813.58 \text{ [M+K]}^+$; $m/z=1881.49 \text{ [M+Ag]}^+$).

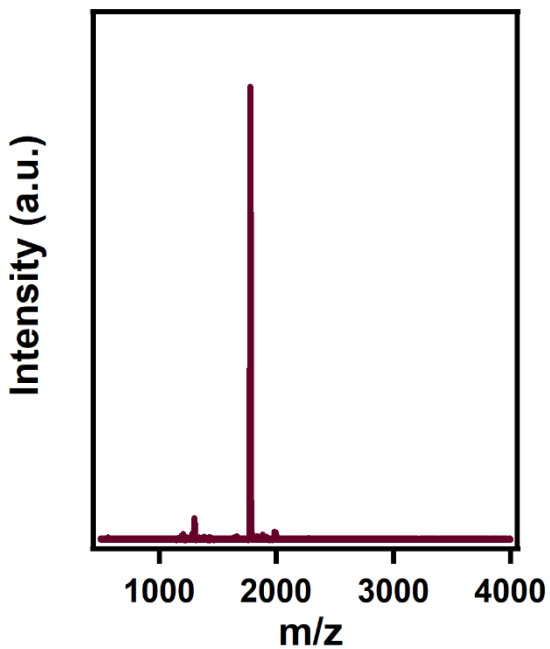


Figure S48. MALDI-MS spectra of MC 1 after acidification with 3.0 equivalents of $\text{CF}_3\text{CO}_2\text{H}$, equilibration for 1 hour, and neutralization with Et_3N showing recovery of the macrocycle with no fragmentation. ($m/z=1774.89 \text{ [M+H]}^+$).

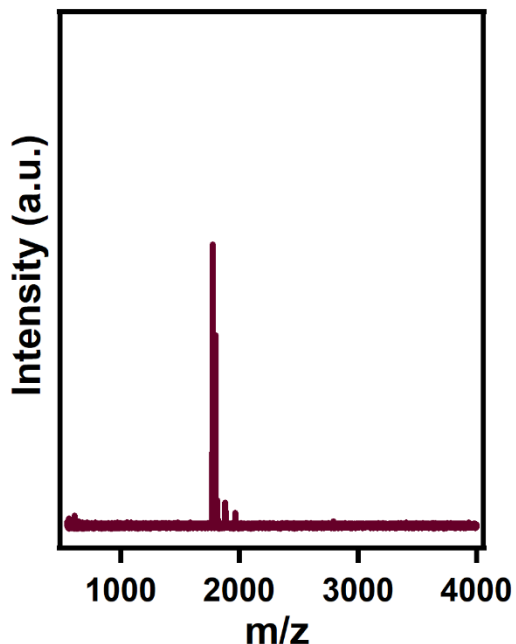


Figure S49. MALDI-MS spectra of MC 1 after acidification with 2.0 equivalents of $\text{CF}_3\text{CO}_2\text{H}$, equilibration for 1 hour, and neutralization with Et_3N showing recovery of the macrocycle with no fragmentation. ($m/z=1774.73$ $[\text{M}+\text{H}]^+$; $m/z=1798.66$ $[\text{M}+\text{Na}]^+$; $m/z=1811.45$ $[\text{M}+\text{K}]^+$).

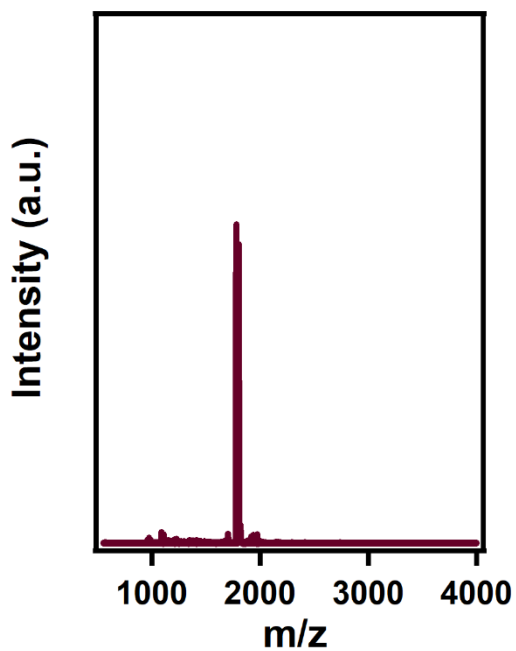


Figure S50. MALDI-MS spectra of MC 1 after acidification with 1.0 equivalents of $\text{CF}_3\text{CO}_2\text{H}$, equilibration for 1 hour, and neutralization with Et_3N showing recovery of the macrocycle with no fragmentation. ($m/z=1774.75$ $[\text{M}+\text{H}]^+$; $m/z=1796.73$ $[\text{M}+\text{Na}]^+$; $m/z=1809.75$ $[\text{M}+\text{K}]^+$).

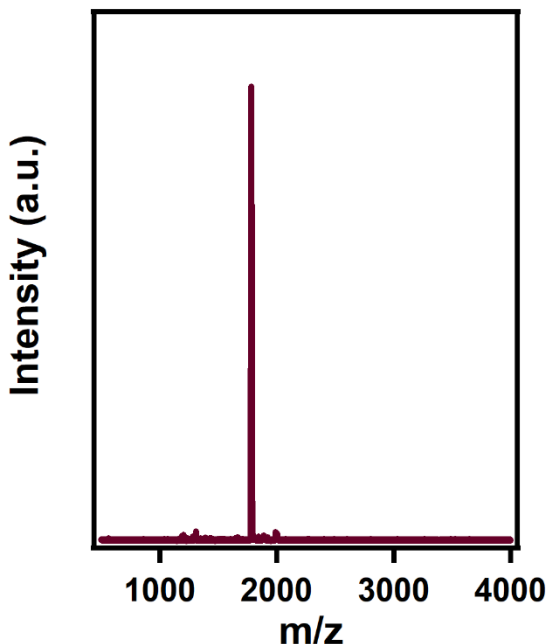


Figure S51. MALDI-MS spectra of MC 1 after acidification with 0.4 equivalents of CF₃CO₂H, equilibration for 1 hour, and neutralization with Et₃N showing recovery of the macrocycle with no fragmentation. ($m/z=1774.91$ [M+H]⁺).

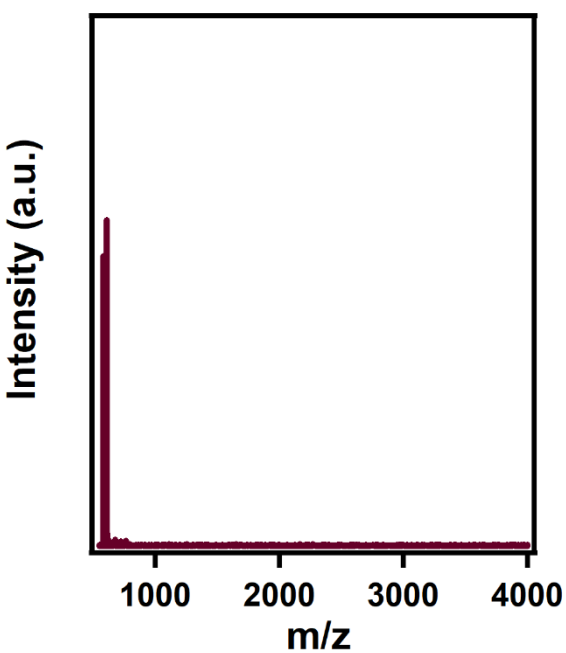


Figure S52. MALDI-MS spectra of MC 2 after acidification with 0.3 equivalents of CF₃CO₂H, equilibration for 1 hour, and neutralization with Et₃N, showing hydrolysis of the desired MC 1nd no remnants of the original macrocycle in solution. ($m/z=609.18$ [1+IDA+H]⁺)

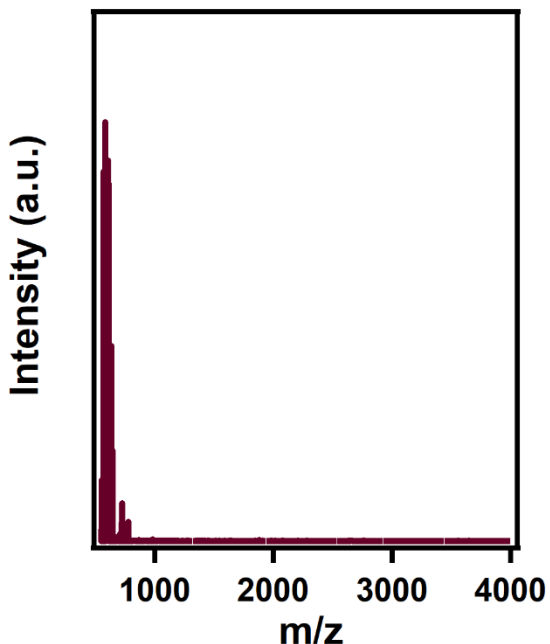


Figure S53. MALDI-MS spectra of MC 2 after acidification with 0.6 equivalents of $\text{CF}_3\text{CO}_2\text{H}$, equilibration for 1 hour, and neutralization with Et_3N , showing hydrolysis of the desired MC 1nd no remnants of the original macrocycle in solution. ($m/z=609.37$ [1+IDA+H] $^+$; $m/z=631.48$ [1+IDA+Na] $^+$; $m/z=648.52$ [1+IDA+K] $^+$)

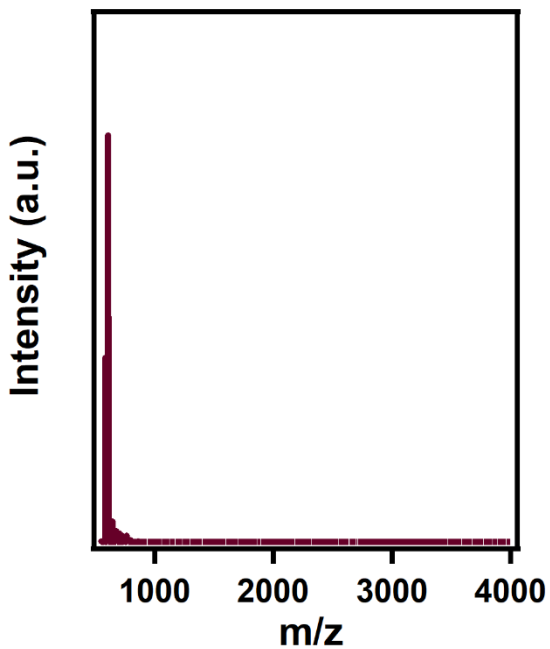


Figure S54. MALDI-MS spectra of MC 2 after acidification with 0.8 equivalents of $\text{CF}_3\text{CO}_2\text{H}$, equilibration for 1 hour, and neutralization with Et_3N , showing hydrolysis of the desired MC 1nd no remnants of the original macrocycle in solution. ($m/z=609.31$ [1+IDA+H] $^+$)

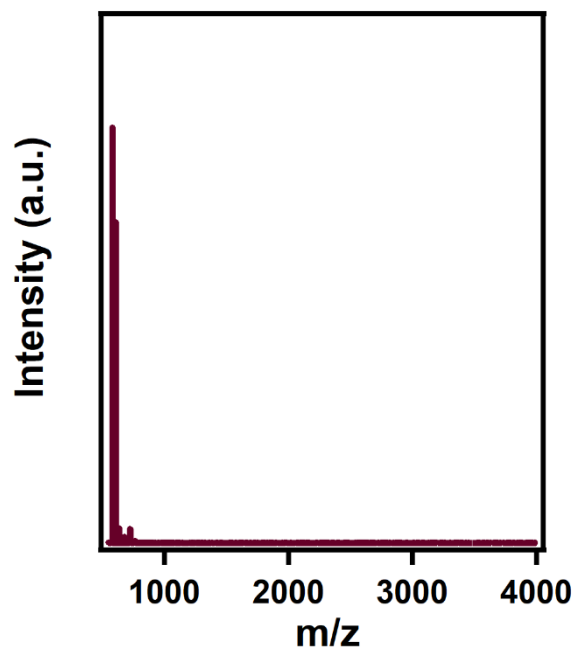


Figure S55. MALDI-MS spectra of MC 2 after acidification with 1.0 equivalents of $\text{CF}_3\text{CO}_2\text{H}$, equilibration for 1 hour, and neutralization with Et_3N , showing hydrolysis of the desired MC 1nd no remnants of the original macrocycle in solution. ($m/z=609.83$ $[1+\text{IDA}+\text{H}]^+$)

V. UV-Vis Spectroscopy

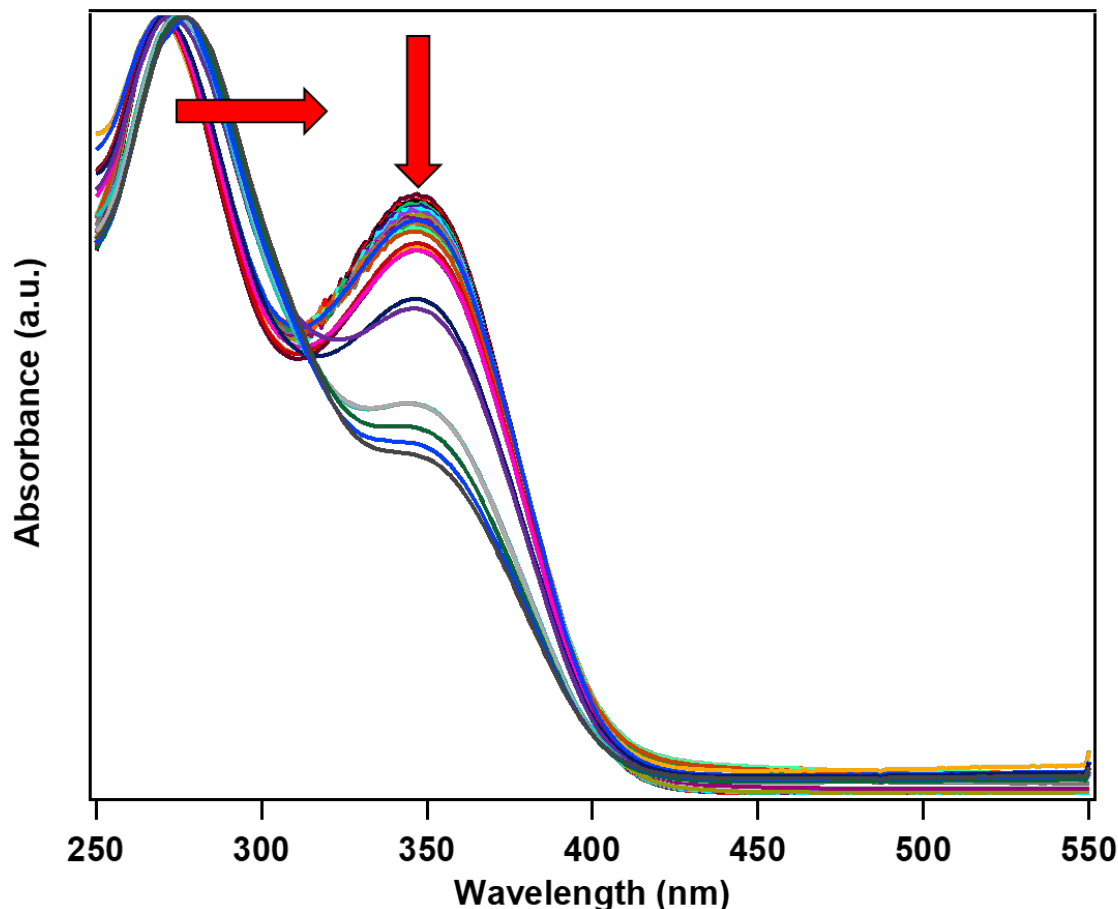


Figure S56. UV-Vis spectra of MC 1 titrated with acid from 0-2000 equivalents of $\text{CF}_3\text{CO}_2\text{H}$. The first absorption band was shown to red shift as a result of $\text{CF}_3\text{CO}_2\text{H}$ being added, while the second absorption band was shown to decrease in intensity. The above UV-Vis spectra were used to determine and appropriate excitation wavelength for subsequent fluorescence experimentation.

VI. Gel Permeation Chromatography (GPC)

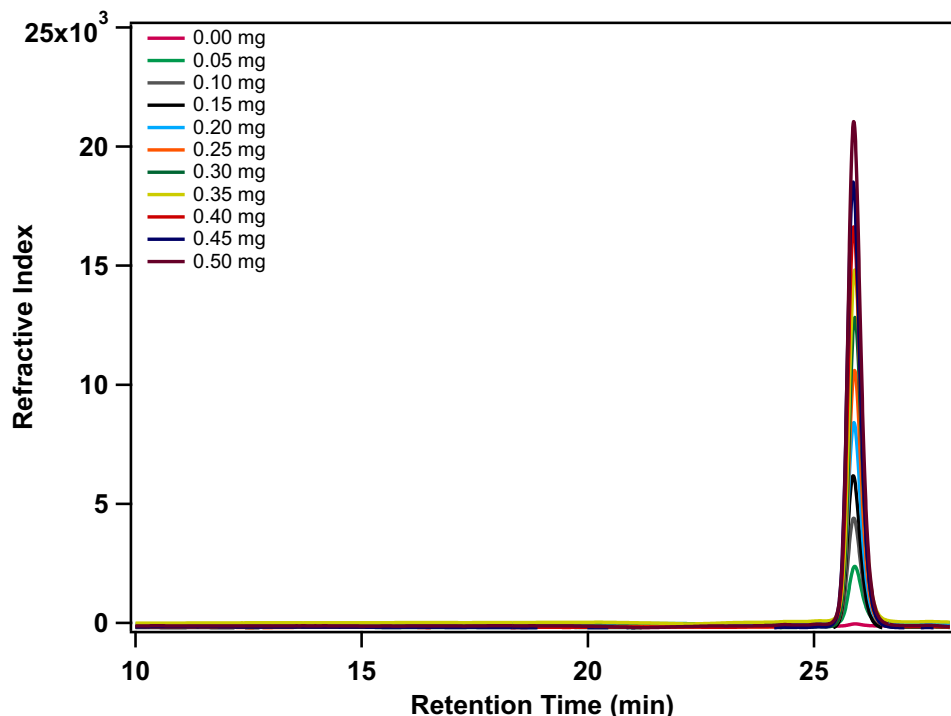


Figure S57. Gel permeation chromatography trace of varying concentrations of MC 1 in THF. All samples were prepared on a 1 mL scale.

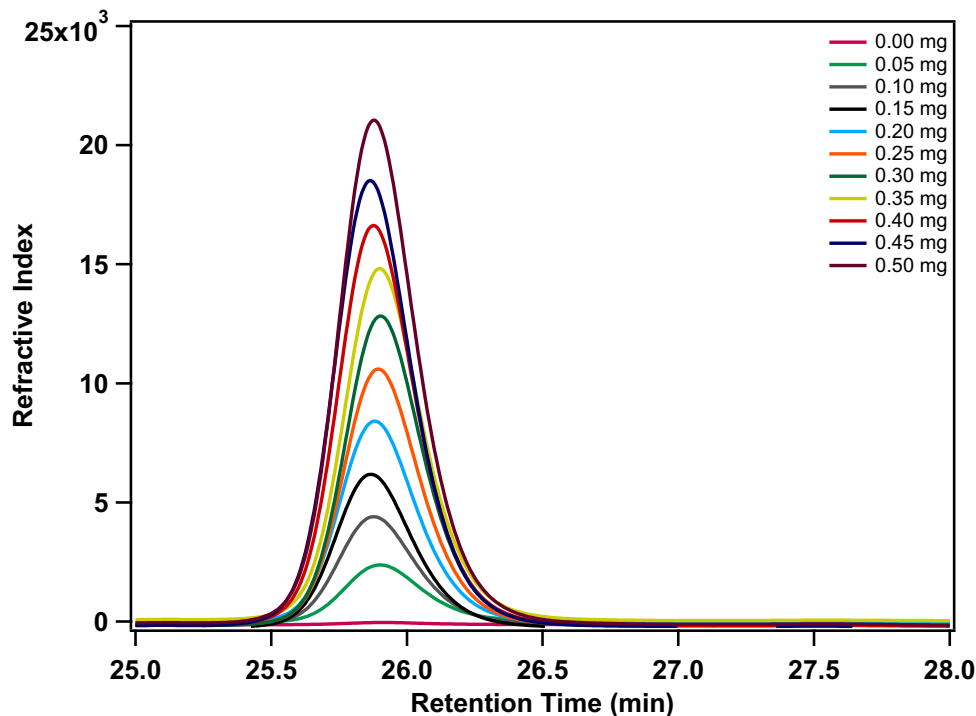


Figure S58. Gel permeation chromatography trace of varying concentrations of MC 1 in THF. All samples were prepared on a 1 mL scale.

Table S1. Data obtained from GPC traces of varying concentrations of MC 1 in THF. Due to the PDI of the solutions remaining constant, response data was taken as the maximum of the elution curve for each respective concentration. Each sample was prepared on a 1 mL scale to ensure accurate measurements.

Macrocyclic Concentration (mg/mL)	Response 1	Response 2	Average Response	Standard Deviation
0	0	0	44.09	0.00
0.05	3035	3194	3035	112.69
0.10	3998	4296	3998	211.03
0.15	5360	5853	5360	348.79
0.20	6618	6833	6618	151.81
0.25	8412	8332	8412	56.50
0.30	10600	9686	10600	646.56
0.35	12301	12032	12301	190.21
0.40	14818	15127	14818	218.50
0.45	16629	16712	16629	58.69
0.50	18512	18826	18512	222.03

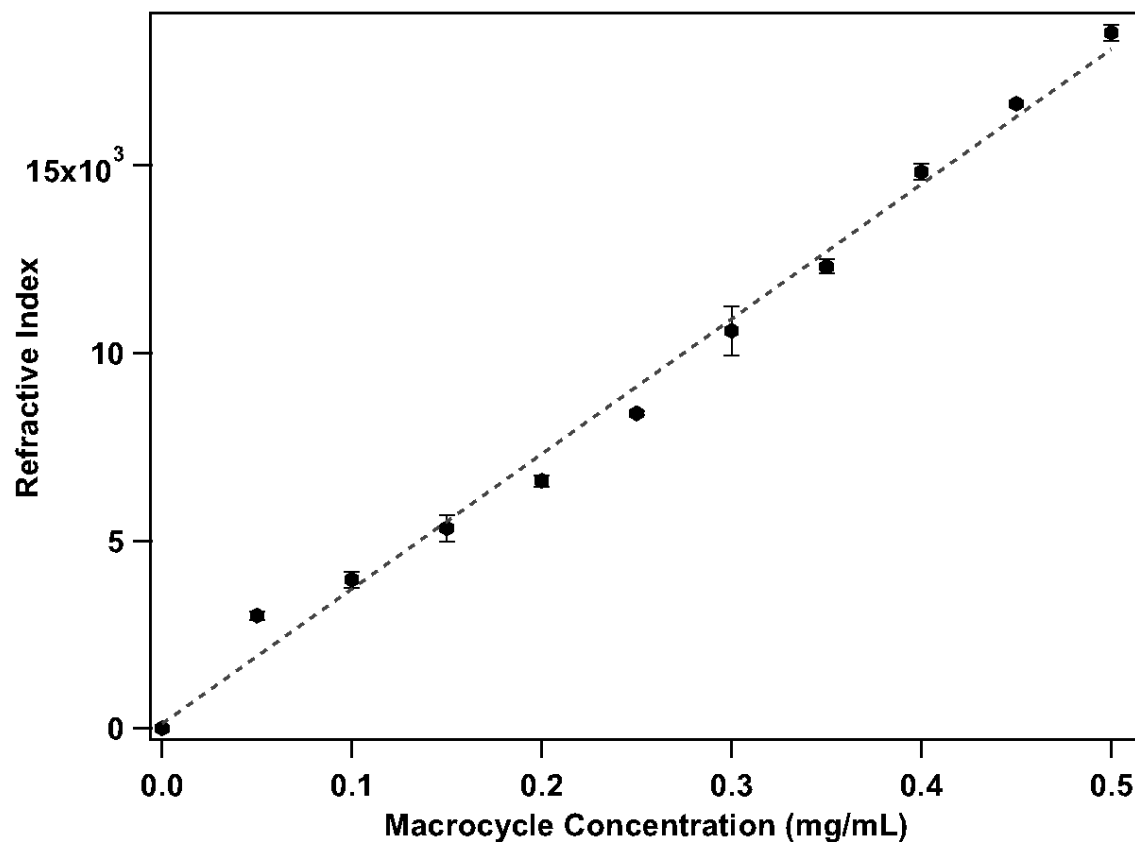


Figure S59. Calibration curve generated from GPC responses of varying concentrations of MC 1. The plot was fit with a linear regression trendline corresponding with the equation $y=35865x+150.27$. The coefficient of linearity was determined to be 0.9917, demonstrating a good fit of the data.

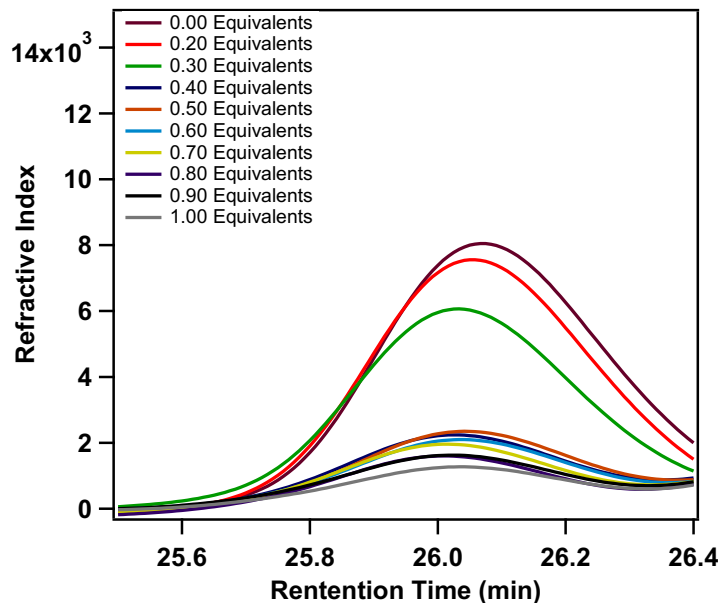


Figure S60. Gel permeation chromatography trace of the acidification of a solution of a 0.15 mg/mL solution of MC 1, in THF with 0.3 mM tetrabutylammonium perchlorate, with 0-1.0 equivalents of CF₃CO₂H.

Table S2. Data obtained from GPC traces of varying acid loadings to a 0.15 mg/mL solution of MC 2 in THF with 0.3 mM tetrabutylammonium perchlorate.

Acid Equivalents	Response 1	Response 2	Response 3	Average Response	Std. Dev.
0.000	5110.55	5111.28	5330.55	5184.13	126.81
0.050	5383.32	5278.07	5546.45	5402.61	135.23
0.075	5397.43	5232.46	5419.44	5349.78	102.19
0.100	5443.56	5425.60	5149.65	5339.60	164.75
0.150	5007.51	4531.53	4337.83	4625.62	344.61
0.200	3613.08	3648.81	3723.09	3661.66	56.12
0.250	3633.92	3146.85	3558.92	3446.56	262.26
0.300	2545.15	2534.17	2667.19	2582.17	73.83
0.400	1487.07	1580.47	-	1533.77	66.04
0.500	1317.62	1241.77	-	1279.69	53.63
0.600	1258.98	1247.74	-	1253.36	7.95
0.700	1030.25	1222.10	-	1126.18	135.66
0.800	1045.72	1269.91	-	1157.81	158.53
0.900	817.63	1269.62	-	1043.62	319.60
1.000	535.42	911.45	-	723.43	265.89

Table S3. Correlation of data obtained from GPC traces of varying acid loadings to a 0.15 mg/mL solution of MC 1 in THF with 0.3 mM tetrabutylammonium perchlorate, to a percent of macrocycle remaining in solution.

Acid Equivalents	Percent Response 1	Percent Response 2	Percent Response 3	Average Percent	Std. Dev.
0.00	1.000	1.000	1.000	1.000	0.000
0.05	1.053	1.033	1.041	1.042	0.010
0.08	1.056	1.024	1.017	1.032	0.021
0.10	1.065	1.061	0.966	1.031	0.056
0.15	0.980	0.887	0.814	0.893	0.083
0.20	0.707	0.714	0.698	0.706	0.008
0.25	0.711	0.616	0.668	0.665	0.048
0.30	0.498	0.496	0.500	0.498	0.002
0.40	0.291	0.309	-	0.300	0.013
0.50	0.258	0.243	-	0.250	0.011
0.60	0.246	0.244	-	0.245	0.002
0.70	0.202	0.239	-	0.220	0.027
0.80	0.205	0.248	-	0.227	0.031
0.90	0.160	0.248	-	0.204	0.063
1.00	0.105	0.178	-	0.142	0.052

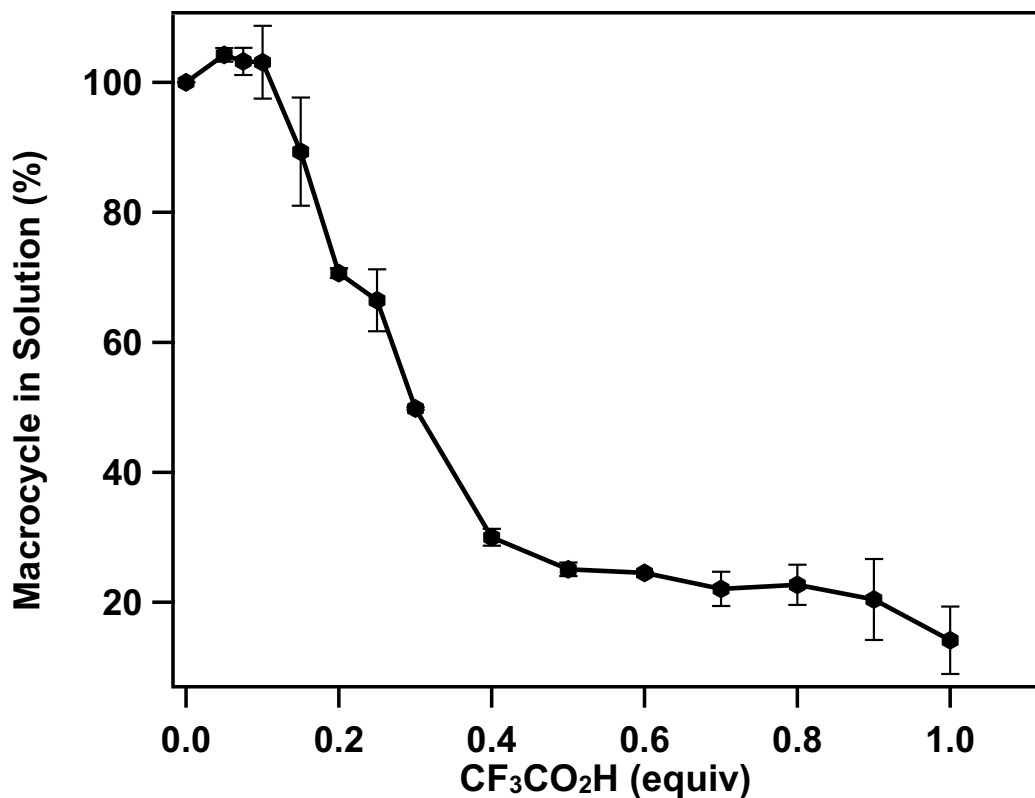


Figure S61. Plot of macrocycles remaining in solution vs. equivalents of acid based on results of GPC traces and quantification using the refractive index detection.

VII. Fluorescence Spectroscopy

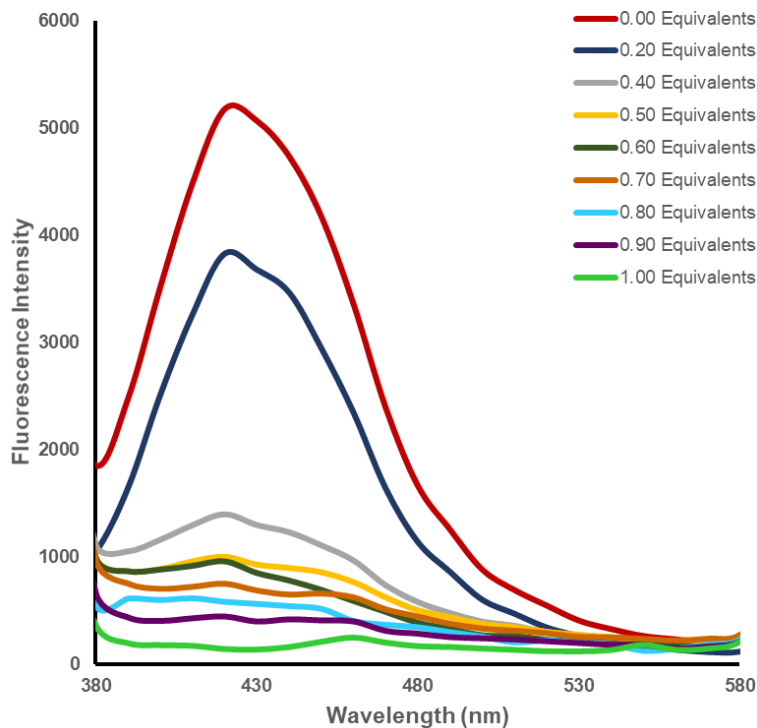


Figure S62. Fluorescence data obtained from 0.5 mg/mL solutions of MC 1 in THF with 0.3 mM tetrabutylammonium perchlorate, which had been acidified with varying equivalents of $\text{CF}_3\text{CO}_2\text{H}$. The solutions were excited at 330 nm and had their emission spectra monitored from 380-580 nm.

Table S4. Fluorescence data obtained from 0.5 mg/mL solutions of MC 1 in THF with 0.3 mM tetrabutylammonium perchlorate, which had been acidified with varying equivalents of $\text{CF}_3\text{CO}_2\text{H}$. The solutions were excited at 330 nm and had their emission monitored at 430 nm.

Acid Equivalents	Emission 1	Emission 2	Average Emission	Std. Dev
0.00	4126.56	4126.56	4126.56	0.00
0.08	3487.55	4165.67	3826.61	479.51
0.10	3042.08	3805.87	3423.97	540.08
0.13	3300.89	3909.49	3605.19	430.35
0.15	3025.61	3803.30	3414.45	549.91
0.18	2839.12	3552.31	3195.71	504.30
0.20	2753.39	3209.90	2981.65	322.80
0.23	2401.90	2598.21	2500.06	138.82
0.25	2186.23	2309.60	2247.92	87.24
0.28	1259.44	1492.54	1375.99	164.83
0.33	1498.46	1577.21	1537.84	55.68
0.35	1673.33	1589.52	1631.43	59.27
0.38	1480.51	1381.94	1431.23	69.70
0.40	1411.76	1255.57	1333.66	110.44
0.45	1236.77	1278.97	1257.87	29.84
0.50	1246.13	1100.40	1173.27	103.05
0.60	1226.30	1117.99	1172.14	76.59
0.70	759.76	670.38	715.07	63.21
0.80	808.21	685.75	746.98	86.59
0.90	731.75	651.29	691.52	56.90
1.00	691.23	673.29	682.26	12.69

Table S5. Fluorescence data (I/I_0) obtained from 0.5 mg/mL solutions of MC 1 in THF with 0.3 mM tetrabutylammonium perchlorate, which had been acidified with varying equivalents of $\text{CF}_3\text{CO}_2\text{H}$. The solutions were excited at 330 nm and had their emission monitored at 430 nm.

Acid Equivalents	Emission 1	Emission 2	Average Emission	Std. Dev
0.0000	1.0000	1.0000	1.0000	0.0000
0.0750	0.8451	1.0095	0.9273	0.0581
0.1000	0.7372	0.9223	0.8297	0.0654
0.1250	0.7999	0.9474	0.8737	0.0521
0.1500	0.7332	0.9217	0.8274	0.0666
0.1750	0.6880	0.8608	0.7744	0.0611
0.2000	0.6672	0.7779	0.7226	0.0391
0.2250	0.5821	0.6296	0.6058	0.0168
0.2500	0.5298	0.5597	0.5447	0.0106
0.2750	0.3052	0.3617	0.3334	0.0200
0.3250	0.3631	0.3822	0.3727	0.0067
0.3500	0.4055	0.3852	0.3953	0.0072
0.3750	0.3588	0.3349	0.3468	0.0084
0.4000	0.3421	0.3043	0.3232	0.0134
0.4500	0.2997	0.3099	0.3048	0.0036
0.5000	0.3020	0.2667	0.2843	0.0125
0.6000	0.2972	0.2709	0.2840	0.0093
0.7000	0.1841	0.1625	0.1733	0.0077
0.8000	0.1959	0.1662	0.1810	0.0105
0.9000	0.1773	0.1578	0.1676	0.0069
1.0000	0.1675	0.1632	0.1653	0.0015

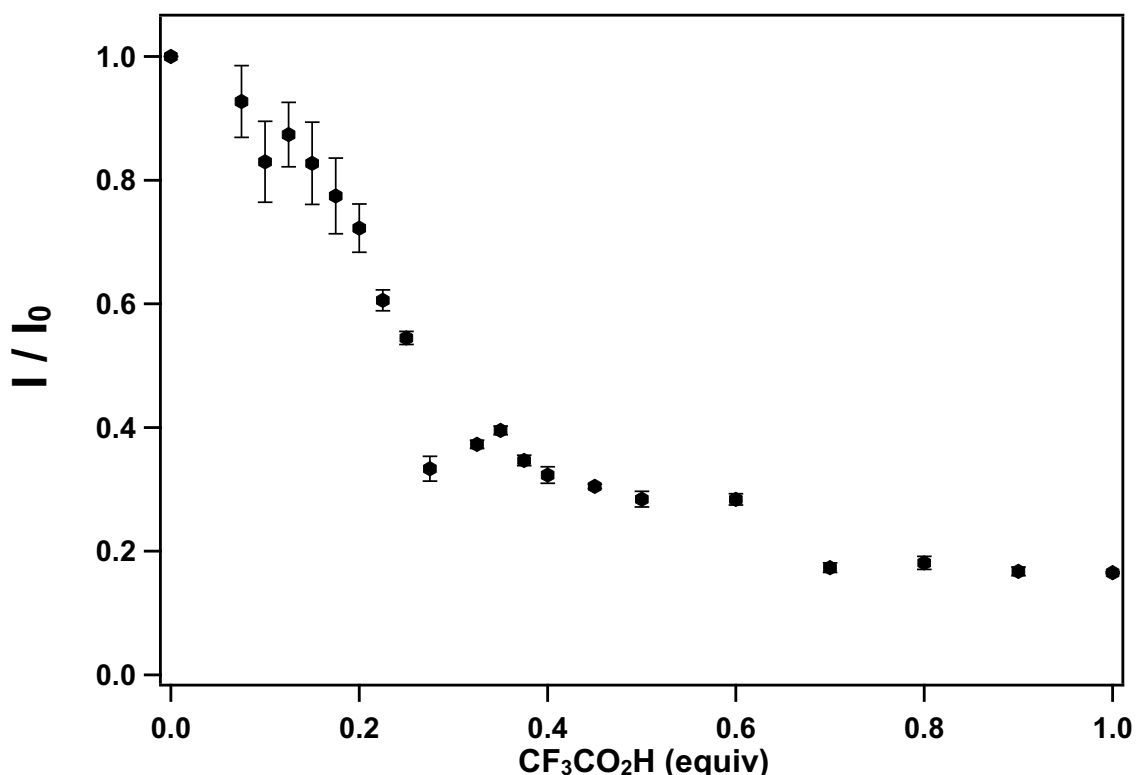


Figure S63. I/I_0 vs. equivalents of acid based on emission values at 430 nm after excitation at 330 nm.

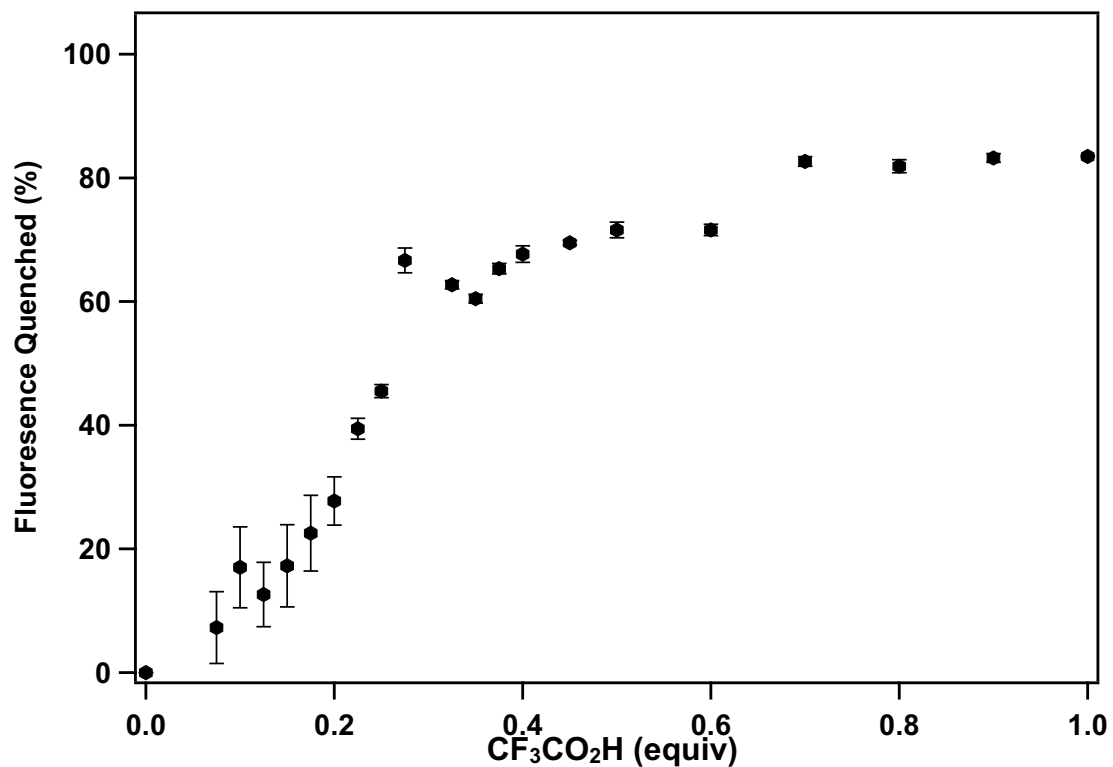


Figure S64. Plot of fluorescence quenched vs. equivalents of acid based on emission values at 430 nm after excitation at 330 nm.

Table S6. Fluorescence data corresponding to the excitation of a 0.5 mg/mL solution of MC 2 in THF with 0.3 mM tetrabutylammonium perchlorate, which had been acidified with varying amounts of $\text{CF}_3\text{CO}_2\text{H}$, at 330 nm and the resulting emission at 430 nm.

Acid Equivalents	Emission 1	Emission 2	Emission 3	Average Emission	Std. Dev.
0	6252.19	6115.48	6281.17	6216.28	88.49
0.1	8311.23	8015.31	8798.80	8375.11	395.63
0.2	6680.56	6632.37	7096.06	6803.00	254.94
0.3	9505.82	9305.12	10127.46	9646.13	428.75
0.4	9721.98	9558.53	10156.36	9812.29	308.98
0.5	9098.05	9347.22	10316.84	9587.37	643.91
0.6	10158.29	10492.76	11315.14	10655.40	595.33
0.7	9926.28	10228.55	9549.38	9901.40	340.27
0.8	9768.91	9143.49	9201.38	9371.26	345.59

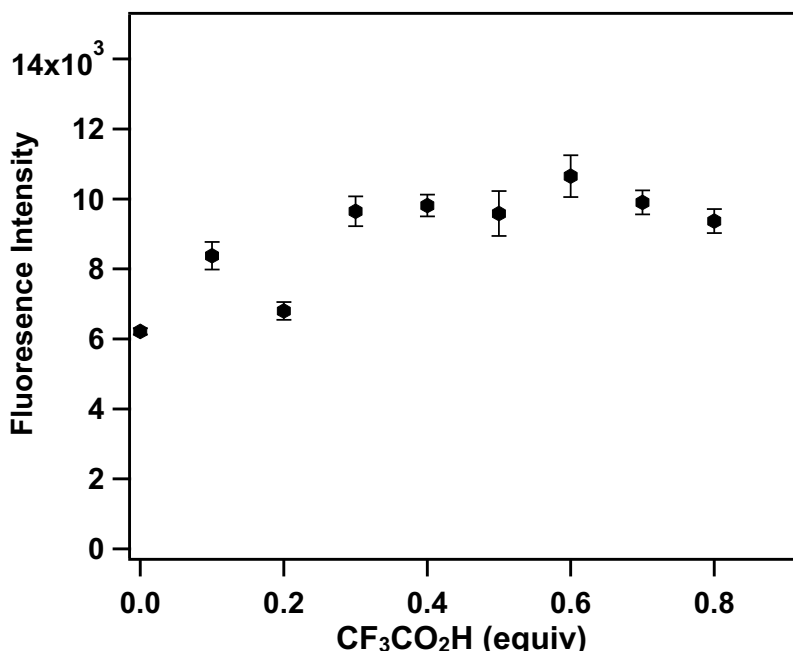


Figure S65. Plot of fluorescence vs equivalents of acid added to a solution of MC 2, in THF with 0.3 mM tetrabutylammonium perchlorate, at 430 nm after excitation at 330 nm. The plot shows a clearly different trend than was observed in MC 1.

Table S7. I/I_0 data calculated from fluorescence data corresponding to the excitation of a 0.5 mg/mL solution of MC 1 in THF with 0.3 mM tetrabutylammonium perchlorate, which had been acidified with varying amounts of $\text{CF}_3\text{CO}_2\text{H}$, at 330 nm and the resulting emission at 430 nm.

Acid Equivalents	I/I_0	Std. Dev
0.000	1.000	0.000
0.075	1.087	0.068
0.100	1.220	0.096
0.125	1.153	0.069
0.150	1.224	0.099
0.175	1.308	0.103
0.200	1.392	0.075
0.225	1.653	0.046
0.250	1.837	0.036
0.275	3.021	0.181
0.325	2.685	0.049
0.350	2.531	0.046
0.375	2.887	0.070
0.400	3.105	0.129
0.450	3.282	0.039
0.500	3.531	0.155
0.600	3.528	0.115
0.700	5.793	0.256
0.800	5.562	0.322
0.900	5.988	0.246
1.000	6.049	0.056

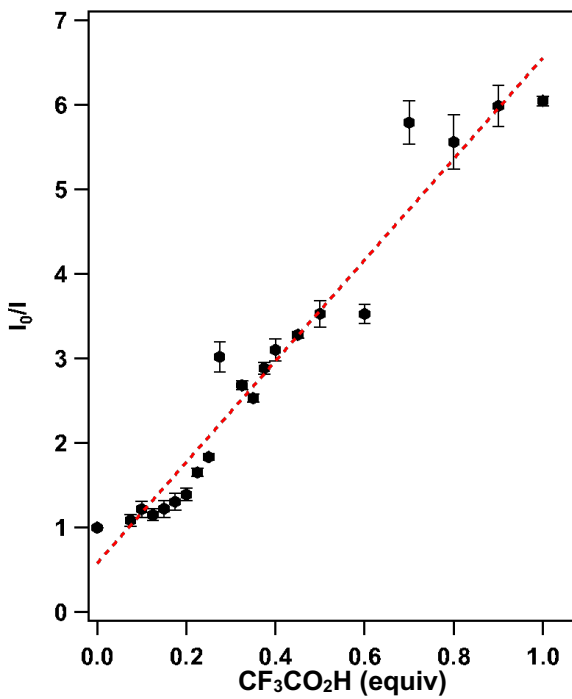


Figure S66. Stern-Volmer plot of data extracted from table S7. The plot was fit with a linear regression trendline corresponding with the equation $y=5.9793x+0.5786$. The coefficient of linearity was determined to be 0.9471, demonstrating a good fit of the data.

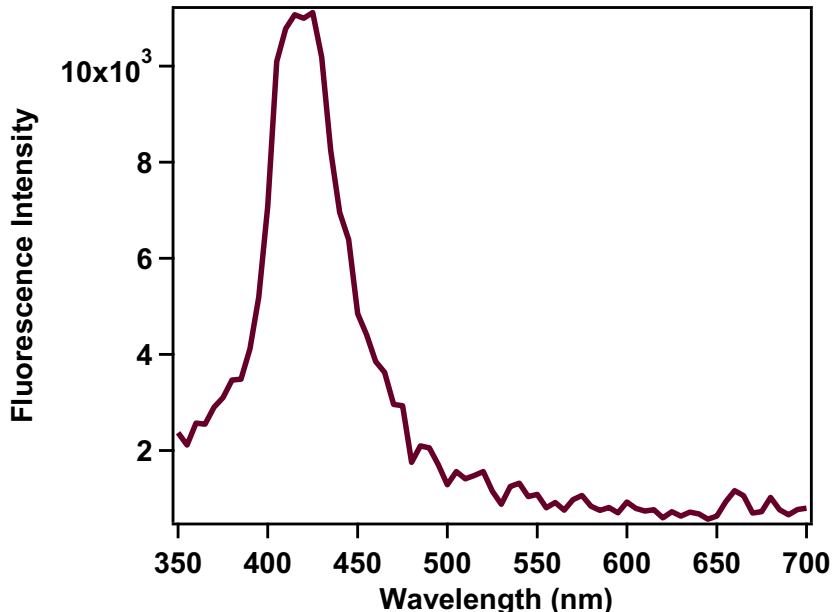


Figure S67. Fluorescence data obtained from a 0.5 mg/mL solution of **2** in THF with 0.3 mM tetrabutylammonium perchlorate, which had been acidified with varying equivalents of $\text{CF}_3\text{CO}_2\text{H}$. The solutions were excited at 330 nm and had their emission spectra monitored from 350-700 nm.

Table S8. Fluorescence data corresponding to the excitation of a 0.5 mg/mL solution of **2** in THF with 0.3 mM tetrabutylammonium perchlorate, which had been acidified with varying amounts of $\text{CF}_3\text{CO}_2\text{H}$, at 330 nm and the resulting emission at 430 nm.

Acid Equivalents	Emission 1	Emission 2	Average Emission	Std. Dev.
0.0	1089.1	1116.5	1102.8	19.43
0.1	1102.7	1058.8	1080.8	31.00
0.2	1098.7	1086.6	1092.6	8.55
0.2	1210.3	1074.7	1142.5	95.89
0.3	985.6	1034.7	1010.1	34.73
0.3	1062.5	996.6	1029.6	46.61
0.4	974.9	1029.3	1002.1	38.49
0.5	961.4	1021.8	991.6	42.71
0.6	863.9	886.7	875.3	16.17
0.7	975.4	1024.1	999.7	34.47
0.8	1127.7	1084.6	1106.2	30.42
0.9	1074.2	973.8	1024.0	71.03
1.0	1044.6	1031.9	1038.2	8.97

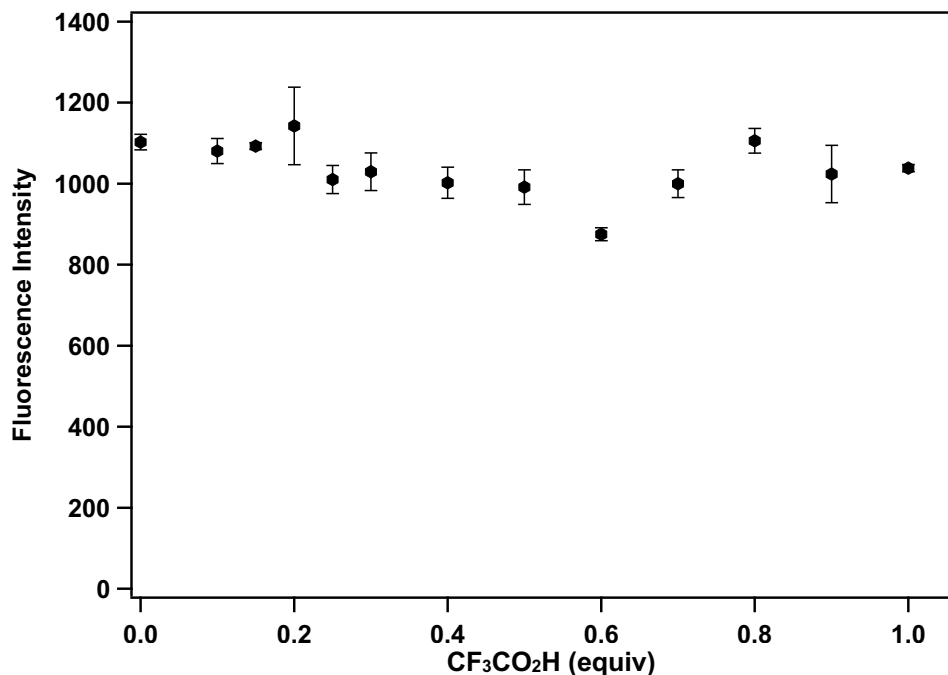


Figure S68. Plot of fluorescence vs equivalents of acid added to a solution of **2** in THF, with 0.3 mM tetrabutylammonium perchlorate, at 430 nm after excitation at 330 nm.

Table S9. I/I₀ data calculated from fluorescence data corresponding to the excitation of a 0.5 mg/mL solution of **2** in THF, with 0.3 mM tetrabutylammonium perchlorate, which had been acidified with varying amounts of CF₃CO₂H, at 330 nm and the resulting emission at 430 nm.

Acid Equivalents	I ₀ /I	Std. Dev.
0.00	1.0000	0.0000
0.10	1.0211	0.0473
0.15	1.0094	0.0257
0.20	0.9694	0.0984
0.25	1.0921	0.0183
0.30	1.0727	0.0674
0.40	1.1009	0.0229
0.50	1.1127	0.0283
0.60	1.2600	0.0011
0.70	1.1034	0.0186
0.80	0.9976	0.0450
0.90	1.0802	0.0939
1.00	1.0623	0.0279

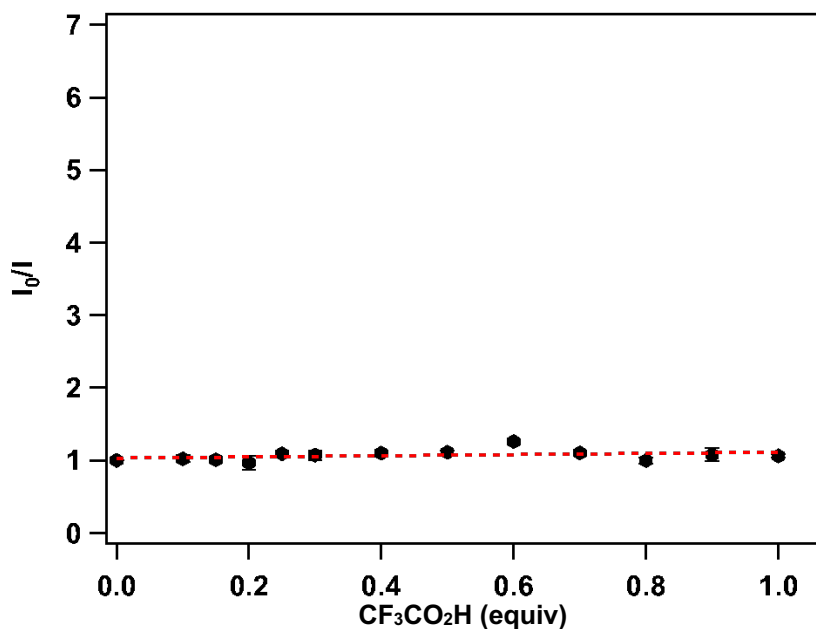


Figure S69. Stern-Volmer plot of data extracted from table S9. The plot was fit with a linear regression trendline corresponding with the equation $y=0.0793x+1.0318$.

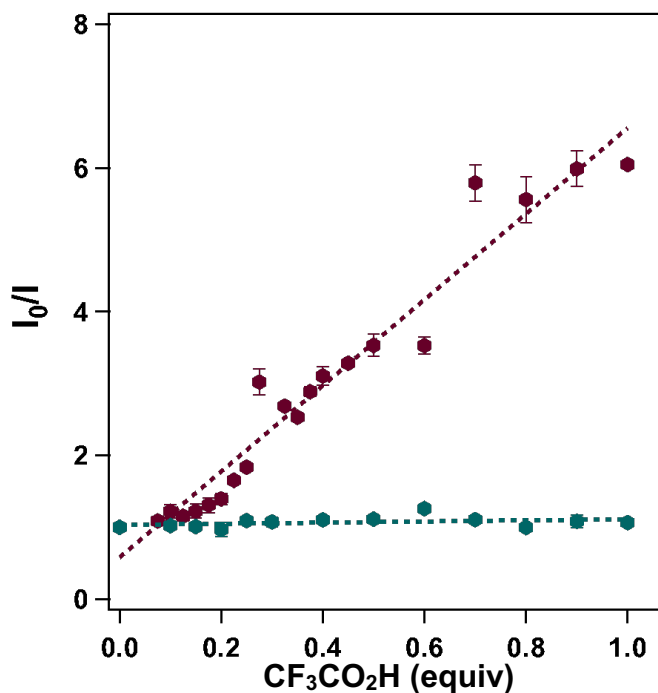


Figure S70. Stern-Volmer comparison of fluorescence quenching behavior of MC 1 and 2.

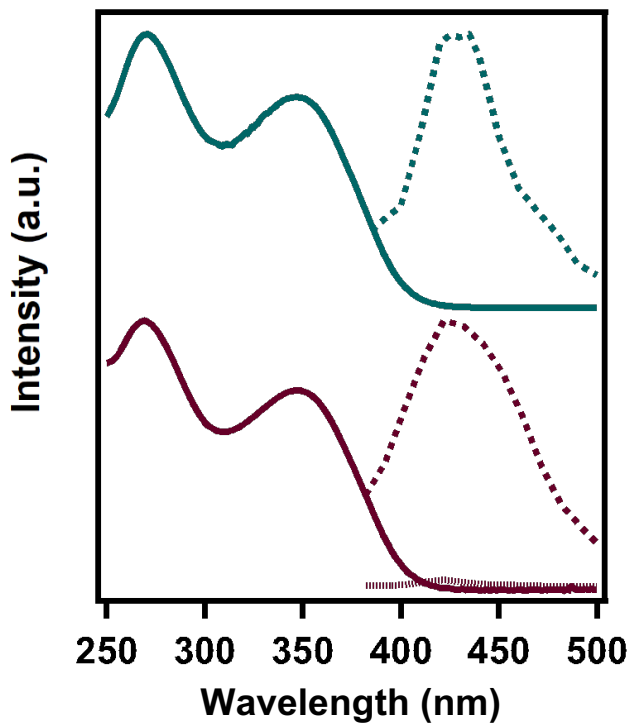


Figure S71. Comparison of MC 1 (maroon) UV-Vis (solid line) and fluorescence (dashed) spectra with that of the model compound (2) (teal). The addition of 1 equivalent of $\text{CF}_3\text{CO}_2\text{H}$ to a solution of MC 1 in THF with 0.3 mM TBAP causes a drastic decrease in fluorescence intensity corresponding with nanotube formation. These comparisons establish that the tetraphenyl benzene core of the truncated node is the fluorophore being studied.

VII. Comparison of GPC and Fluorescence Results

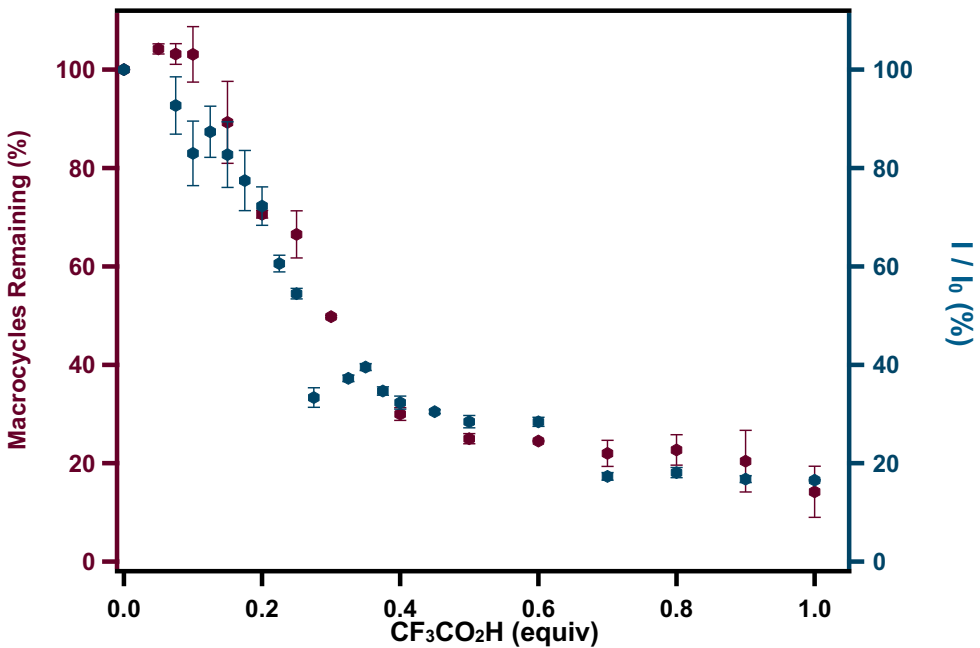


Figure S72. Plot of macrocycle consumption as a function of acid loading, as determined by gel permeation chromatography, and the corresponding fluorescence data obtained by the emission at 430 nm after an excitation at 330 nm.

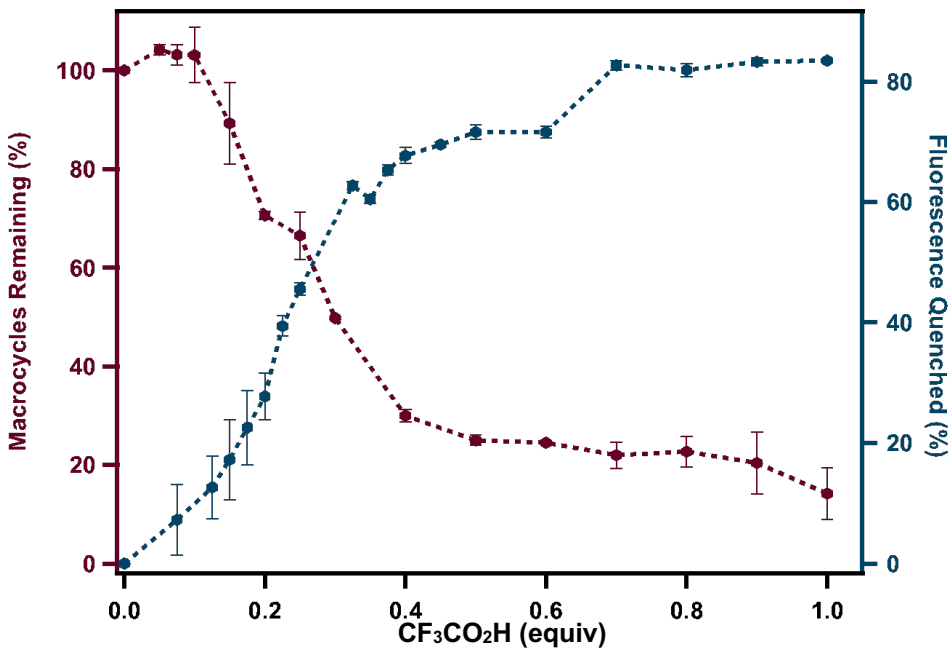


Figure S73. Plot of macrocycle consumption as a function of acid loading, as determined by gel permeation chromatography, and the corresponding data of fluorescence quenching as a percentage.

F. Touch-Spun Fiber Characterization
I. Transmission Electron Microscopy

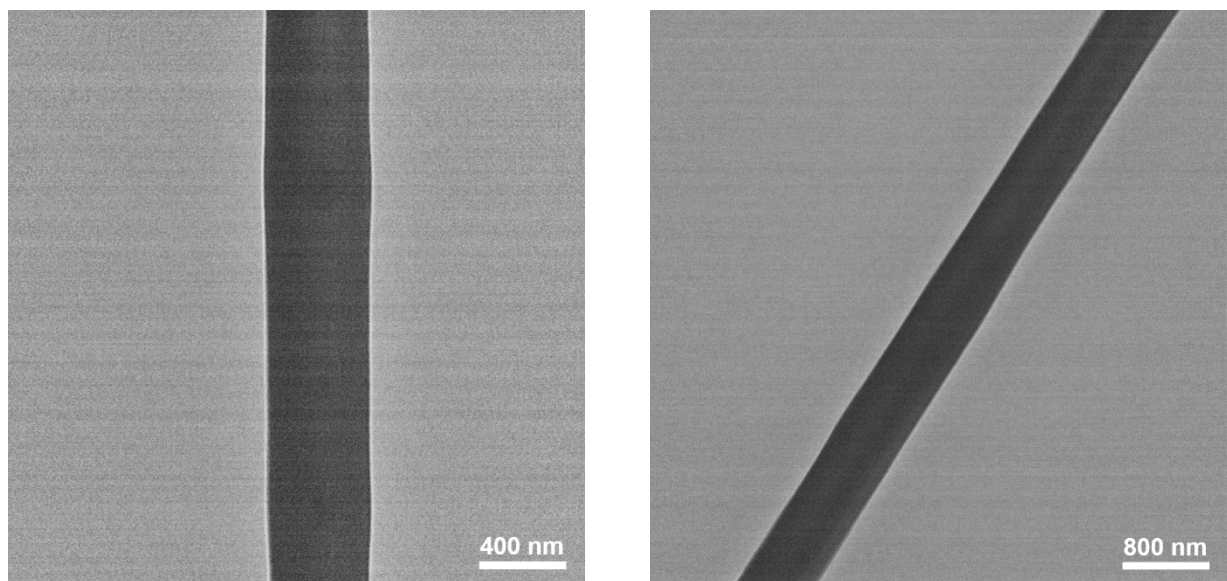


Figure S74. Transmission electron micrographs of touch-spun fibers of poly(ethylene oxide) (PEO). The diameter of the fibers used for mechanical testing was measured to be 298 ± 31 nm.

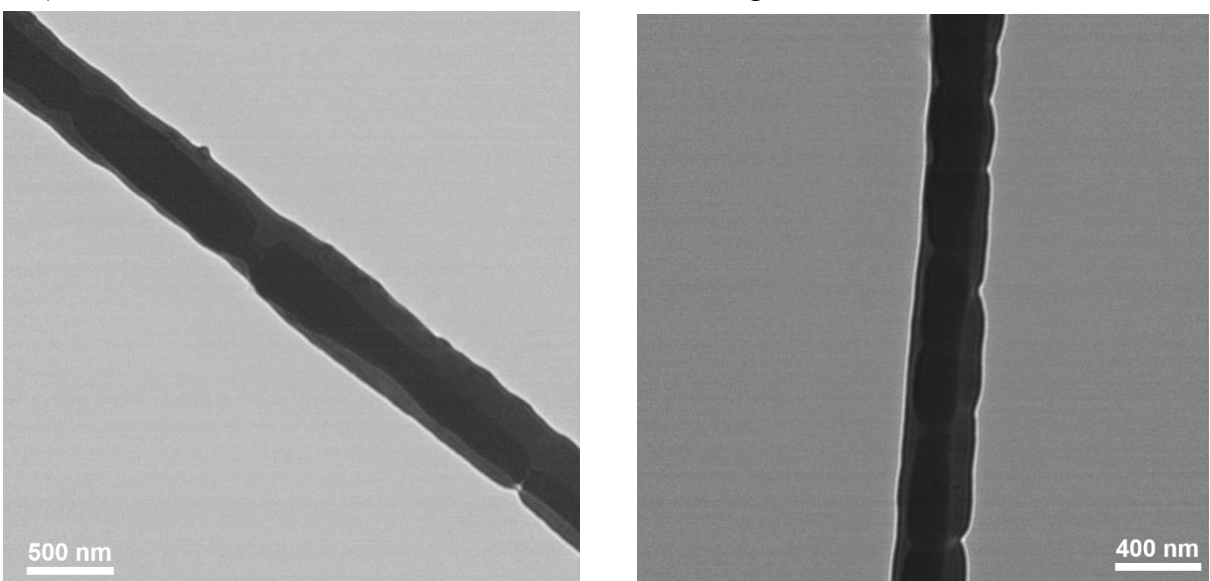


Figure S75. Transmission electron micrographs of touch-spun fibers of nanotubes with 0.5 wt% PEO. The diameter of the fibers used for mechanical testing was measured to be 320 ± 59 nm.

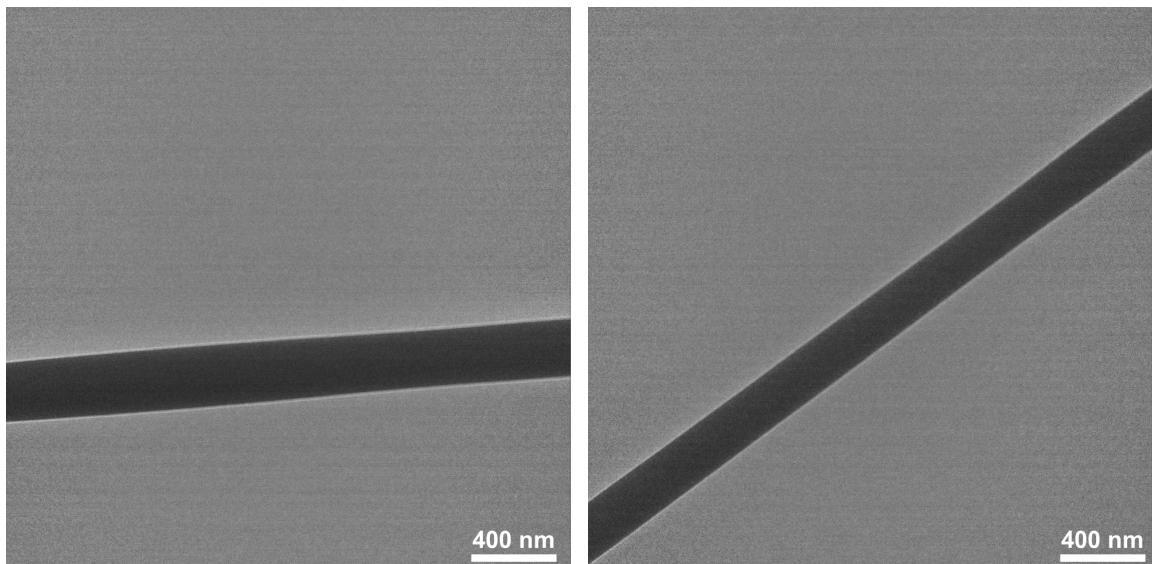


Figure S76. Transmission electron micrographs of touch-spun polycaprolactone (PCL) fibers. The diameter of the fibers used for mechanical testing was measured to be 326 ± 34 nm.

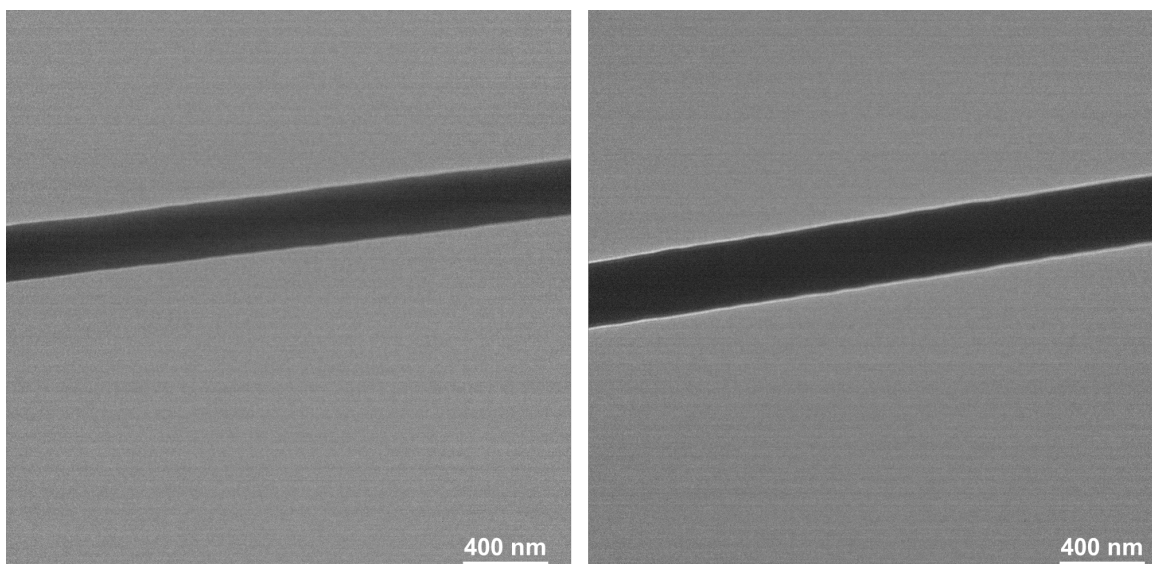


Figure S77. Transmission electron micrographs of touch-spun poly(ester urea) (PEU) fibers. The diameter of the fibers used for mechanical testing was measured to be 328 ± 52 nm.

II. Scanning Electron Microscopy

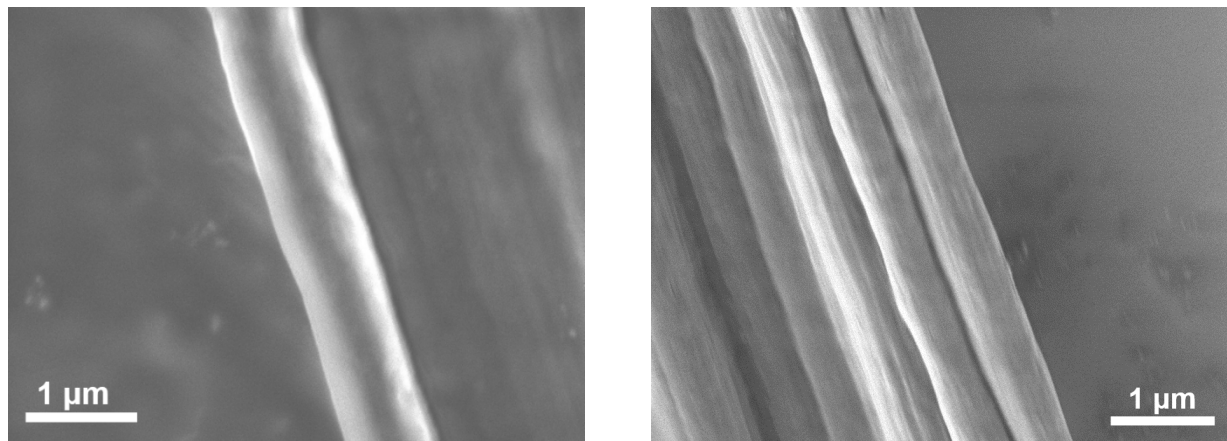


Figure S78. Scanning electron micrographs of touch-spun fibers of PEO.

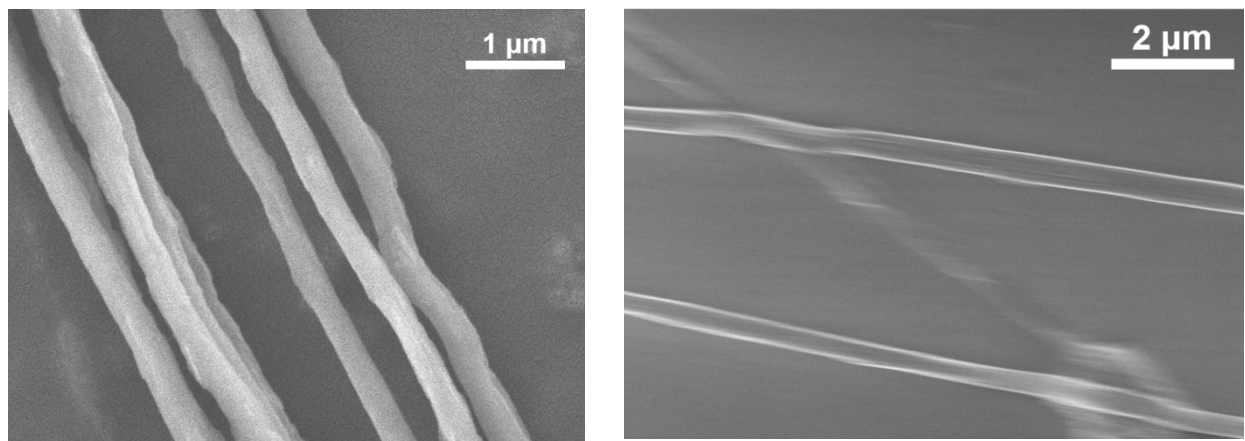


Figure S79. Scanning electron micrographs of touch-spun fibers of nanotubes with 0.5 wt% PEO.

III. Atomic Force Microscopy

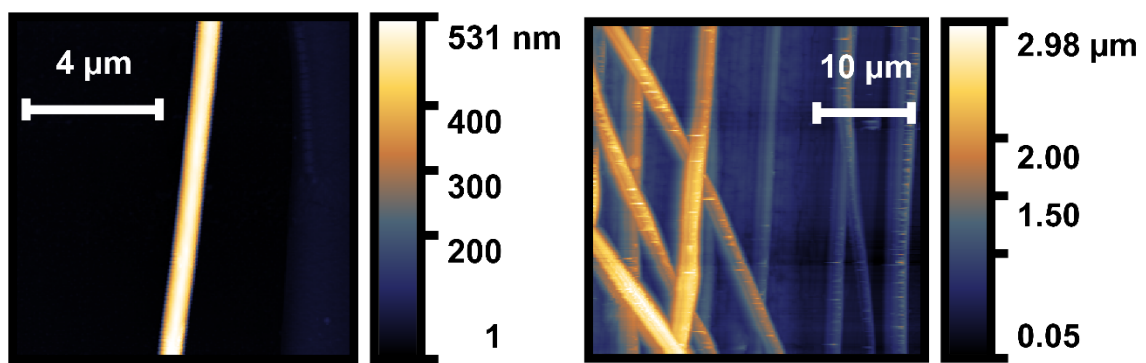


Figure S80. Atomic force micrographs of touch-spun PEO fibers.

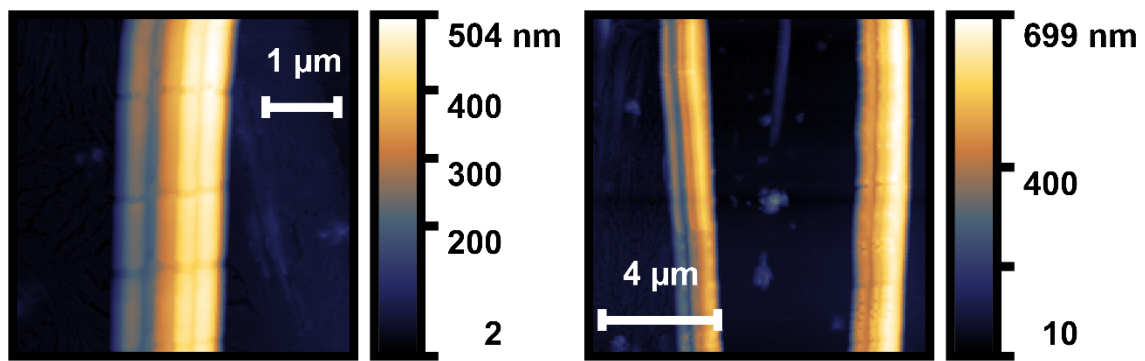


Figure S81. Atomic force micrographs of touch-spun fibers of nanotubes with 0.5 wt% PEO.

IV. Infrared Spectroscopy

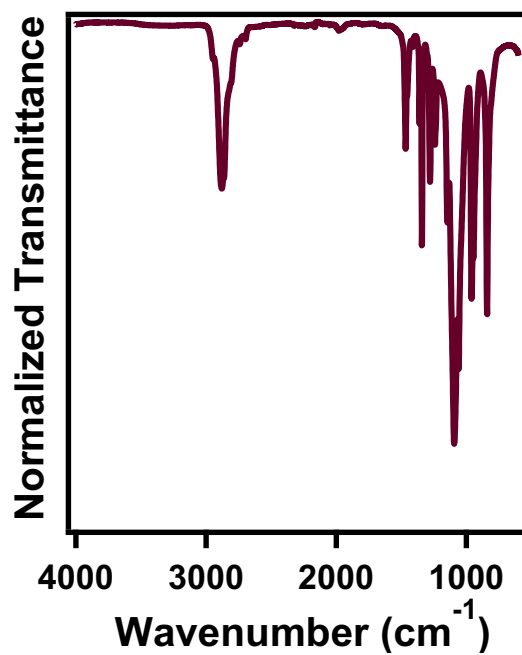


Figure S82. FT-IR spectra of touch-spun PEO fibers.

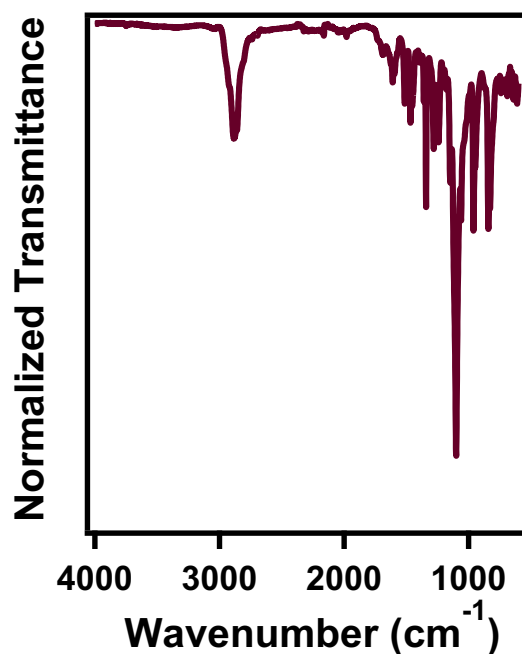


Figure S83. FT-IR spectra of the touch-spun nanotube fibers with 0.5 wt% PEO showing the appearance of a C=N stretch corresponding to the imines of the nanotubes at 1610 cm⁻¹.

V. Matrix Assisted Laser Desorption Ionization Mass Spectrometry

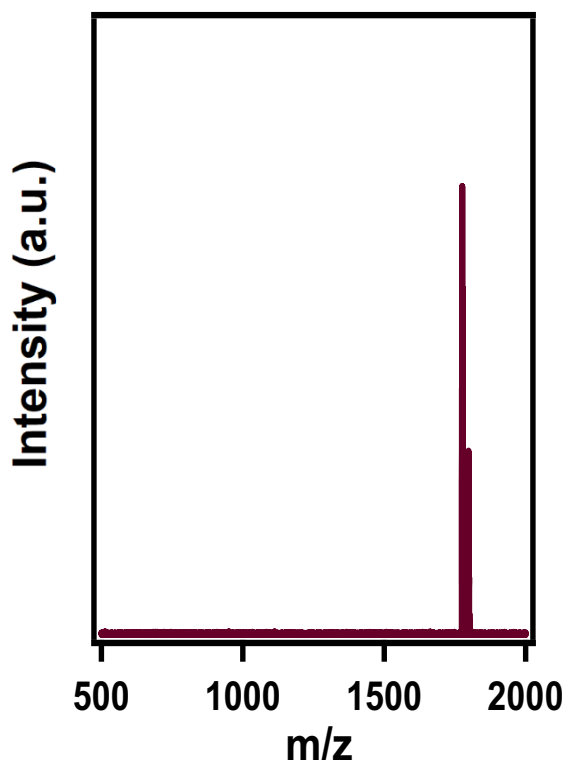


Figure S84. MALDI-MS spectra following the deprotonation and disassembly of the nanotubes showing full recovery of **MC 1** ($m/z = 1774.85$ [$M+H]^+$), thus proving that the touch-spinning process does not result in macrocycle degradation.

VI. Mechanical Testing of Touch-Spun Fibers

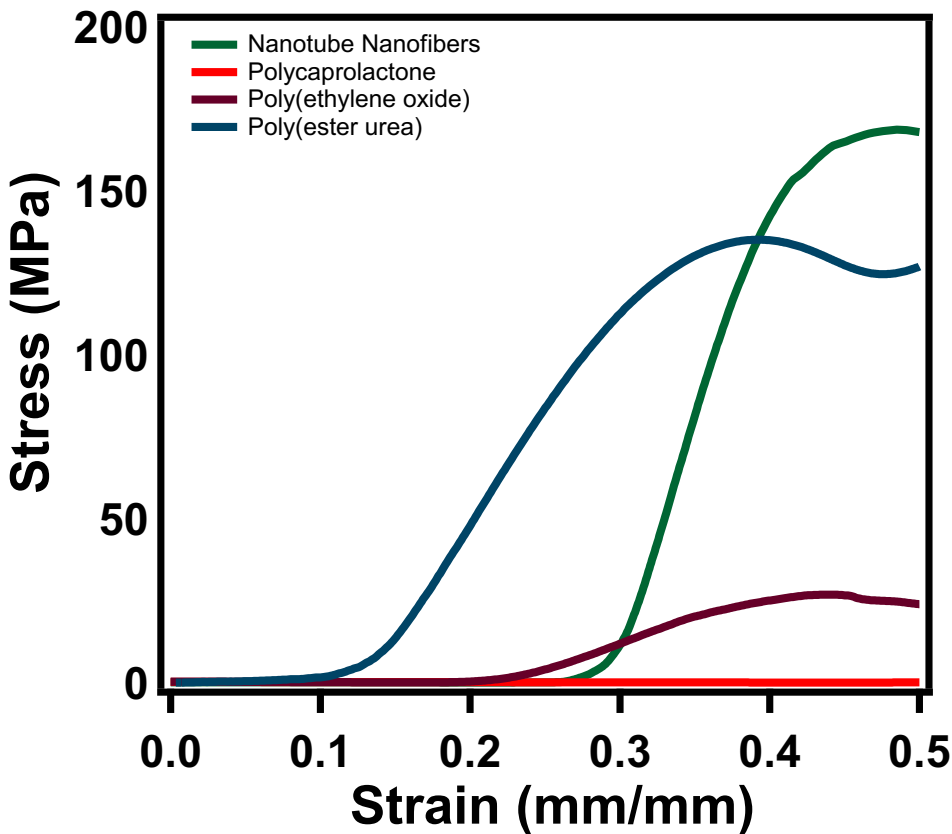


Figure S85. Stress vs. strain plot of all touch-spun nanofibers.

Table S10. Mechanical testing results from nanotube nanofibers.

Sample Name	Modulus (GPa)	True Stress	True Strain (mm/mm)	Engineering Stress (MPa)	Engineering Strain (mm/mm)	Toughness (MPa)
NT 1	1.758	552.942	1.08	187.78	1.95	341.19
NT 2	1.145	59.753	0.64	31.59	0.89	80.05
NT 3	1.55	120.523	0.60	65.93	0.83	40.08
Average	1.48	244.41	0.77	95.10	1.22	153.77
Std. Dev.	0.31	268.92	0.27	82.08	0.63	163.53

Table S11. Mechanical testing results from PEO nanofibers.

Sample Name	Modulus (GPa)	True Stress	True Strain (mm/mm)	Engineering Stress (MPa)	Engineering Strain (mm/mm)	Toughness (MPa)
PEO 1	0.22	45.64	0.70	22.73	1.01	21.02
PEO 2	0.12	6.95	0.69	3.49	0.99	8.28
PEO 3	0.20	69.05	0.58	38.55	0.79	19.95
Average	0.18	40.55	0.66	21.59	0.93	16.42
Std. Dev.	0.05	31.36	0.06	17.56	0.12	7.07

Table S12. Mechanical testing results from PCL nanofibers.

Sample Name	Modulus (GPa)	True Stress	True Strain (mm/mm)	Engineering Stress (MPa)	Engineering Strain (mm/mm)	Toughness (MPa)
PCL 1	0.03	32.28	1.17	9.98	2.24	15.32
PCL 2	0.02	30.51	1.82	4.95	5.17	32.03
PCL 3	0.02	35.03	1.48	7.99	3.38	21.19
Average	0.02	32.61	1.49	7.64	3.60	22.84
Std. Dev.	0.00	2.28	0.32	2.53	1.48	8.48

Table S13. Mechanical testing results from PEU nanofibers.

Sample Name	Modulus (GPa)	True Stress	True Strain (mm/mm)	Engineering Stress (MPa)	Engineering Strain (mm/mm)	Toughness (MPa)
PEU 1	0.68	****	****	****	****	20.90
PEU 2	0.71	138.98	1.33	36.75	2.78	135.85
PEU 3	0.64	160.69	0.72	78.04	1.06	74.22
Average	0.68	149.83	1.03	57.40	1.92	76.99
Std. Dev.	0.04	15.35	0.43	29.20	1.22	57.53

VII. Touch-Spinning of MC 1 with No Acid

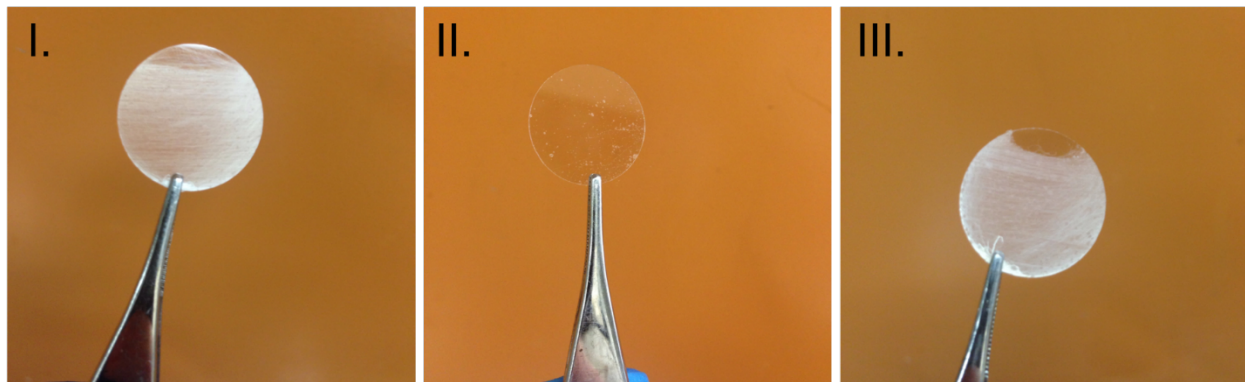


Figure S86. Images of the results of touch-spinning solutions of (I) PEO, (II) neutral MC 1 with 0.5 wt% PEO, and (III) nanotubes assembled from MC 1 with 0.5 wt% PEO

G. References

1. Silantyeva, E. A.; Nasir, W.; Carpenter, J.; Manahan, O.; Becker, M. L.; Willits, R. K., Accelerated neural differentiation of mouse embryonic stem cells on aligned GYIGSR-functionalized nanofibers. *Acta Biomaterialia* **2018**, *75*, 129-139.
2. Yu, J.; Lin, F.; Lin, P.; Gao, Y.; Becker, M. L., Phenylalanine-Based Poly(ester urea): Synthesis, Characterization, and in vitro Degradation. *Macromolecules* **2014**, *47* (1), 121-129.
3. Sun, C.; Shen, M.; Chavez, A. D.; Evans, A. M.; Liu, X.; Harutyunyan, B.; Flanders, N. C.; Hersam, M. C.; Bedzyk, M. J.; Olvera de la Cruz, M.; Dichtel, W. R., High aspect ratio nanotubes assembled from macrocyclic iminium salts. *Proc. Natl. Acad. Sci. U.S.A.* **2018**.
4. Tokarev, A.; Asheghali, D.; Griffiths, I. M.; Trotsenko, O.; Gruzd, A.; Lin, X.; Stone, H. A.; Minko, S., Touch- and Brush-Spinning of Nanofibers. *Adv. Mater.* **2015**, *27* (41), 6526-32.
5. Schindelin, J.; Arganda-Carreras, I.; Frise, E.; Kaynig, V.; Longair, M.; Pietzsch, T.; Preibisch, S.; Rueden, C.; Saalfeld, S.; Schmid, B.; Tinevez, J.-Y.; White, D. J.; Hartenstein, V.; Eliceiri, K.; Tomancak, P.; Cardona, A., Fiji: an open-source platform for biological-image analysis. *Nature Methods* **2012**, *9*, 676.
6. Blackledge, T. A.; Swindeman, J. E.; Hayashi, C. Y., Quasistatic and continuous dynamic characterization of the mechanical properties of silk from the cobweb of the black widow spider *Latrodectus hesperus*. *J. Exp. Bio.* **2005**, *208* (10), 1937-1949.
7. Ge, J.; Wang, X.; Liu, T.; Shi, Z.; Xiao, Q.; Yin, D., Assembly of substituted phenanthridines via a cascade palladium-catalyzed coupling reaction, deprotection and intramolecular cyclization. *RSC Advances* **2016**, *6* (23), 19571-19575.
8. Ankner, T.; Hilmersson, G., Instantaneous Deprotection of Tosylamides and Esters with SmI₂/Amine/Water. *Org. Lett.* **2009**, *11* (3), 503-506.
9. Chavez, A. D.; Evans, A. M.; Flanders, N. C.; Bisbey, R. P.; Vitaku, E.; Chen, L. X.; Dichtel, W. R., Equilibration of Imine-Linked Polymers to Hexagonal Macrocycles Driven by Self-Assembly. *Chem. Eur. J.* **2018**, *24* (16), 3989-3993.
10. Smith, M. K.; Powers-Riggs, N. E.; Northrop, B. H., Rational synthesis of bis(hexyloxy)-tetra(hydroxy)-triphenylenes and their derivatives. *RSC Advances* **2014**, *4* (72), 38281-38292.